

**POLITECNICO DI MILANO**

Facoltà di Ingegneria Industriale

Corso di Laurea in  
Ingegneria Meccanica



Development of a methodology for batteries' integration  
in full electric vehicles

Relatore: Prof. Massimiliano GOBBI

Tesi di Laurea di:  
Alessio SEVARIN

Matr. 801682

Anno Accademico 2014 - 2015







# Aknowledgments

I am grateful to many people who shared with me their time during the development of this work.

Nevertheless, without appearing banal, the first persons I would like to thank are the member of my family, in particular my sisters Giulia and Noemi, for all the support that they gave me during the entire time at the university.

I am also grateful to all the staff of the "Camping Villagge dei Fiori" that I have had the pleasure to meet during my working periods.

I would like also to thank Professor Massimiliano Gobbi for the trust that he gave me and the possibility to develop my thesis abroad at the TU Graz, where I had an amazing experience and I have had the pleasure to meet splendid people.

Between these, I am particularly grateful to my supervisor, Peter Luttenberger, for all the patience and time that he gave me.

I would like to express my gratitude also to Wolfgang Sinz for all the precious advices and to Ellersdorfer Christian for the support also beyond my thesis.

Last, but surely not less important, I would like to thank Weinberger Martin for the friendship established during the developing of this work.

A special thank goes also to Julia Thonhauser for all the support and the patience in the most stressful moments of this work.



# Index

<b>List of the figures</b>	5
<b>List of the tables</b>	10
<b>Abstract</b>	11
<b>Sommario</b>	11
<b>Estratto</b>	12
<b>Introduction</b>	14
<b>Chapter 1 State of the Art</b>	15
<b>Chapter 2 Description of the methodology</b>	18
<b>2.1 Energy requirements ‘evaluation</b>	19
<b>2.2 Battery pack’s mass and volume evaluation</b>	22
<b>2.3 Boundary conditions</b>	23
<b>2.4 Safety</b>	25
<b>2.5 Crash test simulations</b>	27
<b>Chapter 3 Evaluation parameters</b>	29
<b>3.1 Center of gravity</b>	30
3.1.1 Center of gravity height	30
3.1.2 Center of gravity longitudinal position	33
<b>3.2 Rotational inertia moments of the vehicle</b>	34
3.2.1 Yaw inertia moment	34
3.2.2 Roll inertia moment	35
3.2.3 Pitch inertia moment	35
<b>3.3 Safety</b>	35

<b>Chapter 4</b>	<b>Application of the methodology</b>	37
4.1	Description of the vehicle's model	37
4.2	Description of the cells considered	39
4.2.1	Cylindrical cells	39
4.2.2	Prismatic cells	42
4.2.3	Pouch cells	44
4.3	Description of the analysis	47
4.3.1	Boundary conditions	47
4.3.2	Evaluation parameters	49
4.3.3	Conclusions	55
<b>Chapter 5</b>	<b>Results and discussion</b>	56
5.1	Designs using the Boston Power Swing 5300 cells	57
5.2	Designs using the Boston Power Swing 442 modules	59
5.3	Design using the Kokam series 255 75 Ah cells	61
5.4	Designs using the Kokam KBM 255 75 Ah modules	63
5.5	Designs using the Panasonic NCR 18650 A cells	65
5.6	Designs using the Panasonic concept modules	67
5.7	Discussion	69
<b>Chapter 6</b>	<b>Crash test simulations</b>	74
6.1	Frontal crash test against a rigid wall	77
6.2	Pole crash test	80
6.3	Frontal crash test against a deformable barrier	84
6.3.1	Frontal crash test against a deformable barrier with 100 % overlap	84
6.3.2	Frontal crash test against a deformable barrier with 40% overlap	88
6.4	Oblique crash test	91
6.5	Discussion	93
	<b>Conclusion and future works</b>	95
	<b>References</b>	97
<b>Appendix A</b>	<b>Vehicles 'classes</b>	103



<b>Appendix B</b>	<b>Electric vehicles ‘definition and main components</b>	107
<b>Appendix B</b>	<b>Electric vehicles ‘market</b>	118
<b>Appendix D</b>	<b>Accidents in urban scenario</b>	125
<b>Appendix E</b>	<b>EuroNCAP crash tests</b>	130
<b>Appendix F</b>	<b>Application of the methodology to other vehicles</b>	133



## List of the figures

1.1	Different battery packs in the current market	15
1.2	Example of the results of a thermal analysis on a battery pack	16
1.3	Example of a pole crash test simulation the real crash test	17
2.1	Scheme of the methodology	18
2.2	New European Driving Cycle graph	20
2.3	Energy consumption by vehicle mass	21
2.4	Battery pack's components 'mass distribution	22
2.5	Example of the division of the vehicle in zones	23
2.6	Example of the parameters of the vehicle considered	25
2.7	Map of probability of deformation of a passenger cars	26
2.8	Example of the application of the map of probability of deformation	26
2.9	Graphic explanation of the position of the accelerometers	26
3.1	Example of the inertia moments of a passenger car	29
3.2	Example of the center of gravity height for a passenger car	30
3.3	Example of rollover for a simple object	31
3.4	Graphic explanation of the terms involved in the calculation of the SFF	32
3.5	Example of an oversteering and understeering behaviour of a car	33
3.6	Explanation of the main inertia moments of a car	34
3.7	Example of the map of probability of deformation discretized	36
4.1	Comparison between the Geo Metro and the FE model	38
4.2	Photo of a Panasonic NCR 18650 A cell	39
4.3	3D model of the concept Panasonic module	40
4.4	Photo of a Boston Power Swing 5300 cell	42
4.5	Photo of a Boston Power Swing 442 module	43
4.6	Photo of a Kokam Series 255 75 Ah cell	44
4.7	Photo of a Kokam KBM 255 75 Ah module	46
4.8	Graphic explanation of the division in zones of a vehicle	47
4.9	Example of the division in zones and the application of boundary conditions 'values	48

4.10	Comparison of the variation of the average score in different scenarios	50
4.11	Example of the best models for three scenarios	50
4.12	Example of the best models for four scenarios	51
4.13	Trend of the ratio between the $I_{zz}$ and $I_{yy}$ score for 5 scenarios	51
4.14	Comparison of the average score in different scenarios	53
4.15	Comparison of the score of the models between the second and the baseline scenario	54
4.16	Comparison of the score of the models between the third and the baseline scenario	54
4.17	Variation of the safety score in the best models	55
5.1	Explanation of the coordinate system used	56
5.2	Example of the integration of a battery pack designed with the Boston Power 5300 cells into the vehicle	58
5.3	Example of the integration of a battery pack designed with the Boston Power 442 modules into the vehicle	60
5.4	Example of the integration of a battery pack designed with the Kokam Series 255 75 Ah cells into the vehicle	62
5.5	Example of the integration of a battery pack designed with the Kokam KBM 255 75 Ah modules into the vehicle	64
5.6	Example of the integration of a battery pack designed with the Panasonic NCR 18650 A cells into the vehicle	66
5.7	Example of the integration of a battery pack designed with the Panasonic concept modules into the vehicle	68
5.8	Example of the integration of the battery pack in 3 EVs	69
5.9	Center of gravity longitudinal position transfer in the best and worst models	70
5.10	Example of the best designs for four different cells or modules	71
5.11	Transfer of the height of the center of gravity for the best and worst models	71
5.12	Variation of the SFF for the best and worst models	72
5.13	Critical speed comparison for the best and worst models	72
5.14	Transfer of the longitudinal position of the center of gravity in the best and worst models	73
6.1	Comparison between the original FE model and the FE model of the EV	74
6.2	Explanation of the position of the accelerometers	76
6.3	Frontal crash test against a rigid wall configuration	77
6.4	Energies 'trends in the frontal crash test against a rigid wall simulation	77

6.5	Maximum Von Mises stress in the frontal crash test against a rigid wall simulation	78
6.6	Maximum strain in the frontal crash test against a rigid wall simulation	78
6.7	Deformation of the vehicle in two moments of the simulation	79
6.8	Acceleration pulses ‘comparison	79
6.9	Acceleration pulses in the EV	80
6.10	EuroNCAP configuration for the pole crash test	80
6.11	Configurations for the pole crash test simulations	81
6.12	Energies ‘trends in the pole crash test simulations	81
6.13	Maximum strain in the pole crash test simulations	82
6.14	Maximum Von Mises stress in the pole crash test simulations	82
6.15	Deformation of the vehicle in two moments of the simulations	83
6.16	Intrusion depth in the pole crash test simulations	83
6.17	Frontal crash test against PDB with 100 % overlap configuration	84
6.18	Energies ‘trends in the frontal crash test against a PDB with 100 % overlap simulation	85
6.19	Maximum Von Mises stress in the frontal crash test against a PDB with 100% overlap simulation	85
6.20	Maximum strain in the frontal crash test against a PDB with 100% overlap simulation	86
6.21	Acceleration pulses ‘comparison	86
6.22	Maximum Von Mises stress comparison	87
6.23	Maximum strain comparison	87
6.24	Frontal crash test against ODB with 40 % overlap configuration	88
6.25	Energies ‘trends in the frontal crash test against an ODB with 40 % overlap simulation	88
6.26	Maximum Von Mises stress in the frontal crash test against a ODB with 40% overlap simulation	89
6.27	Maximum strain in the frontal crash test against a ODB with 40% overlap simulation	89
6.28	Deformation of the vehicle in two moments of the simulations	90
6.29	Deformation of the vehicle in the zone of the feet of the driver	90
6.30	Oblique crash test against a MPDB configuration	91
6.31	Energies ‘trends in the oblique crash test against an MPDB simulation	91

6.32	Maximum Von Mises stress in the oblique crash test against a MPDB simulation	92
6.33	Maximum strain in the oblique crash test against a MPDB simulation	92
6.34	Acceleration pulses ‘comparison	93
A.1	Photo of two vehicle of the supermini class	105
A.2	Photo of a vehicle of the small family car class	105
A.3	Photo of a vehicle of the large family car class	105
A.4	Photo of a vehicle of the executive class	106
A.5	Photo of a vehicle of the roadster sport class	106
B.1	Photo of an electric road vehicle	107
B.2	Photo of a hybrid electric vehicle	107
B.3	Scheme of a DC motor	108
B.4	Scheme of a PMS motor	109
B.5	Scheme of an ES motor	110
B.6	Scheme of an induction motor	110
B.7	Structure of a cylindrical cell	113
B.8	Photo of a 18650 cylindrical cell	114
B.9	Structure of a prismatic cell	114
B.10	Structure of a pouch cell	115
B.11	Photos of the variation of volume of a pouch cell	115
B.12	Example of the assembly of a battery pack	116
B.13	Components of a cell module	116
C.1	Forecast of the drop of the cost of EVs´cells	119
C.2	Forecast of the matriculation of EVs in the world	120
C.3	Forecast of the grown of the EVs´ fleet	120
C.4	EV matriculations in Europe	121
C.5	EV and ICE vehicles growth rate comparison	122
C.6	Matriculation growth rate in Austria by energy source	123
C.7	Matriculation growth rate in Germany by energy source	123
C.8	Matriculation by energy source in Austria in 2013	124
C.9	Matriculation by energy source in Germany in 2013	124
D.1	Accidents distribution by road type in Europe	125
D.2	Accidents distribution by road type in Germany	125
D.3	Accidents distribution by road type in Italy	126
D.4	Accidents trends by road type in Italy	126
D.5	Accidents trend in Italy from 2002 to 2011	127
D.6	Accidents ‘forecast in Italy	127
D.7	Ratio forecasted between the total number of accidents and the accidents in urban roads in Italy	128
D.8	Injuries distribution in urban scenario accidents	128
D.9	PDoF frequencies in urban accidents	129

D.10	PDoF frequencies in junction accidents	129
E.1	Frontal crash test against a rigid wall configuration by EuroNCAP	130
E.2	Frontal crash test against an ODB configuration by EuroNCAP	131
E.3	Pole crash test configuration by EuroNCAP	131
E.4	Side crash test configuration by EuroNCAP	132
F.1	Example of the result of the application of the methodology to a Dodge Neon	133
F.2	Example of the result of the application of the methodology to a concept L7e vehicle	134
F.3	Example of the result of the application of the methodology to a Renault Twizy	134

## List of the tables

4.1	Main characteristics of the Geo Metro	38
4.2	Characteristics of the Panasonic NCR 18650 A cell	39
4.3	Characteristics of the battery pack modelled with the Panasonic NCR 18650 A cells	40
4.4	Characteristics of the Panasonic concept module	41
4.5	Characteristics of the battery pack modelled with the Panasonic concept modules	41
4.6	Characteristics of the Boston Power Swing 5300 cell	42
4.7	Characteristics of the battery pack modelled with the Boston Power Swing 5300 cells	43
4.8	Characteristics of the Boston Power Key 442 module	43
4.9	Characteristics of the battery pack modelled with the Boston Power Swing Key 442 modules	44
4.10	Characteristics of the Kokam Series 255 75 Ah cell	45
4.11	Characteristics of the battery pack modelled with the Kokam Series 255 75 Ah cells	45
4.12	Characteristics of the Kokam KBM 255 75 Ah module	46
4.13	Characteristics of the battery pack modelled with the Kokam KBM 255 75 Ah modules	46
4.14	Characteristics of the analysis	49
4.15	Sensitivity analysis's scenarios	49
5.1	Results of the battery packs modelled with the Boston Power Swing 5300 cells	57
5.2	Results of the battery packs modelled with the Boston Power Swing Key 442 modules	59
5.3	Results of the battery packs modelled with the Kokam Series 255 75 Ah cells	61
5.4	Results of the battery packs modelled with the Kokam KBM 255 75 Ah modules	63
5.5	Results of the battery packs modelled with the Panasonic NCR 18650 A cells	65
5.6	Results of the battery packs modelled with the Panasonic concept modules	67
6.1	Resume of the crash test simulations developed	75
B.1	Comparative view of the characteristics of the main shapes for Li-ion cells	113
C.1	Comparison between the matriculation of EVs and ICE vehicles in Europe	122



## Abstract

The application of alternative sources of energy, in particular electricity, for the propulsion of passenger cars is a rapid growing sector of the automotive industry. Due to the new hazards introduced by the integration of high-energy batteries into the vehicles, the placement of themselves represents an important task in order to guarantee the safety of the vehicle and the passengers.

This work develops a methodology for the design and positioning of the battery pack for electric vehicles by using the probability of deformation in real accidents, in order to determine the most adequate positions that satisfy the design boundary conditions, increase the safety of the cells and reduce the influence of the added mass on the dynamic performance of the vehicle.

Moreover, the results of the methodology are analysed by simulating real crash tests with the purpose to identify possible improvements in the vehicle's structure.

**Key words:** electric vehicle, battery pack design, deformation frequency, crash test simulation, finite element method.

## Sommario

L'applicazione di fonti alternative di energia, in particolare elettrica, per la propulsione di autoveicoli è un settore dell'industria automobilistica in rapida crescita.

A causa dei nuovi pericoli introdotti dall'integrazione di batterie ad alta energia nei veicoli, la collocazione delle stesse rappresenta una decisione importante allo scopo di garantire la sicurezza dell'automobile e dei passeggeri.

Questo studio sviluppa una metodologia per il design ed il posizionamento del battery pack per veicoli elettrici sfruttando la probabilità di deformazione in incidenti reali, allo scopo di determinare le posizioni più adeguate che soddisfino i vincoli di progetto, aumentino la sicurezza e riducano l'influsso della massa aggiunta sulle performance dinamiche del veicolo.

Inoltre, i risultati della metodologia sono analizzati simulando crash test reali allo scopo di identificare possibili miglioramenti nella struttura del veicolo.

**Parole chiave:** veicolo elettrico, battery pack design, frequenza di deformazione, simulazione di crash test, metodo agli elementi finiti.

## Estratto

Il mercato dei veicoli elettrici ha subito negli ultimi anni una notevole espansione, grazie al numero crescente di ricerche di una fonte alternativa di energia per la propulsione di autoveicoli.

Tuttavia, nello stato dell'arte attuale, non è presente alcuna metodologia pubblica in grado di facilitare il design ed il posizionamento del battery pack per veicoli elettrici.

Questo lavoro punta a limitare tale mancanza fornendo uno strumento che permetta il facile design di concepts di battery packs allo scopo di diminuire i tempi di progettazione e, potenzialmente, i costi di sviluppo.

Lo strumento in questione è un programma, sviluppato con il software Matlab, in grado di creare modelli 3D di battery packs, considerando i vincoli del design, nonché le dimensioni caratteristiche del veicolo, cercando al tempo stesso di massimizzare la sicurezza del battery pack.

Per tale obiettivo viene sfruttata una mappa di probabilità di deformazione nei veicoli di classe M1, ossia auto caratterizzate da meno di 9 posti ed adibite al trasporto di passeggeri (si veda appendice A).

Mediante la definizione delle celle desiderate per il battery pack, l'intero veicolo viene discretizzato in volumi con le stesse dimensioni delle celle selezionate; l'algoritmo procede successivamente alla scelta delle posizioni che massimizzano la sicurezza, con rispetto delle condizioni di vincolo definite, fino al raggiungimento del numero di celle necessario per ottenere l'autonomia desiderata.

Grazie alla relativa velocità di esecuzione dell'algoritmo, risulta possibile la creazione di un elevato numero di concepts.

Nasce quindi la possibilità non solo selezionare il concept che più si adatta alle condizioni di vincolo imposte, ma, anche, che influenza nel modo desiderato le caratteristiche dinamiche del veicolo, in particolare la posizione del baricentro e i momenti di rollio, beccheggio e imbardata.

Poiché non è presente in letteratura alcuna informazione riguardo la possibile importanza relativa dei parametri dinamici selezionati, nell'applicazione della metodologia viene fornita la possibilità di definire tale caratteristica; viene inoltre fornita un'analisi sull'influenza dei vari parametri nel design dei battery packs.

Applicando tale metodologia su uno stesso veicolo, variando la tipologia di celle scelte, è stato possibile individuare che, indipendentemente dalle dimensioni delle celle stesse, un design comune permette di ottimizzare l'influenza del battery pack

sulle caratteristiche dinamiche del veicolo, massimizzando la sicurezza (si veda capitolo 5).

Inoltre, al fine di verificare l'effettiva sicurezza dei concepts prodotti, un concept è stato implementato in un modello di veicolo esistente e sono stati simulati, mediante il metodo ad elementi finiti, tipici crash tests attualmente impiegati per la verifica della sicurezza dei passeggeri.

Nonostante l'approssimativo modello di battery pack utilizzato, la metodologia ha dimostrato buoni risultati nella maggioranza dei test, offrendo al contempo importanti informazioni sul possibile e/o miglioramento del veicolo e del battery pack stesso (si veda capitolo 6).

## Introduction

The electric vehicles 'market is a sector in continue growth in the last years thanks to the improvements in the technology and the increasing researches in an alternative and economical source of energy for the automobile propulsion. [1]

Nevertheless is not available in the literature a methodology for the easy design and implementation of the main components of an electric vehicle, in particular the batteries, into an existing automobile.

This work aims to define a methodology for the simple design of battery pack concepts and for their positioning inside the vehicle with respect to the dynamic and structural features of the vehicle itself.

As most of the manufacturing costs are already defined in the concept phase, the possibility to define fast multiple solutions can decrease the design phase time and reduce the further production expenses. [2]

The results of the methodology can provide a guideline for the detailed design of the battery pack and for the improvements or modifications needed in the structure of vehicle, still from the earliest phase of the development of the car.

Moreover, as the methodology permits the design of a wide number of battery pack models (more than 10000), further analyses can be developed, considering the influence of the battery pack design in some important dynamic parameters of the automobile.

# Chapter 1

## State of the art

The safety of EVs is an important topic both for producers and consumers, as the components necessary for the electric propulsion introduce new risks for the users in case of crash. [3]

As the number of car producers that pointed their attention to the EV's market increased, the range of different solutions for the implementation of the batteries in the vehicles raised. [4]

Since the damage of the battery pack can lead to high hazards for the EV's users, its position and design has to be chosen carefully. Moreover, due to its notable mass, the battery pack can influence the dynamic performance of the automobile. Every car producer makes use of its own internal knowledge in order to find a compromise between the dynamic performance of the vehicle and the safety of the battery pack, always considering the costs of the manufacturing process and the ease of production and integration.

Although many researches have been developed regarding the design of the battery pack and the test of the safety of the cells, no design method that considers the safety, as well as the dynamic influence of the battery pack, is currently available.

The solution commonly adopted by EV's producers is the installation of the battery pack in the lower middle part of the vehicle, nevertheless a wide range of shapes is found in the current market, as shown in figure 1.1.



**Figure 1.1** Example of different battery packs present in the current market. From the left, Tesla model S battery pack [5], Chevrolet Volt battery pack [6] and Nissan Leaf battery pack [7].

The safety of the cells is ensured by the design of the battery pack's housing that has to:

- avoid the penetration of external objects inside the battery pack in case of crash;
- avoid the deformation of the cells in case of crash;

- permit the needed thermal management of the cells;
- integrate all the instruments for the control of the correct operation of the batteries.

This leads to the design of compact battery packs in which the cells are organised in modules in order to achieve the energy requirements, decrease the production costs and improve the safety through the possibility of disconnect the single batteries 'modules in case of emergency. Moreover, other safety precautions are necessary regarding the connection to the electric engine. [3]

Before the series manufacturing of the battery packs, a campaign of test is always developed in order to check the safety of the product. The campaign includes both Finite Element Analyses (FEAs) and tests on real models, which have to fulfill the current regulations. [8] [9] [10]

A wide range of FEAs has been developed so far, including mechanical and electro-thermal characteristics of the battery packs.

Electro-thermal analyses (figure 1.2) target to simulate the behaviour of the cells when an overcharge or a malfunction of the recharging system happens.

In addition, they aim to check the thermal loads under normal conditions, in order to provide the correct thermal management of the cells. [11]

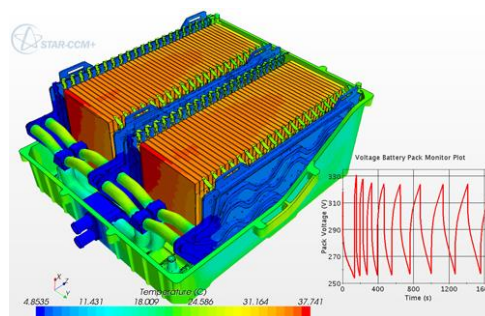


**Figure 1.2** Example of the results of a thermal analysis on a battery pack. [12]

Moreover is common to compare the results of the FEAs to which of the real tests in order to validate the analyses.

Mechanical FEAs permit the identification of the deformations and stresses to which the battery pack is subjected before the effective production and test. [13] However, it has to be noted that no mechanical FEA alone can predict events whose cause is influenced also by chemical and/or thermal factors.

A wide number of simulation approaches is available in literature spacing from battery pack's impact tests to simulations of a complete EV in case of crash. [14] [15]

However, a common step is the simulation of the behaviour of the complete battery pack in case of crash.

This is usually developed reproducing the contact of the battery pack with an external object, that can be part of the vehicle itself as well as part of the environment, and observing the deformation of the cells. [16]

If no deformation in the cell can be found, it is then possible to judge the safety of the battery pack; nevertheless it has to be noted that this type of simulation do not consider the position of the battery pack inside the vehicle.

Various methods are currently used to simulate the mechanical behaviour of the cells through finite elements (FE) models. [17] [18]

As the correct modelling of every component of the cells requires an elevated effort, an approach can be the modelling of the batteries through the use of a representative volume element (VRE) that reproduces the local features of the battery. [17]

A final assessment of the safety of the battery pack is developed simulating the behaviour of the entire vehicle in case of crash, at first, then testing in real crash tests the EV (see figure 1.3).

Every country is subjected to his mandatory regulations, however these always include the evaluation of the safety of the automobile in case of frontal crash, side impact against a rigid pole and against a mobile trolley, representing another vehicle. [19]

If all the tests are successfully fulfilled, the public sale of the car is approved. [8] [9] [10]

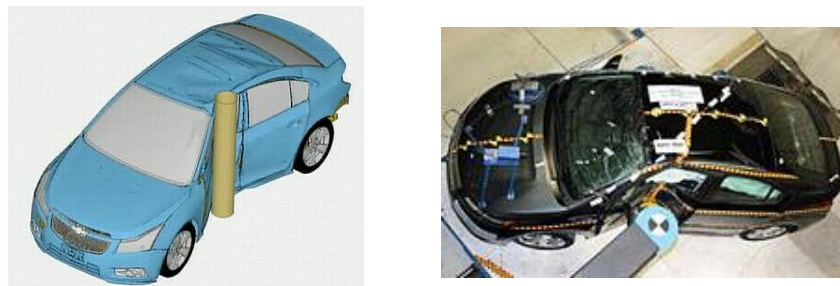


**Figure 1.3** Example of a simulation of a pole crash test (left) [20] and the real pole crash test [21].

## Chapter 2

### Description of the methodology

In this work an innovative methodology for the design of EVs' battery packs is presented.

The methodology considers mainly three factors: the energy requirements of the vehicle, the structure of the car itself and the probability of deformation associated to every zone of the automobile.

The combination of these factors permits, using a novel algorithm, the selection of the best positions for the cells that both satisfy the boundary conditions and maximize the safety of the batteries.

A resuming scheme of the methodology is proposed in figure 2.1.

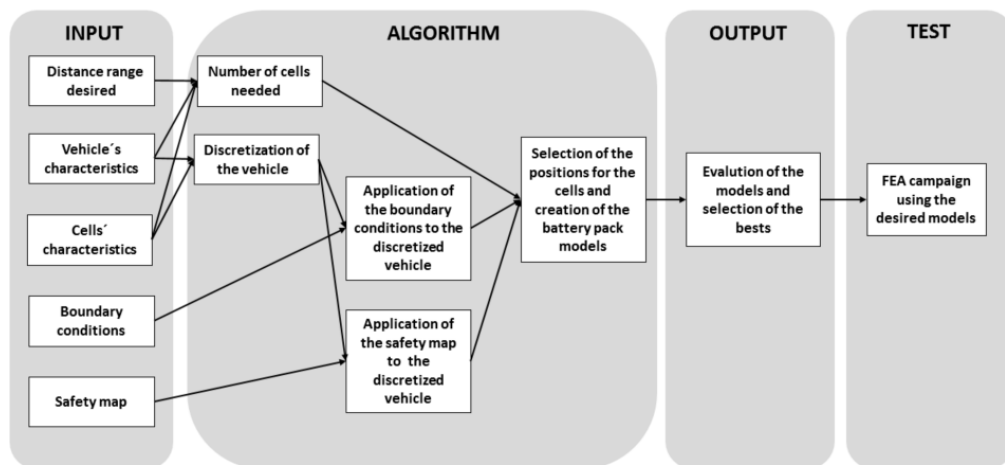


**Figure 2.1** Scheme of the methodology.

The methodology consists in 5 phases which can be defined as:

1. inputs definition;
2. calculation of the energy requirements;
3. discretization of the vehicle and search of the best positions for the cells;
4. analysis of the battery pack models;
5. crash test simulations of the vehicle after the integration of the battery pack.



In the first phase, the parameters of the vehicle and of the design, as well as the cells 'features, should be defined.

The second phase, using the information of the previous phase as inputs, focuses on the calculation of the energy needed for the propulsion of the vehicle for the design distance range, then, through the definition of the desired cells, an estimation of the number of batteries is provided.

In the third phase, in order to define the positions of the cells, the algorithm arranges a discretization of the vehicle in elementary volumes with the same dimensions of the batteries, then, the safety of every elementary volume is evaluated depending on the probability of deformation of its position in the vehicle.

Moreover, in this phase, the algorithm provides the selection of the best positions until the goal number of cells is achieved.

As usually more than a single solution is found, in the fourth phase, the application of an evaluation method based on dynamic and safety parameters permits the identification of the most suitable models for the selected automobile.

In the last phase, in order to test the effectiveness of the result, a campaign of FEAs, reproducing real crash tests, is developed and used as examination method.

## 2.1 Energy requirements 'evaluation

The energy available is one of the main characteristics of an EV's battery pack as it determines the autonomy of the car.

The energy needed is influenced by many factors that can be mainly divided in:

- design factors: as the usage of the electric motor, the maximum degree of discharge (DOD) of the cells and the design distance range;
- parameters of the vehicle: as ,primarily , the mass and the shape of the vehicle;
- external factors, as the skills of the driver and the scenario in which the vehicle will be used.

In order to remove the external factors from the analyses, the energy consumption of a vehicle is calculated upon standard driving cycles, which consider a certain number of acceleration's and deceleration's periods, followed by intervals with a standard duration and a defined speed of the vehicle.

An example of a driving cycle is presented in figure 2.2. [22]

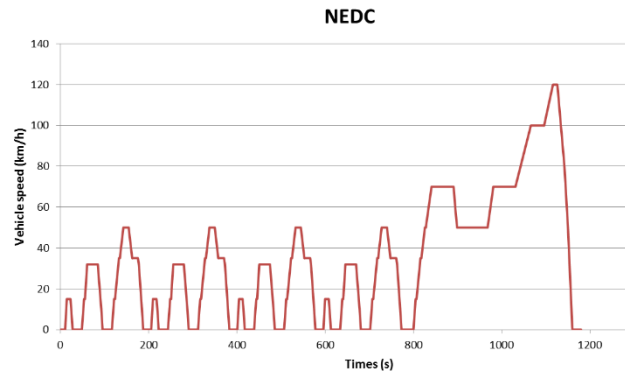


**Figure 2.2** Speeds versus time graph of the New European Driving Cycle (NEDC).

The mass of the vehicles plays an important role because, as known, as the mass increases, the energy needed to accelerate the vehicle and to maintain the speed raises. [23]

The shape of the vehicle has also to be taken into account as the aerodynamic friction can produce a considerable dissipation of energy. [23]

Moreover, the energy use is influenced by the characteristics of the electric motor, because usually motors with higher performance require more energy to run, independently by the efficiency. [23]

The maximum DOD of a battery is a parameter that should be patiently analysed. It defines the percentage of energy of the cell that can be used. In fact every battery allows a maximum DOD in order to assure a safe life cycle, moreover every batteries' producer indicates a recommended DOD with the purpose to guarantee a longer life of the cell.

It can be summarized that the higher the DOD is, the shorter is the life of the battery. Furthermore, it has to be considered that the cost of a single cell is usually not elevated but the same consideration can not be stated regarding the battery pack, for this reason EVs' producers do not consider the replacement of the battery pack during the life of the vehicle.

It is then obvious that a 100% DOD is not a good "economical" decision; the maximum DOD is normally set to 80% but this is a topic of high interest for electric vehicles' and cells' producers. [24]

Previous works permit the evaluation of the energy consumption for a vehicle with a certain mass for a desired driving cycle. In particular, the energy consumption can be defined as in equation 2.1. [25]

$$m_{batt} * (\rho_{ele,batt} * SOC) - [a * (m_{vei} + m_{batt}) + b] * s_{ele} = m_{batt} * \frac{(a * m_{vei} + b)}{\frac{\rho_{ele,batt} * SOC}{s_{ele}} - a} \quad (2.1)$$

**Equation 2.1** Equation for the evaluation of the energy consumption depending on the mass of the vehicle.

The terms of the equation have the following meanings:

- $m_{batt}$  is the mass of the battery pack [kg];
- $m_{vei}$  is the mass of the vehicle without the battery pack [kg];
- $\rho_{ele,batt}$  is the specific energy density of the battery system [kWh/ kg];
- SOC is the minimum state of charge of the battery pack [%];
- $a$  is the cycle specific mass gradient [kWh/(kg\*km)];
- $b$  is the cycle specific basic consumption [kWh/km] and expresses the losses due to air and powertrain friction and the energy absorbed by auxiliary components;
- $s_{ele}$  is the design distance range [km].

The method was applied to vehicles with different mass and for different driving cycles. The results are proposed in figure 2.3. [25]

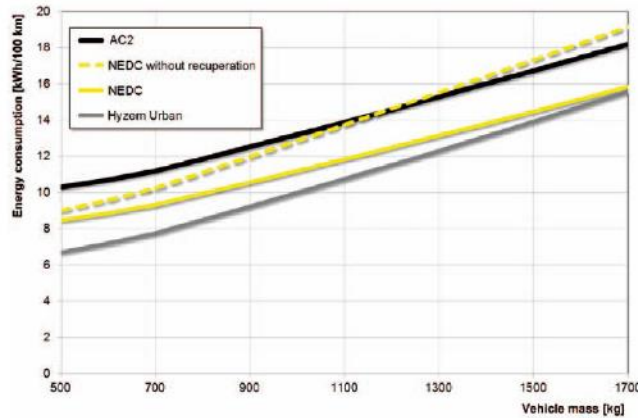


**Figure 2.3** Vehicle's energy consumption for 100 km as found in the literature.

Considering the NEDC cycle with recuperation, it is possible to estimate the energy needed for an electric vehicle with a certain mass and a defined design distance range, as exposed in equation 2.2.

$$E_{\text{need}} = \frac{a \cdot m_{\text{vei+batt}} + b}{1 - SOC} \cdot \text{Sele} \quad (2.2)$$

**Equation 2.2** Formula used for the estimation of the energy needed for the propulsion of the desired vehicle.

Where the terms of the equation have the same meanings as in equation 2.1 with the exception of  $m_{\text{vei+batt}}$  that indicates the mass of the vehicle plus the battery pack [kg] and  $E_{\text{need}}$  that expresses the needed energy [kWh].

After the definition of the characteristics of the cells, in order to evaluate the correct number of batteries needed, it is necessary to find the appropriate disposition of the cells in parallel and series to achieve both the desired voltage for the electric motor and the energy required for the design distance range.

## 2.2 Battery pack mass and volume evaluation

The cells are not the only component of a battery pack (see appendix B), thus the complete definition of the mass and volume of the battery pack is not possible in the concept phase. Nevertheless, a common mass distribution between the main components can be found in the current state of art (see figure 2.4). [26]

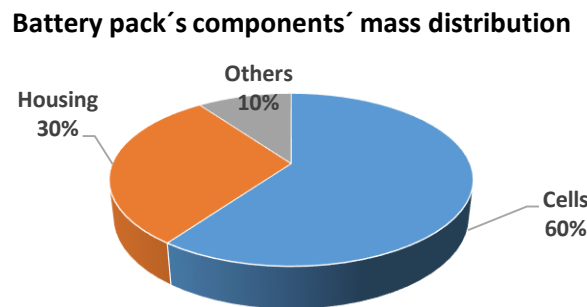


**Figure 2.4** Distribution of the total mass of the battery pack between the main components, as found in the literature.

Thus, knowing the mass of the cells, an estimation of the total mass of the battery pack can be provided using equation 2.3.

$$m_{B-P} = \frac{m_{batt} * 100}{60} \quad (2.3)$$

**Equation 2.3** Formula used for the estimation of the total mass of the battery pack.

The terms in equation 2.3 assume the following meanings:

- $m_{B-P}$  is the total mass of the battery pack;
- $m_{batt}$  is the total mass of the cells.

Moreover, the total volume of the battery pack should be estimated in order to define the required space inside the vehicle.

As a high percentage of the total volume of the battery pack is represented by the cells, the volume of the other components has been neglected. [27]

Nevertheless, in order provide an appropriate prediction of the complete volume needed by the battery pack, it is necessary to consider the need of a certain distance between the cells, due to the necessity of a correct thermal management. This parameter, which varies for every design, can in the concept phase only be estimated. Nevertheless, it was considered, increasing the cells dimensions, in order to respect the common state of art.

## 2.3 Boundary conditions

In order to reproduce all the actual battery pack's shapes and to extend the design possibilities, a standard vehicle was divided in 12 zones that can be found in common passenger car as shown in figure 2.5.

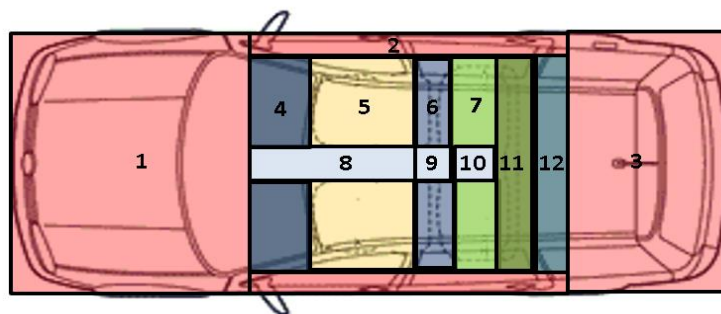


**Figure 2.5** Example of the division of the vehicle in zones at the height of the floor pan.

The zones assume the following meanings:

1. represents the space from the front bumper to a distance from the front axle specified by the user;
2. represent the lateral frame of the vehicle plus a “safety zone” decided by the user;
3. represents the trunk of the vehicle, this zone extends from a line specified by the user to the rear bumper of the vehicle;
4. represents the zone of the cockpit from the front seats to the end of the cockpit itself,
5. represents the zone under the front seats;
6. represents the zone between the front and the rear seats;
7. represents the zone under the rear seats until the rear cross beam;
8. represents the tunnel from the beginning of the cockpit to the end of the front seats;
9. represents the tunnel between the front and the rear seats;
10. represents the middle zone under the front seats
11. represents the rear cross beam;
12. represents the space between the rear cross beam and the beginning of the selected zone for the trunk.

In order to permit the application of the methodology to an as wide as possible range of vehicles, the creation of the zones is developed using some important parameters of the car, that can be found in every vehicle member of the M1 or L7e class.

The main parameters used can be resumed in:

- the number of seats of the vehicle;
- the total length of the vehicle;
- the total width of the vehicle;
- the dimensions of the tunnel;
- the distance between the front bumper and the front axle;
- the wheel base of the vehicle;
- the distance between the rear bumper and the rear axle;
- the distance of the rear cross beam from the front bumper, or in case of absence of this component, the distance between the front bumper and the B pillar.;
- the position of the seats;

- the frame dimensions.

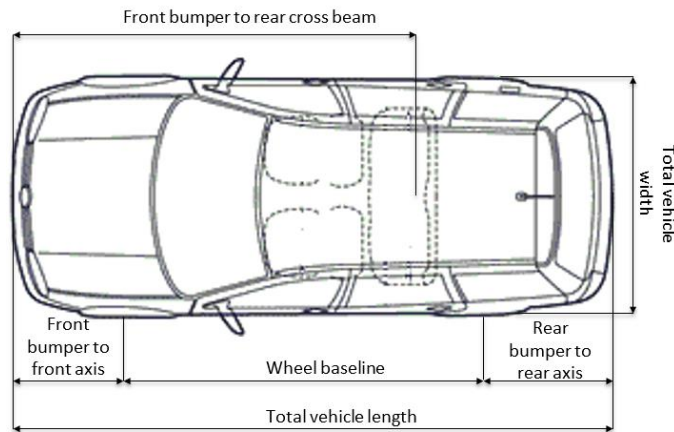


**Figure 2.6** Example of some of the parameters of the vehicle used.

The use of a particular zone for the battery pack depends from many factors like:

- the physical availability of that zone;
- the previous experience;
- the modifications needed to the vehicle in order to use that zone;
- the influence of the use of a particular zone for the battery pack in the dynamic of the vehicle.

As every EVs` producer adopts his own strategy based also upon the internal knowledge, it is not possible to find in the state of art common indications or advices.

For this reason, in the methodology, a value can be applied to every zone, expressing the will of use the selected area.

This permits to avoid the integration of the batteries in a certain zone, if previous experiences show that it would not lead to a good design, and ,on the other hand, to explore a wide range of solutions.

## 2.4 Safety

The safety of a battery pack is not an easy factor to determinate, as it is influenced by many variables regarding the design of the battery pack`s housing, the position of the battery pack itself and the structure of vehicle too.

With the aim of founding a solution independent from the vehicle and from the design of the battery pack`s housing, the safety of the battery pack is evaluated through statistical data in real crashes.

A map of the probability of deformation of passenger cars was found in the literature (see figure 2.7). [28]

The map was retrieved after analysing more than 6000 accidents present in the GIDAS database and shows the deformation frequency in automobiles in real crashes. Due to the slight variations of the probability of deformation with the height of the section considered in proximity of the floor pan, the map at the height of the floor pan was taken as reference.

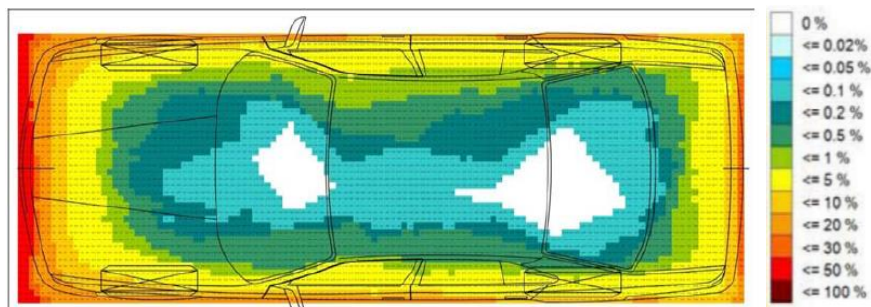


**Figure 2.7** Map of the probability of deformation for the floor pan level of an automobile.

It is then assumed that the sum of the probability of deformation of the zones, where the battery pack is set, can be directly linked to the safety of the battery pack itself and can be used as guideline for a concept design.

The map was taken as reference for the evaluation of the safety of the battery pack, using a range of four values:

- 0 = probability of deformation = 0% ;
- -1 =  $0\% < \text{probability of deformation} \leq 0.1\%$  ;
- -2 =  $0.1\% < \text{probability of deformation} \leq 5\%$  ;
- -3 =  $5\% < \text{probability of deformation} \leq 50\%$  ;
- -4 = probability of deformation  $> 50\%$  .

As describe previously the map of probability of deformation appears like in figure 2.8.

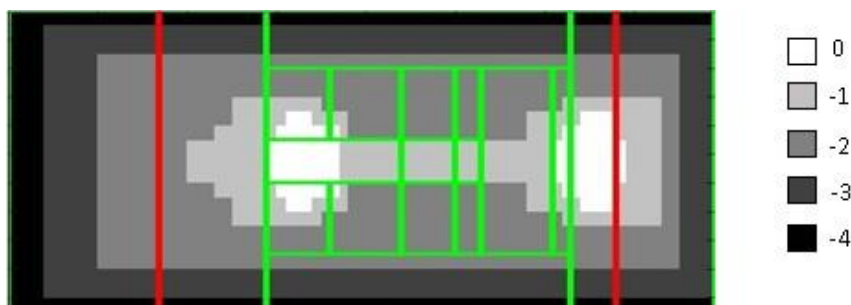


**Figure 2.8** Example of the application of a discretized map of probability of deformation to a vehicle member to the supermini segment.



It has to be noted that the integration of the battery pack into the vehicle can actively influence the map of deformation, nevertheless due to the reduced number of EVs, in comparison to ICE vehicles (see appendix B), an assessment is, so far, not possible.

## 2.5 Crash test simulations

A FEAs´campaign was selected as the method to test the effectiveness of the solutions.

Simulating common crash tests, the behaviour of the battery pack can be evaluated in term of safety for the battery pack itself and for the driver.

In order to cover the widest range possible of urban accidents, seven critical crash tests were selected (see appendix D):

- a frontal crash test against a rigid wall;
- two frontal crash tests against a deformable barrier with a 100% overlap;
- a frontal crash test against a deformable barrier with a 40% overlap;
- an oblique crash test against a moving deformable barrier;
- two pole crash tests.

The evaluation of the safety of the battery pack is then judged taking into consideration the deformations´ and stresses ´trends of the cells.

As the deformation can directly expresses the damage of the battery pack, its value has to be taken in consideration; however it is not possible to find in the literature a maximum value of cells ´deformation that can be accepted as limit, as usually these informations are part of the EV´ s producer´ s internal knowledge. [14]

It has to be stated that the damage of the battery pack or of a single cell is usually visually evaluated by experts trough the presence of exterior signs of damage or hazard (leakage, venting, fire,...). [1]

Models that predict the effective damage of a cell requires the cell to be modelled in all its components (housing, cover, internal jelly,...); in order to offer a fast advice, in this work, the cells are simulated macroscopically, without taking into consideration the effective internal structure of the battery itself and the different mechanical properties of the components.

This permits a fast modelling of the battery pack, nevertheless more accurate analyses are needed once the battery pack model is defined.

Moreover, as the analysis of the accelerations ‘pulses of the vehicle can provide indicative but important information about the safety of the occupants and possible improvements in the vehicle’s structure, this has been taken into consideration, providing the EV with two accelerometers and comparing the acceleration pulses to the original vehicle (see figure 2.9). [29]

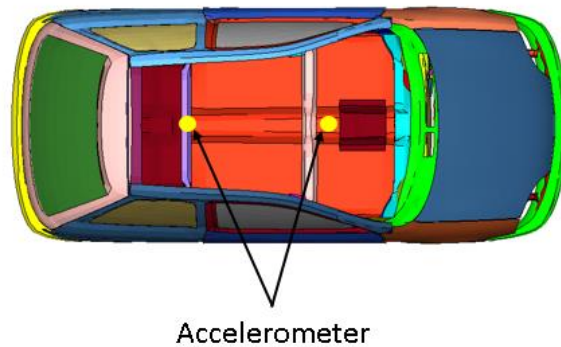


**Figure 2.9**      **Graphic explanation of the position of the accelerometers.**

## Chapter 3

### Evaluation parameters

As normally more than a single solution that satisfies the boundary conditions and the energy requirements is found, it is necessary to introduce the use of some evaluation parameters with the purpose of a fast identification of the most suitable battery pack's concept for the vehicle.

The parameters used consider both dynamic and safety factors. Although the algorithm provides an automatic selection of the best positions depending on the safety, this selection process is influenced by the boundary conditions, thus different boundary conditions lead to models with a diverse safety.

The dynamic parameters considered are (see also figure 3.1):

- the coordinates of the center of gravity of the entire vehicle after the integration of the battery pack;
- the variation of the inertia moments of the vehicle after the installation of the battery pack.

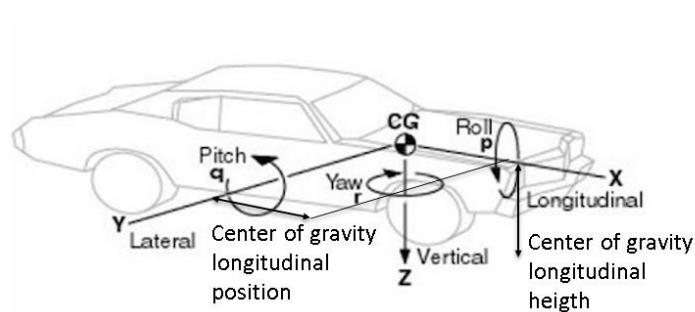


**Figure 3.1 Synthetic example of the inertia moments and coordinates of the center of gravity considered.**

Moreover, the safety of the battery pack is considered as evaluation parameter through the comparison to the map of probability of deformation described in chapter 2.4.

### 3.1 Center of gravity

The center of gravity is a geometric property of an object and it indicates the mean location of the mass of an object.

In dynamic, the center of gravity is commonly used, as it is possible to accurately describe the motion of an object just referring to the translation of its center of gravity.

Moreover, in automobile dynamic the center of gravity assumes still more importance as it strongly influences the behaviour of the vehicle. [30]

As usually the distance between the position of the center of gravity and the longitudinal symmetry plane of the vehicle is almost negligible, only two coordinates of the center of gravity are considered: the height and the longitudinal position.

#### 3.1.1 Center of gravity height

The height of the center of gravity influences heavily the dynamic behaviour of the vehicle; it is calculated measuring the distance between the center of gravity and the road plane as shown in figure 3.2.

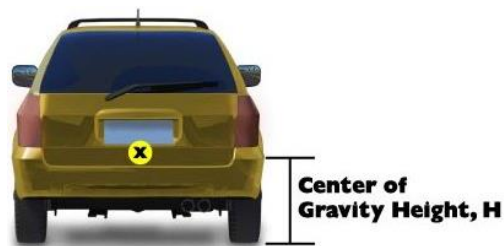


Figure 3.2 Example of the center of gravity height for a road vehicle.

The main effect of the center of gravity height regards the load transfer; in fact, as the height of the center of gravity increases, more load shifts from the front to the rear wheels while accelerating and vice versa while braking. Moreover, it has to be considered that the load acting on the wheels strongly affects the maximum available traction. Thus in sport and racing vehicles much attention is dedicated to the height of the center of gravity in order to maximize the handling and steering characteristics of the car. [31]

Nevertheless, lowering the center of gravity is not an easy task as the achievement of a standard of comfort for the vehicle's users imposes boundaries for the height of the entire vehicle. In order to avoid this problem lightweight materials are often used in the upper part of the car (usually the roof) with the goal of limiting the

center of gravity height. However, this solution leads unavoidably to an increase of the production costs as the material and manufacturing costs increase. [32]

Furthermore, it has to be noted that not just the pitch behaviour of the vehicle is influenced by the center of gravity height but also the roll one. In fact, acting just like previously exposed for the pitching, the load ratio between the wheels on opposite sides of the vehicle can vary, during a cornering, modifying the steering qualities of the car. [30]

The roll of the vehicle plays an important role, regarding not only the dynamic behaviour of the automobile but also the safety of the vehicle itself. [33]

In fact, for every object, when the projection of the center of gravity to the base falls outside the base itself, the object switches to an unstable position that leads to the rollover, as shown in figure 3.3.

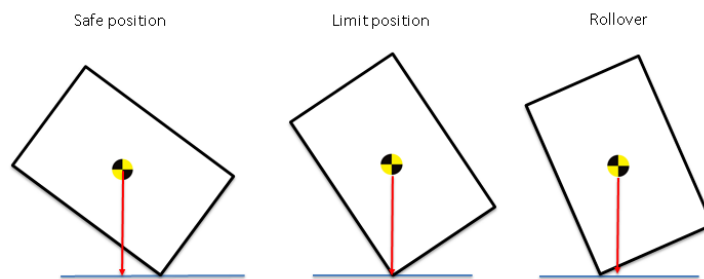


**Figure 3.3** Explication of the influence of the rollover for a simple object.

The same happens to an automobile when the center of gravity falls outside the wheelbase.

For this reason, it is defined by NHTSA a Static Stability Factor (SSF) defined as one half of the track width ( $t/2$ ) divided by the height of the center of gravity ( $h$ ) (equation 3.1). [33]

$$SSF = \frac{t/2}{h} \quad (3.1)$$

**Equation 3.1** Definition of the SSF.

Moreover the SSF can be also interpreted as "equal to the lateral acceleration in g's at which rollover begins in the most simplified rollover analysis of a vehicle represented by a rigid body without suspension movement or tire deflections" as shown in figure 3.4. [33]

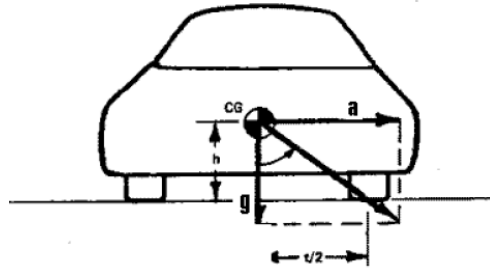


**Figure 3.4** Graphical explanation of the terms involved in the calculation of the SSF. [33]

It is then obvious that the deeper the SSF is, the stronger is the acceleration needed to cause the rollover of the automobile, thus a decrease of the center of gravity can be directly linked to a safer response against rollover.

The height of the center of gravity affects also another important parameter: the critical speed to produce rollover in an impact.

This is defined as the speed necessary to cause the rollover of the vehicle, when the vehicle, sliding sideways, hits an obstacle with both the wheels on the same side. [33]

This parameter does not take into account the use of active controls and/or the movement and deflections of tires and suspensions but permits an easy interpretation of the changes in the safety against rollover. [33]

The critical speed is defined in equation 3.2. [33]

$$v = \sqrt{2g * \sqrt{\left(\frac{t}{2}\right)^2 + h^2} - h} \quad (3.2)$$

**Equation 3.2** Definition of the critical speed for rollover. For the meanings of the terms of the equation see figure 3.4.

As the EV's battery pack can cover an important percentage of the total mass of the vehicle, its position and shape can actively influence, positively or negatively, the height of the center of gravity; thus the variation of this parameter, due to the introduction of the battery pack, is considered as evaluation factor.

### 3.1.2 Center of gravity longitudinal position

The longitudinal position of the center of gravity mainly influences the steady-state cornering behaviour of the vehicle, as well as the load distribution.

The characteristics of an automobile in this driving occasion are, of course, not only determined by the center of gravity but also from the tires' and suspensions' performance and settings.

It is possible to state that the less the distance between the center of gravity and the front axle is, the more the vehicle will show an understeering behaviour in steady state cornering and vice versa (see figure 3.5). [30]



**Figure 3.5** Example of an oversteering (left) and understeering (right) behaviour of a car. [30]

It is not possible to find in the state of art recommended longitudinal positions for the center of gravity, since the choice of this parameter depends from the desired behaviour of the vehicle, considering also the response of the tires and the suspensions. Moreover, the position of the center of gravity is often the result of a compromise between different design parameters.

Nevertheless is commonly accepted that a location of the center of gravity in the middle between the front and rear axle (also referred to 50/50 weight distribution) produces the preferred handling compromise. [34]

However, in case of sport and racing vehicles, a 50/50 weight distribution does not provide a satisfying behaviour, due to a tendency of understeering in the initial corner entry. Therefore, in these cases, a more rearward weight distribution is preferred in order to improve the performance in a sport driving situation, leading to a 45/55 or 40/60 weight distribution. [34]

The evaluation of the battery pack through the longitudinal position of the center of gravity is then judged by the distance between the center of gravity of the vehicle with the battery pack and the desired position of center of gravity, defined by the user.

## 3.2 Rotational inertia moment of the vehicle

Considering the dynamic of the vehicle, three rotational inertia moments assume particular importance: the yaw, the pitch and the roll of the vehicle (figure 3.6).

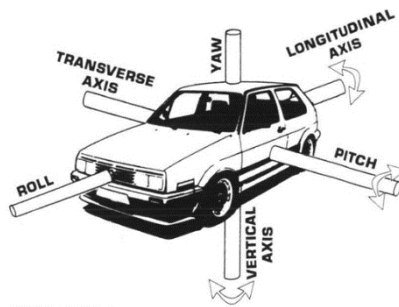


Figure 3.6- Graphic explanation of the three main inertia moments of car. [30]

These inertia moments influence the handling and the response of the vehicle and so, indirectly, its performance and comfort, thus they deserve particular attention. It has to be noted that in steady state cornering the inertia moments have no influence, but they affect the behaviour of the vehicle in every occasion that implies a variation of the direction of the movement. [30]

### 3.2.1 Yaw inertia moment

When considering the safety of the vehicle the yaw inertia is, surely, an important parameter because it represents the most sollicitated rotational axis of the vehicle. The yaw inertia is responsible for the time needed by the vehicle to redistribute the lateral forces on the wheels when entering a corner or in case of a change of the curvature of the turn. [35]

It is then easy to understand that, in case of need of an emergency manoeuvre in order to avoid an obstacle, the yaw inertia can play an important role as it conditions the ease of changing direction.

It is possible to conclude that reduced yaw inertia leads to more agile vehicles, with increased handling. [35]

For these reasons, it is considered important to limit the increase of the yaw inertia due to the application of the battery pack, therefore the battery pack models are also evaluated depending by the increase of the yaw inertia of the entire vehicle produced by the integration of the cells.



### 3.2.2 Roll inertia moment

The roll inertia is responsible for the load transfer between wheels on opposite sides of the automobile when changing the direction of motion.

The comfort of the passengers can be strongly influenced by the roll inertia, as a higher inertia moment around this axis leads to a longer time for the vehicle to settle down and follow the steering. During this time, the distribution of the loads between the wheels of different sides of the car is unequal and can lead to losses of traction. [36]

This behaviour is particularly important in sport and racing cars, nevertheless in passenger cars this parameter has to be taken into consideration too.

Although the influence of the roll inertia for a safe behaviour of the vehicle is not as important as the yaw inertia, this parameter will be anyway taken into account in the evaluation of the battery packs.

### 3.2.3 Pitch inertia moment

The pitch inertia has no direct influence in the safety of the vehicle but it strongly influences the behaviour and the loads acting on the suspensions as well as the comfort of the passengers. [36]

In fact, the suspensions have to be correctly set in order to reduce the oscillations around the pitch axis.

It has also to be noted that the pitch inertia influences the response of the vehicle in case of periodic undulations of the road surface.

Therefore the change of the pitch inertia of the vehicle due to the application of the battery pack is taken into consideration.

## 3.3 Safety

As the development of a safe battery pack is one of the main topics of the thesis, the safety is an important parameter of evaluation.

As in the current state of art it is not available a method for the evaluation of the safety of a battery pack based upon its position before its simulations in real crashes or crash tests, a statistical method depending on the probability of deformation of every zone of the vehicle is used, as exposed in chapter 2.3.

As the boundary conditions influence the position of the cells inside the vehicle, every model of battery pack is analysed through the map of probability of deformations exposed in chapter 2.3.

In particular, every model of battery pack is compared to the previously exposed map and the sum of the probability of deformation of every zone occupied by a

cell of the battery pack leads to the possibility of an estimation of an overall safety score of the battery pack(see figure 3.7).

This safety score has a range from 0 (that indicates that the cells are set only where the probability of deformation is 0) to a minimum that is dependent by the number of cells and their position.

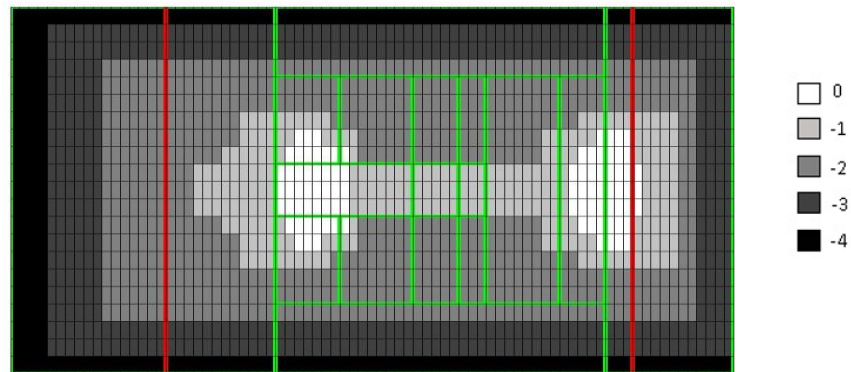


**Figure 3.7** Example of the map of probability of deformation discretized with the division in zones applied to a vehicle of the supermini class.

## Chapter 4

### Application of the methodology

In order to ensure the validity of the methodology, it is necessary to demonstrate its application in the most different types of vehicles as possible and to test the crashworthiness of the results.

Nevertheless, as this work focuses on vehicles intended for the use in urban scenarios, the attention is pointed primarily in car's types that appear most frequently in that environment.

The Geo Metro model R3 was analysed as representative of a wide number of vehicles currently on the market and as a validated Finite Element model is available. [37]

The results of the application of the methodology to different type of vehicles can be found in appendix F.

Moreover, the methodology was applied to the selected vehicle using cells and modules with different characteristics with the aim of analysing the impact of the energy source's dimensions in the battery pack design.

As the evaluation parameters influence the judgment of the most adequate models for the integration into the vehicle, a sensitivity analysis has been developed in order to identify the effects of different weighting value in the shape of the battery pack models.

#### 4.1 Description of the vehicle model

The Geo metro was a variation of the Suzuki Cultus available in North America from 1989 to 2001; it was available in two main version: a 3 door hatchback and a 4 door sedan. [38]

As representative of many vehicles that belong to the supermini segment (see appendix A) the 3 door hatchback version was selected for the analysis.

The main characteristics of the vehicle, retrieved from the FE model, are shown in table 4.1.

### Geo Metro main characteristics

<b>Total vehicle length</b>	3750 mm
<b>Total vehicle width</b>	1580 mm
<b>Front bumper to front axle distance</b>	805 mm
<b>Track width</b>	2370 mm
<b>Rear bumper to rear axle distance</b>	575 mm
<b>Number of seats</b>	5
<b>Center of gravity distance from front axle</b>	802 mm
<b>Center of gravity height</b>	511 mm
<b>Roll inertia</b>	$2.853 \cdot 10^8 \text{ kg} \cdot \text{mm}^2$
<b>Yaw inertia</b>	$1.361 \cdot 10^9 \text{ kg} \cdot \text{mm}^2$
<b>Pitch inertia</b>	$1.193 \cdot 10^9 \text{ kg} \cdot \text{mm}^2$
<b>Total mass</b>	926 kg

**Table 4.1** Main characteristics of the Geo Metro R3 model.

Moreover, in figure 4.1 it is shown a comparison between the Geo Metro and the model used.



**Figure 4.1** Comparison between the Geo Metro (left) [38] and the FE model of the vehicle (right) [37].

As the vehicle is designed for the use in an urban environment an autonomy range of 100 km was selected; applying the parameters of the vehicle to equation 2.1 (see chapter 2.1) a total energy of the battery pack equal to 15 kWh was estimated, in order to satisfy the autonomy requirements.

## 4.2 Description of the cells considered

A wide range of cells ‘types is currently available in the market and the selection process of the most suitable cell has to consider the electric and chemical characteristics of the cells, as well as the mechanical properties and the economic factors. A detailed description of the currently most used cells for EVs is available in appendix B.

In order to ensure the application of the methodology independently by the batteries ‘dimensions, three cells, representative of three frequent cells ‘type, have been selected: a cylindrical cell, a prismatic cell and a pouch cell.

Moreover, the methodology was tested considering the application of entire modules, with the purpose of checking the differences in the battery pack shapes depending on the dimensions of the source of energy used.

### 4.2.1 Cylindrical cells

Cylindrical cells are a common choice for the propulsion of EVs thanks to their good thermal performances, an elevated mechanical stability and the possibility to lead to a good space utilisation (see appendix B for details). [39]

As representative of the cylindrical cells, the 18650 model manufactured by Panasonic (figure 4.2) was taken as reference thanks to the wide availability of electric characteristics, reported in table 4.2. [40]



Figure 4.2 Picture of the cylindrical cell considered: the Panasonic NCR 18650A.  
**Panasonic NCR 18650 A**

<b>Height</b>	65.2 mm
<b>Diameter</b>	18.6 mm
<b>Nominal voltage</b>	3.7 V
<b>Nominal capacity (minimal)</b>	2700 mAh
<b>Nominal capacity (typical)</b>	2950 mAh
<b>Mass</b>	45 g
<b>Mass energy density</b>	238 Wh/kg
<b>Volumetric energy density</b>	151.3 Wh/l
<b>Energy pro cell</b>	10.7 Wh

Table 4.2 Resuming table of the main features of the Panasonic NCR18650A cell.

In order to provide the needed energy, 1440 cells are required, moreover a configuration of 80s18p was selected providing a total tension of 296 Volt and an energy equal to 15451 Wh.

Applying the procedure exposed in chapter 2.2, an estimation of the total weight and volume of the battery pack is possible, after the decision of the distance between the cells. A resuming view of the battery pack's parameters used is proposed in table 4.3.

### Battery pack using the Panasonic NCR 18650 A cells

<b>Number of cells</b>	1440
<b>Configuration</b>	80s16p
<b>Output tension</b>	296 V
<b>Energy</b>	15451 Wh
<b>Distance between the cells in height direction</b>	0,8 mm
<b>Distance between the cells in length direction</b>	1,4 mm
<b>Distance between the cells in width direction</b>	1,4 mm
<b>Cells' mass</b>	64.8 kg
<b>Housing's mass</b>	32.4 kg
<b>Other components' mass</b>	10.8 kg
<b>Total mass of the battery pack</b>	108 kg
<b>Total volume of the battery pack</b>	38.016 l

**Table 4.3** Resuming table of the main features of battery pack modelled using the Panasonic NCR 18650A cell.

It was not possible to find in the current state of art a module manufactured using the previously exposed cells, nevertheless Panasonic provided a module concept that was used as reference (see figure 4.3). [41]



**Figure 4.3** 3D model of the module, using the cylindrical cell Panasonic NCR 18650A, taken as reference.

The main characteristics of the concept module are proposed in table 4.4.

#### **Panasonic concept module**

<b>Height</b>	100 mm
<b>Length</b>	430 mm
<b>Width</b>	150 mm
<b>Nominal voltage</b>	25.2 V
<b>Nominal capacity</b>	58 Ah
<b>Weight</b>	8 kg
<b>Mass energy density</b>	177 Wh/kg
<b>Volumetric energy density</b>	430 Wh/l
<b>Energy per module</b>	1412 Wh
<b>Number of cells</b>	140 cells
<b>Configuration</b>	7s20p

**Table 4.4** Resuming table of the main features of the concept module by Panasonic.

Applying the same energy requirements previously exposed, a battery pack composed by the Panasonic concept modules presents the characteristics shown in table 4.5.

#### **Battery pack using the Panasonic concept module**

<b>Number of modules</b>	11
<b>Modules' configuration</b>	11s1p
<b>Output tension</b>	277,2 V
<b>Energy</b>	16077 Wh
<b>Cells' mass</b>	69.3kg
<b>Housing's mass</b>	32.4
<b>Other components' mass</b>	10.8
<b>Total mass of the battery pack</b>	113 kg
<b>Total volume of the battery pack</b>	36 l

**Table 4.5** Resuming table of the main features of the battery pack modelled with the concept Panasonic modules.

### 4.2.2 Prismatic cells

Prismatic cells offer the best thermal performances among the cells considered thanks to their shape, moreover they have the advantage of a high energy density and an acceptable mechanical stability (see appendix B for details). [39]

The Boston Power Swing 5300, shown in figure 4.4, is taken as reference for this type of cells; the characteristics of the cell are exposed in table 4.6. [42]



**Figure 4.4** Photo of a Boston Power Swing 5300 cell.

#### Boston Power Swing 5300

<b>Height</b>	64.8 mm
<b>Length</b>	37.3 mm
<b>Width</b>	19.2 mm
<b>Nominal voltage</b>	3.7 V
<b>Nominal capacity (typical)</b>	5300 mAh
<b>Mass</b>	94 g
<b>Mass energy density</b>	207 Wh/kg
<b>Volumetric energy density</b>	407 Wh/l
<b>Energy per cell</b>	19.3 Wh

**Table 4.6** Resuming table of the characteristics of the Boston Power Swing 5300 cell.

The energy requirements are satisfied using 800 cells in a configuration 80s10p. The characteristics of the battery pack model based on the Boston Power Swing 5300 cells are presented in table 4.7.



### Battery pack using the Boston Power Swing 5300 cells

<b>Number of cells</b>	800
<b>Configuration</b>	80s10p
<b>Output tension</b>	296 V
<b>Energy</b>	15688 Wh
<b>Distance between the cells in height direction</b>	10.2 mm
<b>Distance between the cells in length direction</b>	9.7 mm
<b>Distance between the cells in width direction</b>	0.8 mm
<b>Cells' mass</b>	74.8 kg
<b>Housing's mass</b>	37.4 kg
<b>Other components' mass</b>	12.4 kg
<b>Total mass of the battery pack</b>	124.6 kg
<b>Total volume of the battery pack</b>	56,4 l

**Table 4.7** Resuming table of the characteristics of the battery pack modelled with the Boston Power Swing 5300 cells.

As the producer offers also the possibility to utilize already build modules for the direct implementation into EVs, the Boston Power Swing Key 442 was taken as reference (figure 4.5). The characteristics of the module are resumed in table 4.8. [43]



**Figure 4.5** Photo of the Boston Power Swing Key 442 module.

### Boston Power Swing Key 442 module

<b>Height</b>	40 mm
<b>Length</b>	185 mm
<b>Width</b>	70 mm
<b>Nominal voltage</b>	3.7 V
<b>Nominal capacity</b>	42 Ah
<b>Mass</b>	0.9 kg
<b>Mass energy density</b>	170 Wh/kg
<b>Volumetric energy density</b>	300 Wh/l
<b>Energy pro module</b>	155 Wh
<b>Number of cells</b>	8
<b>Configuration</b>	1s8p

**Table 4.8** Resuming table of the features of the Boston Power Swing Key442 modules.

The energy requirements are met with a battery pack as presented in table 4.9.

### Battery pack using the Boston Power Swing Key 442 modules

<b>Number of modules</b>	96
<b>Modules' configuration</b>	96s1p
<b>Output tension</b>	355.2 V
<b>Energy</b>	14918 Wh
<b>Cells' mass</b>	72.2kg
<b>Housing's mass</b>	35.2 kg
<b>Other components' mass</b>	10 kg
<b>Total mass of the battery pack</b>	117.4 kg
<b>Total volume of the battery pack</b>	49.7 l

**Table 4.9** Resuming table of the features of the battery pack based on the Boston Power Swing 442 modules.

### 4.2.3 Pouch cells

Pouch cells differ from the other two types of cells considered, as they do not present a rigid case, due to the sensible volume variation, to which the cells are subjected during the charging and discharging cycle.

For this reason they exhibit the worst mechanical stability between the cells considered, nevertheless their particular shape offers the advantage of the achievement of a high energy density and, at the same time, acceptable thermal performances. [39]

The Kokam Series 255 75Ah cell (figure 4.6) has been considered as reference for the pouch cells; its features are resumed in table 4.10. [44]



**Figure 4.6** Photo of the Kokam Series 255 75 Ah pouch cell.

### Kokam Series 255 75 Ah

<b>Height</b>	268 mm
<b>Length</b>	265 mm
<b>Width</b>	12 mm
<b>Nominal voltage</b>	3.7 V
<b>Nominal capacity (typical)</b>	7500 mAh
<b>Mass</b>	1630 g
<b>Mass energy density</b>	170 Wh/kg
<b>Volumetric energy density</b>	325.6 Wh/l
<b>Energy per cell</b>	277.5 Wh

**Table 4.10** Resuming table of the features of the Kokam Series 255 75Ah pouch cell.

Thanks to the high energy available per cell, the battery pack consists only on 57 cells with a disposition of 57s1p. The features of such a battery pack are exposed in table 4.11.

### Battery pack using the Kokam Series 255 75 Ah cells

<b>Number of cells</b>	57
<b>Configuration</b>	57s1p
<b>Output tension</b>	210.9 V
<b>Energy</b>	15817 Wh
<b>Distance between the cells in height direction</b>	2 mm
<b>Distance between the cells in length direction</b>	5 mm
<b>Distance between the cells in width direction</b>	10 mm
<b>Cells' mass</b>	92.9 kg
<b>Housing's mass</b>	46.4 kg
<b>Other components' mass</b>	15.4 kg
<b>Total mass of the battery pack</b>	154.7 kg
<b>Total volume of the battery pack</b>	91.6 l

**Table 4.11** Resuming table of the features of the battery pack modelled with the Kokam Series 255 75Ah pouch cells.

It is worth noting the low value of the total tension provided by this battery pack in comparison to the others presented. This can lead to a difficult selection and operation of the electric motor, nevertheless, due to the considerable variation in the total energy that other solutions provide, it was taken as reference for the further analyses for this cells 'type.

As the cell producer manufactures also complete modules the Kokam KBM 255 75 Ah (figure 4.7) has been taken as reference; the main characteristics of the module are proposed in table 4.12. [45]



**Figure 4.7** Photo of the Kokam KBM 255 75 Ah module.

#### **Kokam KBM 255 75 Ah module**

<b>Height</b>	145.4 mm
<b>Length</b>	305 mm
<b>Width</b>	308.4 mm
<b>Nominal voltage</b>	29.6 V
<b>Nominal capacity</b>	75 Ah
<b>Mass</b>	19.7 kg
<b>Mass energy density</b>	133 Wh/kg
<b>Volumetric energy density</b>	162 Wh/l
<b>Energy per module</b>	2220 Wh
<b>Number of cells</b>	8
<b>Configuration</b>	8s1p

**Table 4.12** Resuming table of the features of Kokam KBM 255 75 Ah module.

The features of a battery pack using such a module are presented in table 4.13.

#### **Battery pack using the Kokam KBM 255 75 Ah modules**

<b>Number of modules</b>	7
<b>Modules' configuration</b>	7s1p
<b>Output tension</b>	207.2 V
<b>Energy</b>	15540 Wh
<b>Cells' mass</b>	91.3 kg
<b>Housing's mass</b>	46 kg
<b>Other components' mass</b>	15.1 kg
<b>Total mass of the battery pack</b>	152.1 kg
<b>Total volume of the battery pack</b>	96 l

**Table 4.13** Resuming table of the features of battery pack designed with the Kokam KBM 255 75 Ah module.

### 4.3 Description of the analysis

#### 4.3.1 Boundary conditions

In order to provide the possibility of a comparison between the results achieved with different cells and modules, the analysis was developed without changing the boundary conditions.

As this methodology aims to help the designer in the concept phase, an automatic variation of the boundary conditions was provided in order to analyse a wide range of possible solutions.

The zones that define the boundary conditions are exposed in figure 4.8.

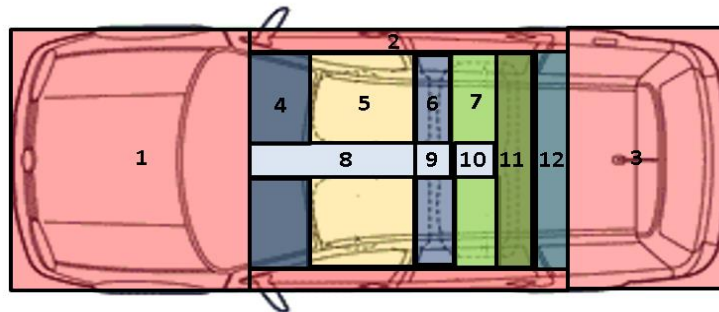


**Figure 4.8** Graphic explanation of the division in boundary zones of the vehicle.

The boundary conditions were automatically varied using three different values, which were chosen in the same range of the safety values (see chapter 2.4) in order not to overrate the design boundary conditions:

- 0, indicating a desirable position for the integration of the cells;
- -2, indicating a less preferred position for the integration of the cells,
- -4, indicating an undesired position for the integration of the cells.

It has also to be noted that 6 zones present a constant value:

- the bonnet: this zone was avoided for the integration of the batteries, thus its value was posed equal to -20 with the purpose of eliminate the possibility of the placement of the cells in this area;
- the trunk, as for the bonnet the use of this zone was avoided for the positioning of the cells, thus its value was set equal to -20;
- the side external frame: in order to improve the safety of the battery pack, the use of the space of the side external frame, plus a “safety zone” of 100 mm, was averted and its value was posed equal to -20;
- the tunnel and the central zone between the rear seats: in order to avoid the possibility to have a separated battery pack that increases the costs due

to the need of two battery management systems (BMS) and as these zones always exhibit the presence of cells, their values were set to 0.

Thus, a possible number of 729 different combinations of the boundary conditions for every cells` and modules` type was analysed; an example is proposed in figure 4.9.

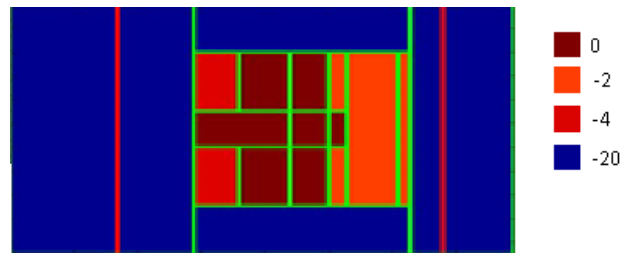


**Figure 4.9** Example of the division of the vehicle in zone and the application of the boundary conditions` values.

Moreover, with the purpose of investigating the influence of the maximum height available for the cells, for the shape and the safety of the battery pack, three different height limits were set:

- 340 mm from the ground, this is 40 mm higher than the lower part of the frame and this height was selected in order to provide the possibility to include a floor pan integration in the results;
- 390 mm from the ground, this is the height of the front seats for the vehicle selected;
- 440 mm from the ground, as it is the distance from the ground of the beginning of the rear seats.

Furthermore, as the mechanical deformation of the cells is not independent by the direction of the force applied, three main orientations for the cells were tested, aligning the biggest dimension of the cells in direction of the X, Y and Z axis of the vehicle.

As the algorithm stops when the desired number of cells is achieved, the starting side influences the results as it leads to different battery pack models. For this reason, for every combination of boundary conditions, cells `orientation and maximum height available, two different models are created: one searching for the best positions from the bonnet side and one scanning in the opposite direction.

This leads to the analysis of 13122 different models for every simulation (see table 4.14).

### Characteristics of the analysis

<b>Possible values per zone</b>	3 ( 0 -2 -4)
<b>Zones with variation of the values</b>	6
<b>Zones with fixed parameters</b>	6
<b>Total number of possible combinations of the boundary conditions</b>	729
<b>Maximum heights available</b>	3 (340 mm, 390 mm 440 mm)
<b>Different orientations of the cells</b>	3
<b>Different directions of position selection</b>	2
<b>Total number of models</b>	13122

**Table 4.14** Resuming table of the characteristics of the analysis.

### 4.3.2 Evaluation parameters

As discussed in chapter 3 not all the dynamic parameters have the same importance regarding the handling and the safety of the vehicle. Nevertheless, it is not possible to find in the literature values that permit to define the relevance of the parameters.

For this reason a sensitivity analysis was developed, with the aim to search a possible ratio between the parameters that both reflects the real importance of the parameters and permits an adequate evaluation of the models.

The models were analysed with different weighting values; in every case a single weighting value was set equal to 10 while the others were kept constant and equal to 1 in order to identify the variations in the classification, which is calculated as the sum of the normalized scores in the six different evaluation parameters divided by the sum of the weights of the parameters (see table 4.15).

### Sensitivity analysis's scenarios

<b>Scenario</b>	<b>X CoG value</b>	<b>Z CoG value</b>	<b>I<sub>zz</sub> value</b>	<b>I<sub>yy</sub> value</b>	<b>I<sub>xx</sub> value</b>	<b>Safety value</b>
<b>1</b>	1	1	1	1	1	1
<b>2</b>	10	1	1	1	1	1
<b>3</b>	1	10	1	1	1	1
<b>4</b>	1	1	10	1	1	1
<b>5</b>	1	1	1	10	1	1
<b>6</b>	1	1	1	1	10	1
<b>7</b>	1	1	1	1	1	10

**Table 4.15** Resuming table of the scenarios analysed.

The results in the different scenarios have then been compared using the first scenario as baseline.

The following considerations take the analysis developed with the Boston Power 5300 cells as example, however similar results have been found for all the cells` and modules` types considered.

In figure 4.10 is exposed the absolute average value of the variation of the total score of a model in comparison to the baseline scenario.

From the analysis, it was shown that the weighting values of the coordinates of the center of gravity have the biggest influence in the variation of the total score of a model (about 25% and 41% respectively for the x and z coordinate, so respectively the second and third scenario). The motivation is that searching for a model that satisfy this characteristics leads to particular battery pack shapes that heavily differ from the majority.

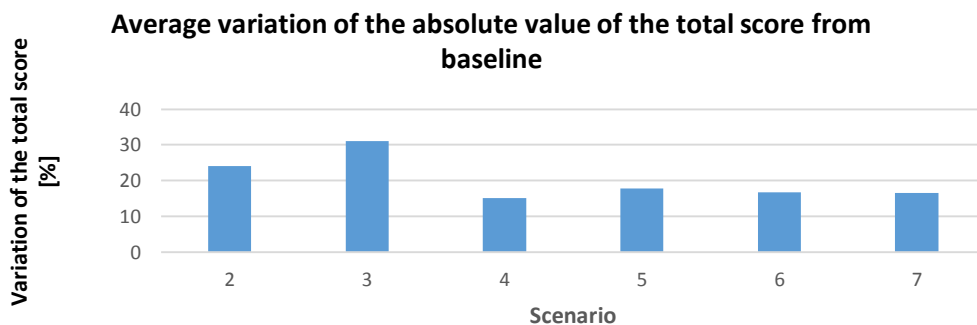


**Figure 4.10** Graphical comparison of the average variation of the score of the models from the baseline scenario.

As example in figure 4.11 the best model for the first, second and third scenarios are exposed.

If the main goal is the achievement of the desired weight distribution the result is a battery pack that expands in the rear part of the vehicle, instead, if the z coordinate of the center of gravity is the goal, the battery pack will be limited in the height, with respect to the boundary conditions. Nevertheless, it has to be noted that these results can only be applied to the vehicle considered, as different goal coordinates for the center of gravity lead inevitably to different battery pack shapes.

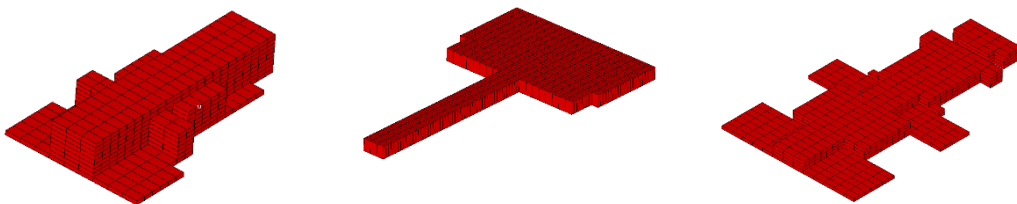


**Figure 4.11** 3D models of the best configuration from the battery pack in the first (left), second (middle) and third (right) scenario.

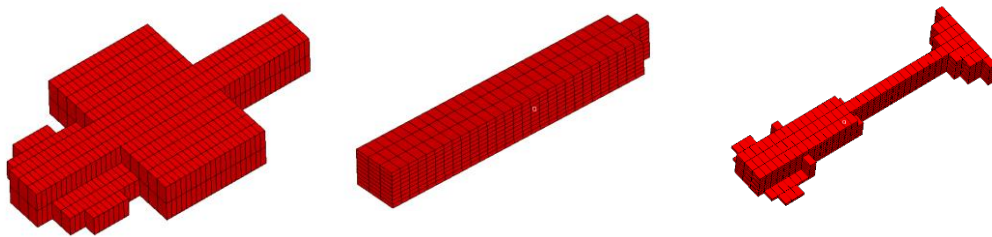


The influence of the other 4 weighting values is reduced in comparison to the first two analysed, as shown also in figure 4.9.

This can be explained analysing the best models for these scenarios, shown in figure 4.12.

The best models for these four scenarios exhibit the common and almost exclusive use of a zone of the vehicle: the tunnel; in fact the battery pack is almost completely set in this zone, if that is possible to respect with the boundary conditions.

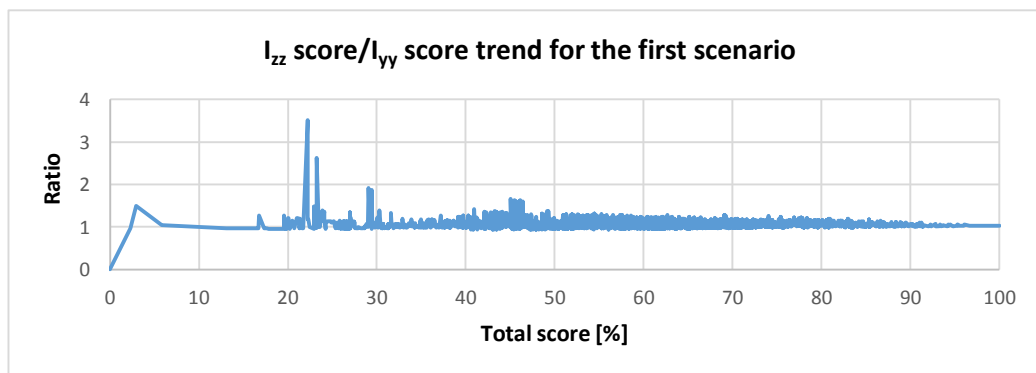
That proves the similar influence of the weighting values of the roll, pitch, yaw inertias and safety, in fact they all lead to a design with a common shape.



**Figure 4.12** 3D models of the best configuration from the battery pack in the fourth and fifth (left), sixth (middle) and seventh (right) scenario.

It is worth noting that the best shape found for the battery pack focusing on the  $I_{zz}$  and  $I_{yy}$  inertias is exactly the same, moreover the same effect is found for different models with the same score.

That can be explained observing the trend of the ratio between the  $I_{zz}$  and  $I_{yy}$  score in different scenarios (see figure 4.13).



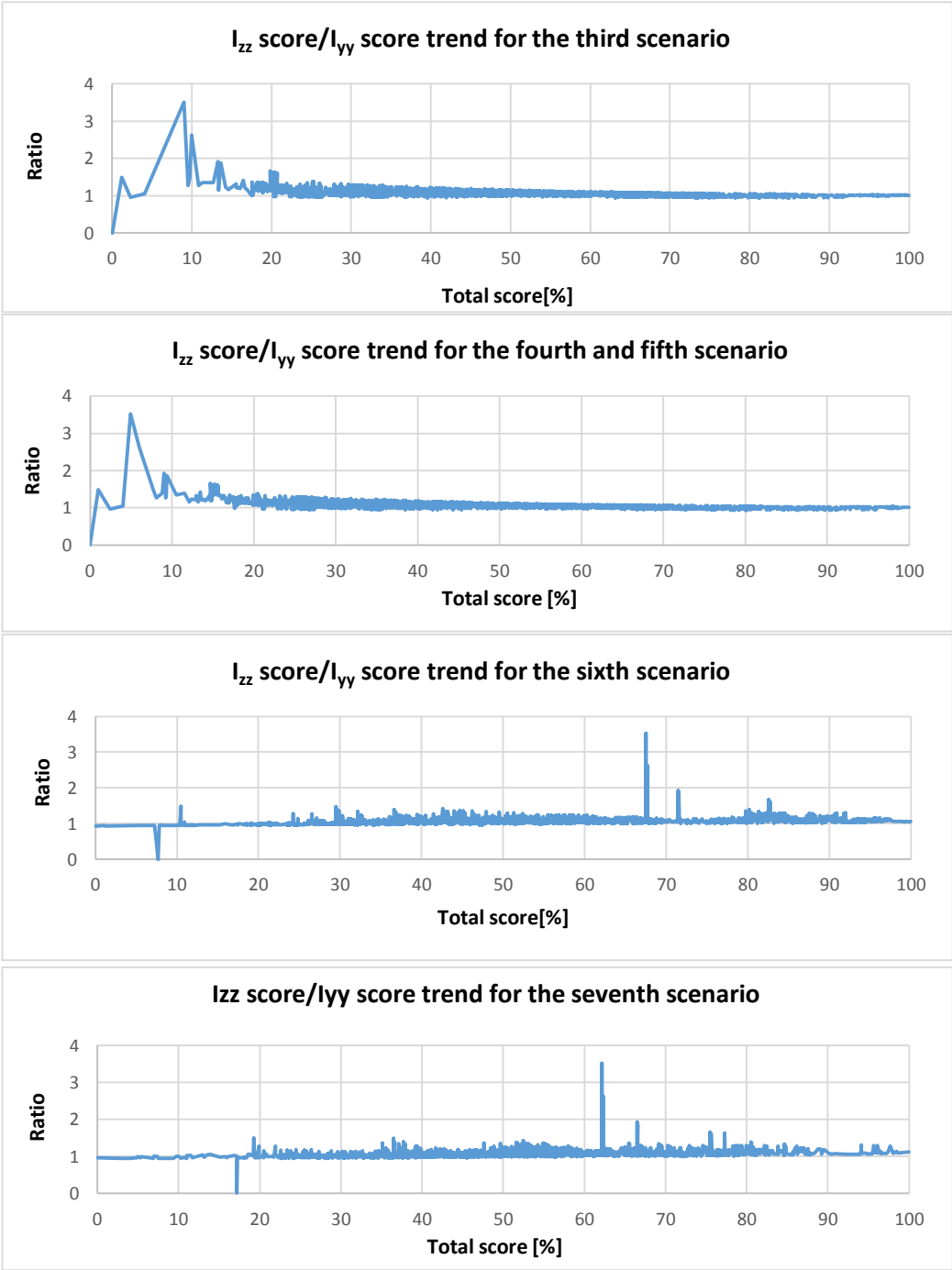
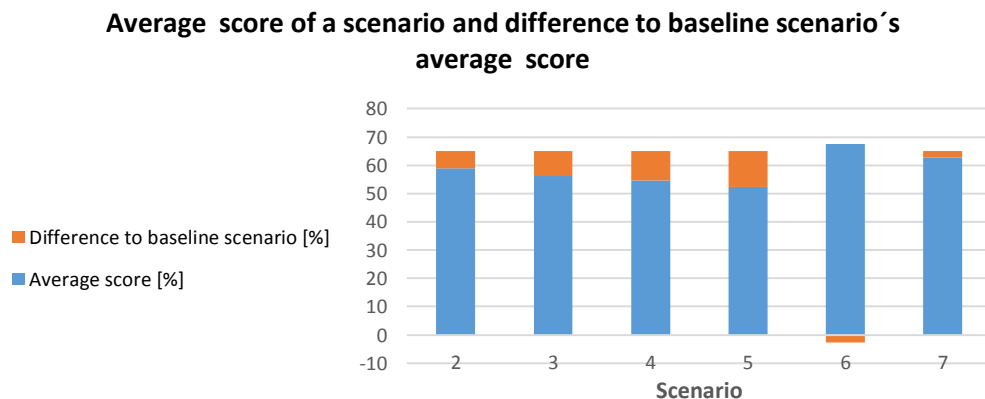


Figure 4.13 Trends of the ratio between  $I_{zz}$  and  $I_{yy}$  for five scenarios.

It is then possible to conclude that the ratio between the normalized score of the  $I_{zz}$  inertia and whose of the  $I_{yy}$  inertia is near to the value of 1 for the majority of the models in all the scenarios that do not weight the center of gravity more than the other parameters. Therefore it can be understood why the weighting the  $I_{zz}$  or  $I_{yy}$  inertia do not lead to a wide variation in the shape of the best battery packs. Therefore is possible to analyse the variations in the average score of the designs in the different scenarios (see figure 4.3).

The models were compared to the baseline scenario and the average score of the models was analysed and compared to the average score of the baseline scenario. In the baseline scenario the average score of the models was 65 %, indicating that the majority of the models presents a good compatibility to the requirements if no particular weighting is applied.

The second and the third scenarios, representing respectively the increase of the weight of the x and z coordinate of the center of gravity, present a reduced variation of the average score, respectively about 5% and 8 %, nevertheless the absolute value of the variation in comparison to the baseline scenario is respectively almost 25% and 31% ( figure 4.14) .



**Figure 4.14** Graphical comparison between the average scores in the different scenarios and the difference to the baseline scenario.

This can be explained observing figure 4.15, showing the total score of the models in the second scenario and the difference of the total score for the same model in the baseline scenario.

It can be observed that the use of a strong weighting value for the x coordinate of the center of gravity leads to a wide difference compared to the baseline scenario. In particular, the best models for the baseline scenario become the worst in the second scenario and vice versa. This “mirroring” effect explains the great difference between the mean of the absolute value of the difference and the simple mean of the difference.

**Total score comparison between the second and the baseline scenario**

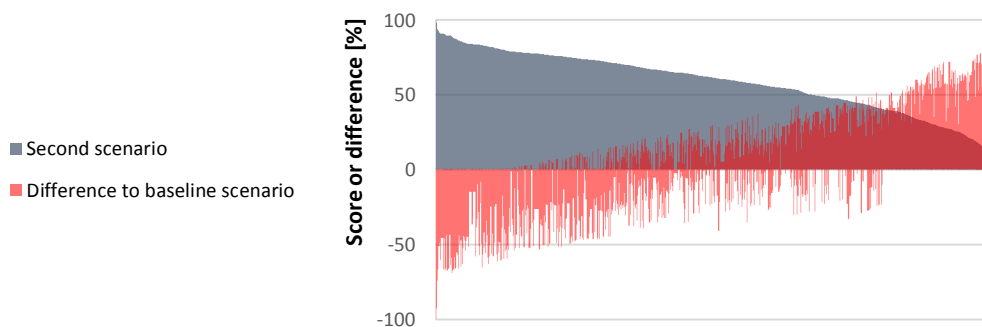


**Figure 4.15** Graphical comparison between the scores of the models in the second scenario and the difference to the baseline scenario.

Similar trends at the extremes can be found also for the Z coordinate of the center of gravity (figure 4.16).

**Total score comparison between the third and the baseline scenario**

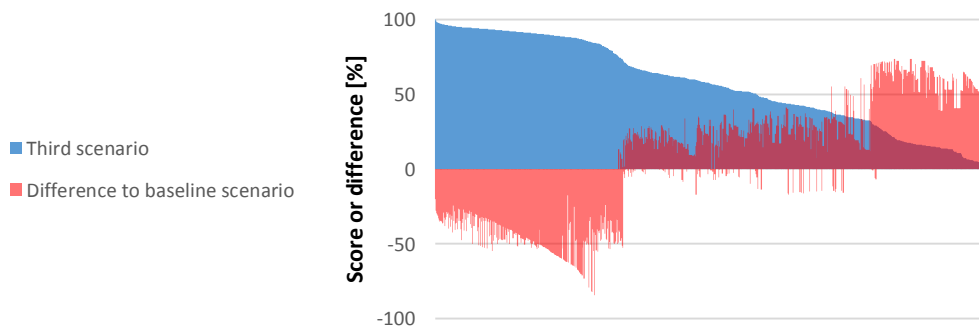


**Figure 4.16** Graphical comparison between the score of the models in the third scenario and the difference to the baseline scenario.

Moreover, it is worth observing the similar but opposite influence that the weighting of the  $I_{xx}$  and safety parameter has in the results.

In particular, increasing the weight for the  $I_{xx}$  score leads to an increase of the average score of the models. This can be explained observing that, due to the boundary conditions and the safety, all the model have in common the use of the tunnel zone. As this zone is exactly in the middle of the automobile, it limits the increase of the roll inertia of the vehicle and permits the model to achieve a good score if evaluated by the  $I_{xx}$  inertia.

Moreover, the reduced influence of the weighting of the safety score in the comparison to the baseline scenario can be explained observing that also in this last scenario the best overall models already exhibit a good safety score. In fact, as shown in figure 4.17, the normalized safety score for the baseline scenario exhibits an average value of 0,68 for a variation of the 16 % of the total score of the models

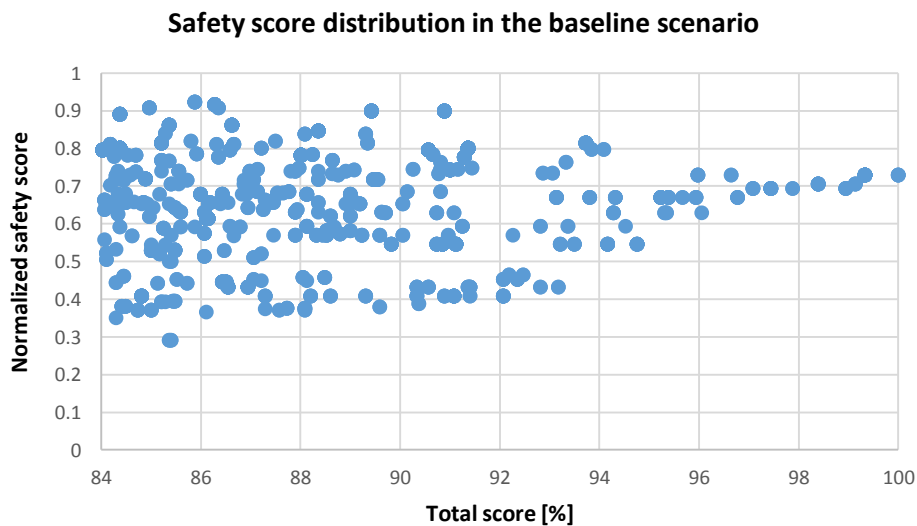


**Figure 4.17** Graphical comparison of the safety score with a variation of 16% of the total score in the baseline scenario

### 4.3.3 Conclusion

From the analysis of the results based upon different scenarios it was possible to observe the influence of the weight of the factors in the battery pack shape. Although it not possible to provide a ratio between the importance of the various parameters, it can be stated that focusing the attention strictly on the coordinate of the center of gravity leads to the design of battery packs that exhibits poor results if evaluated also by the other factors.

## CHAPTER 5

### Results and discussion

Thanks to the wide range of battery pack's designs provided by the application of the methodology, as described in the previous chapter, it is possible to analyse the influence of the cells' dimension in the battery pack's shape.

Before that, it is worth exposing the results of the methodology for the different analyses developed.

For every cell and module analysed a summary table with the main characteristics and the influence of the battery pack in the inertia moments and center of gravity of the vehicle is presented.

It is worth mentioning that in order to obtain an "overall score" of the battery pack design every characteristic of the battery pack has been normalized from 1 to 0 where 1 represents the value of the best model and 0 the value of the worst model for the desired characteristic.

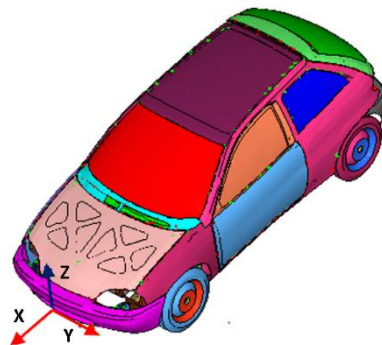
The sum of the normalized score for the 6 evaluation parameters exposed in chapter 3 permits the calculation of an overall score of the design.

Moreover is possible to evaluate a "percentage score", observing the highest and the lowest value of the total score for every analysis developed and normalizing it from 100% to 0%, where 100% represents the best model and 0% the worst.

The lists proposed have been calculated using the first evaluation parameter scenario exposed in chapter 4.3.2.

Moreover in order to understand the results in figure 5.1 the coordinate system used is exposed.

It is worth observing that in the results the coordinates of the center of gravity of the entire EV after the integration of the battery pack are presented, while the inertia moments refers to the battery pack only.

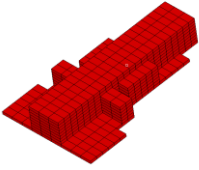
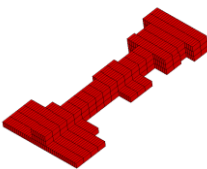
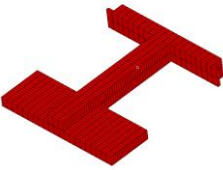
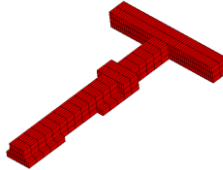



**Figure 5.1** Graphic explanation of the coordinate system used.

## 5.1 Designs using the Boston Power Swing 5300 cells

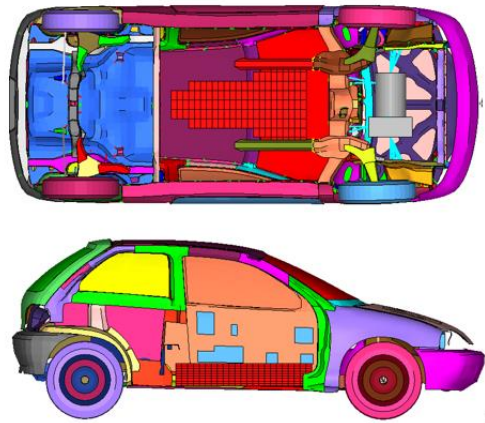
In this paragraph the results of the analysis developed with the Boston Power 5300 cells are exposed. The characteristics of the cell and of the entire battery pack are described in chapter 4.2.2.

The analysis provided 13122 designs of battery packs; here some representative examples are shown in order to simplify the further analysis (see table 5.1).

<b>Total Score</b>	<b>Score [%]</b>	<b>X Cog [mm]</b>	<b>Z Cog [mm]</b>	
0.649	100	-1808	501.6	
<b>I<sub>zz</sub> [kg*mm<sup>2</sup>]</b>	<b>I<sub>yy</sub> [kg*mm<sup>2</sup>]</b>	<b>I<sub>xx</sub> [kg*mm<sup>2</sup>]</b>	<b>Safety score</b>	
1.38e7	1.57e7	4.95e6	-635	
<hr/>				
<b>Total Score</b>	<b>Score [%]</b>	<b>X Cog [mm]</b>	<b>Z Cog [mm]</b>	
0.586	75	-1842	498.62	
<b>I<sub>zz</sub> [kg*mm<sup>2</sup>]</b>	<b>I<sub>yy</sub> [kg*mm<sup>2</sup>]</b>	<b>I<sub>xx</sub> [kg*mm<sup>2</sup>]</b>	<b>Safety score</b>	
4.51e7	4.71e7	6.11e6	-745	
<hr/>				
<b>Total Score</b>	<b>Score [%]</b>	<b>X Cog [mm]</b>	<b>Z Cog [mm]</b>	
0.5226	50	-1856	499.43	
<b>I<sub>zz</sub> [kg*mm<sup>2</sup>]</b>	<b>I<sub>yy</sub> [kg*mm<sup>2</sup>]</b>	<b>I<sub>xx</sub> [kg*mm<sup>2</sup>]</b>	<b>Safety score</b>	
4.73e7	4.68e7	8.19e6	-922	
<hr/>				
<b>Total Score</b>	<b>Score [%]</b>	<b>X Cog [mm]</b>	<b>Z Cog [mm]</b>	
0.4595	25	-1878	499.73	
<b>I<sub>zz</sub> [kg*mm<sup>2</sup>]</b>	<b>I<sub>yy</sub> [kg*mm<sup>2</sup>]</b>	<b>I<sub>xx</sub> [kg*mm<sup>2</sup>]</b>	<b>Safety score</b>	
7.44e7	7.38e7	8.11e6	-768	
<hr/>				
<b>Total Score</b>	<b>Score [%]</b>	<b>X Cog [mm]</b>	<b>Z Cog [mm]</b>	
0.3959	0	-1904	495.45	
<b>I<sub>zz</sub> [kg*mm<sup>2</sup>]</b>	<b>I<sub>yy</sub> [kg*mm<sup>2</sup>]</b>	<b>I<sub>xx</sub> [kg*mm<sup>2</sup>]</b>	<b>Safety score</b>	
9.03e7	8.73e7	1.26e7	-1090	
<hr/>				

**Table 5.1** Resume table of the results of the application of the methodology with the Boston Power Swing 5300 cell.

It is worth observing that, due to the high number of cells needed, the analysis provided an elevated number of models. Nevertheless a wide number of designs do not present a great variation of the shape, due to the modification of the placement of a reduced number of cells. Moreover an example of the integration of the battery pack into the vehicle is proposed in figure 5.2.

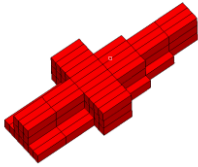
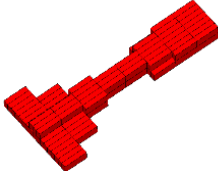
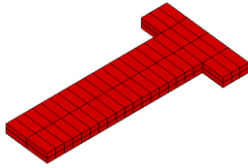
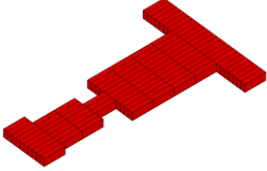
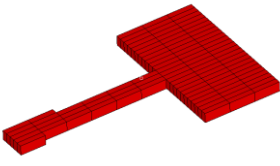


**Figure 5.2** Example of the integration of the battery pack with the best score into the vehicle.



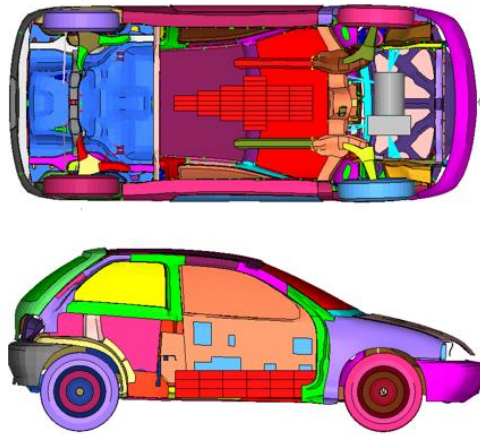
## 5.2 Designs using the Boston Power Swing Key 442 modules

The input for this analysis are proposed in chapter 4.2.2. In table 5.2 it is possible to find a resume and 5 examples of the designs of the battery pack ordered by the overall score.

<b>Total Score</b>	<b>Score [%]</b>	<b>X Cog [mm]</b>	<b>Z Cog [mm]</b>	
0.6991	100	-1800	503.36	
<b>I<sub>zz</sub> [kg*mm<sup>2</sup>]</b>	<b>I<sub>yy</sub> [kg*mm<sup>2</sup>]</b>	<b>I<sub>xx</sub> [kg*mm<sup>2</sup>]</b>	<b>Safety score</b>	
1.07e7	1.27e7	4.1e6	-59	
<b>Total Score</b>	<b>Score [%]</b>	<b>X Cog [mm]</b>	<b>Z Cog [mm]</b>	
0.6282	75	-1827	498.86	
<b>I<sub>zz</sub> [kg*mm<sup>2</sup>]</b>	<b>I<sub>yy</sub> [kg*mm<sup>2</sup>]</b>	<b>I<sub>xx</sub> [kg*mm<sup>2</sup>]</b>	<b>Safety score</b>	
3.65e7	3.9e7	5.51e6	-84	
<b>Total Score</b>	<b>Score [%]</b>	<b>X Cog [mm]</b>	<b>Z Cog [mm]</b>	
0.5582	50	-1845	495	
<b>I<sub>zz</sub> [kg*mm<sup>2</sup>]</b>	<b>I<sub>yy</sub> [kg*mm<sup>2</sup>]</b>	<b>I<sub>xx</sub> [kg*mm<sup>2</sup>]</b>	<b>Safety score</b>	
4.29e7	4.4e7	8.25e6	-136	
<b>Total Score</b>	<b>Score [%]</b>	<b>X Cog [mm]</b>	<b>Z Cog [mm]</b>	
0.4867	25	-1849	495	
<b>I<sub>zz</sub> [kg*mm<sup>2</sup>]</b>	<b>I<sub>yy</sub> [kg*mm<sup>2</sup>]</b>	<b>I<sub>xx</sub> [kg*mm<sup>2</sup>]</b>	<b>Safety score</b>	
6.07e7	5.9e7	1.15e7	-110	
<b>Total Score</b>	<b>Score [%]</b>	<b>X Cog [mm]</b>	<b>Z Cog [mm]</b>	
0.4154	0	-1895	495.10	
<b>I<sub>zz</sub> [kg*mm<sup>2</sup>]</b>	<b>I<sub>yy</sub> [kg*mm<sup>2</sup>]</b>	<b>I<sub>xx</sub> [kg*mm<sup>2</sup>]</b>	<b>Safety score</b>	
8.02e7	7.87e7	1.31e7	-138	

**Table 5.2** Resume table of the results of the application of the methodology with the Boston Power Swing key 442 module.

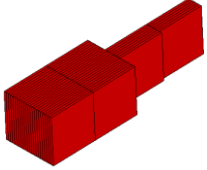
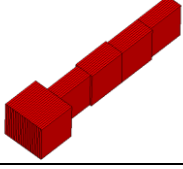
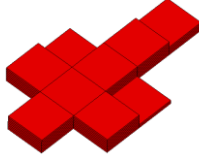
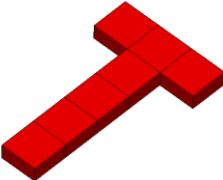
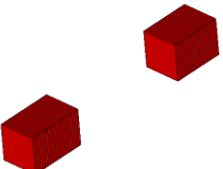
It is important to note the similarity of the models with affine scores with the models of the previous chapter, although the dimensions of the discretization are strongly different. This can indicate the presence of preferred zones for the integration of the batteries, nevertheless it is necessary to compare also the other models in order to provide useful conclusions. Moreover an example of the integration of the battery pack into the vehicle is proposed in figure 5.3.



**Figure 5.3** Example of the integration of the battery pack with the best score into the vehicle.

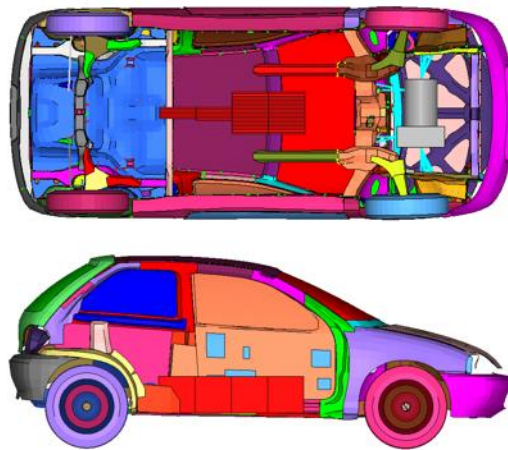
### 5.3 Designs using the Kokam Series 255 75 Ah cells

The features of the battery pack using the pouch cells are exposed in chapter 4.2.3. The analysis provided 13122 models that were evaluated using the first scenario described in chapter 4.3.2. In table 5.3 is possible to find some examples of the design.

<b>Total Score</b>	<b>Score [%]</b>	<b>X Cog [mm]</b>	<b>Z Cog [mm]</b>	
0.688	100	-1823	505	
<b>I<sub>zz</sub> [kg*mm<sup>2</sup>]</b>	<b>I<sub>yy</sub> [kg*mm<sup>2</sup>]</b>	<b>I<sub>xx</sub> [kg*mm<sup>2</sup>]</b>	<b>Safety score</b>	
1.66e7	1.83e7	3.77e6	-13	
<b>Total Score</b>	<b>Score [%]</b>	<b>X Cog [mm]</b>	<b>Z Cog [mm]</b>	
0.607	75	-1849	505	
<b>I<sub>zz</sub> [kg*mm<sup>2</sup>]</b>	<b>I<sub>yy</sub> [kg*mm<sup>2</sup>]</b>	<b>I<sub>xx</sub> [kg*mm<sup>2</sup>]</b>	<b>Safety score</b>	
3.97e7	4.19e7	3.39e6	-27	
<b>Total Score</b>	<b>Score [%]</b>	<b>X Cog [mm]</b>	<b>Z Cog [mm]</b>	
0.5254	50	-1853	490	
<b>I<sub>zz</sub> [kg*mm<sup>2</sup>]</b>	<b>I<sub>yy</sub> [kg*mm<sup>2</sup>]</b>	<b>I<sub>xx</sub> [kg*mm<sup>2</sup>]</b>	<b>Safety score</b>	
3.9e7	3.62e7	1.33e6	-82	
<b>Total Score</b>	<b>Score [%]</b>	<b>X Cog [mm]</b>	<b>Z Cog [mm]</b>	
0.4404	25	-1897	491	
<b>I<sub>zz</sub> [kg*mm<sup>2</sup>]</b>	<b>I<sub>yy</sub> [kg*mm<sup>2</sup>]</b>	<b>I<sub>xx</sub> [kg*mm<sup>2</sup>]</b>	<b>Safety score</b>	
7.61e7	7.39e7	1.2.e7	-82	
<b>Total Score</b>	<b>Score [%]</b>	<b>X Cog [mm]</b>	<b>Z Cog [mm]</b>	
0.3609	0	-1864	505	
<b>I<sub>zz</sub> [kg*mm<sup>2</sup>]</b>	<b>I<sub>yy</sub> [kg*mm<sup>2</sup>]</b>	<b>I<sub>xx</sub> [kg*mm<sup>2</sup>]</b>	<b>Safety score</b>	
9.22e7	9.11e7	6.61e6	-34	

**Table 5.3** Resume table of the results of the application of the methodology with the Kokam series 255 cells.

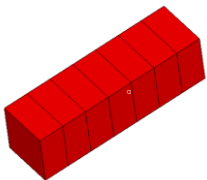
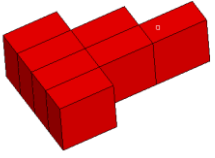
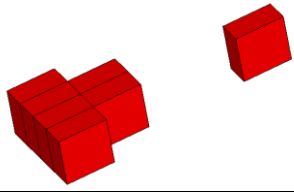
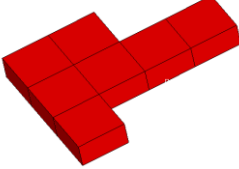
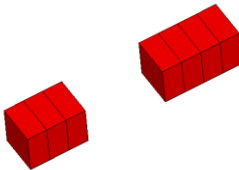
In this analysis the influence of the cells' dimensions is heavily observable in two factors. At first, it was found an high number of models with the same shape, due to the high dimension of the discretization. Then, in this case, various solutions in which the battery pack was divided in two parts were found. Such a solution is not convenient as it increases the cost of the battery pack itself and as it does not provide an acceptable overall score of the battery pack shape. An example of the integration is proposed in figure 5.4.



**Figure 5.4** Example of the integration of the battery pack with the best score into the vehicle.

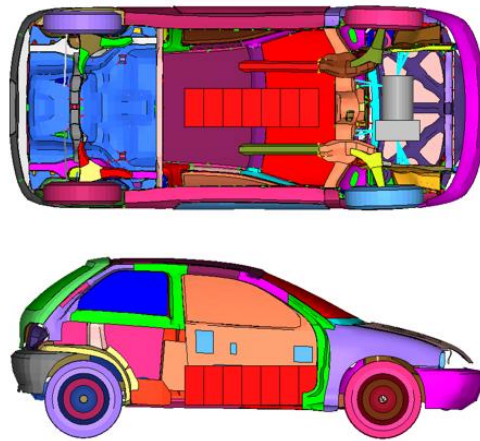
### 5.3 Designs using the Kokam KBM 255 75 Ah modules

The battery packs in this analysis are designed using the Kokam KBM255 75 Ah modules described in chapter 4.2.3. Table 5.4 resumes the features of the models evaluated using the baseline scenario described in chapter 4.3.2.

<b>Total Score</b>	<b>Score [%]</b>	<b>X Cog [mm]</b>	<b>Z Cog [mm]</b>	
0.678	100	-1805	507.86	
<b>I<sub>zz</sub> [kg*mm<sup>2</sup>]</b>	<b>I<sub>yy</sub> [kg*mm<sup>2</sup>]</b>	<b>I<sub>xx</sub> [kg*mm<sup>2</sup>]</b>	<b>Safety score</b>	
2.09e7	1.85e7	7.72e6	-4	
<b>Total Score</b>	<b>Score [%]</b>	<b>X Cog [mm]</b>	<b>Z Cog [mm]</b>	
0.6327	80	-1757	507	
<b>I<sub>zz</sub> [kg*mm<sup>2</sup>]</b>	<b>I<sub>yy</sub> [kg*mm<sup>2</sup>]</b>	<b>I<sub>xx</sub> [kg*mm<sup>2</sup>]</b>	<b>Safety score</b>	
1.82e7	1.63e7	7.18e6	-4	
<b>Total Score</b>	<b>Score [%]</b>	<b>X Cog [mm]</b>	<b>Z Cog [mm]</b>	
0.5561	50	-1773	507	
<b>I<sub>zz</sub> [kg*mm<sup>2</sup>]</b>	<b>I<sub>yy</sub> [kg*mm<sup>2</sup>]</b>	<b>I<sub>xx</sub> [kg*mm<sup>2</sup>]</b>	<b>Safety score</b>	
3.59e7	3.4e7	7.18e6	-4	
<b>Total Score</b>	<b>Score [%]</b>	<b>X Cog [mm]</b>	<b>Z Cog [mm]</b>	
0.4987	21	-1786	493	
<b>I<sub>zz</sub> [kg*mm<sup>2</sup>]</b>	<b>I<sub>yy</sub> [kg*mm<sup>2</sup>]</b>	<b>I<sub>xx</sub> [kg*mm<sup>2</sup>]</b>	<b>Safety score</b>	
2.85e7	2.31e7	1.4e7	-7	
<b>Total Score</b>	<b>Score [%]</b>	<b>X Cog [mm]</b>	<b>Z Cog [mm]</b>	
0.4508	0	-1865	507	
<b>I<sub>zz</sub> [kg*mm<sup>2</sup>]</b>	<b>I<sub>yy</sub> [kg*mm<sup>2</sup>]</b>	<b>I<sub>xx</sub> [kg*mm<sup>2</sup>]</b>	<b>Safety score</b>	
8.02e7	7.78e7	7.72e6	-4	

**Table 5.4** Resume table of the results of the application of the methodology with the Kokam KBM255 75 Ah module.

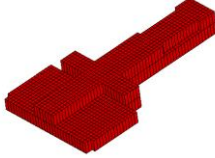
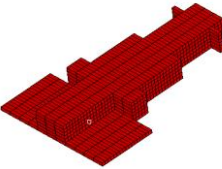
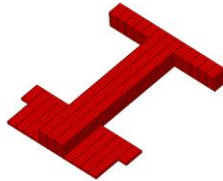
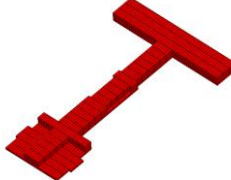
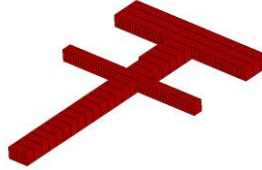
In this analysis the characteristics, already observed in the designs using the Kokam Series 255 75 Ah cells are emphasized. In particular a reduced number of models exhibit a different shape, due to the high dimensions of the elementary volumes in which the vehicle is discretized. This leads to the same battery pack's shape for different boundary conditions. An example of the integration is proposed in figure 5.5.



**Figure 5.5** Example of the integration of the battery pack with the best score into the vehicle.

## 5.5 Designs using the Panasonic NCR 18650 A cells

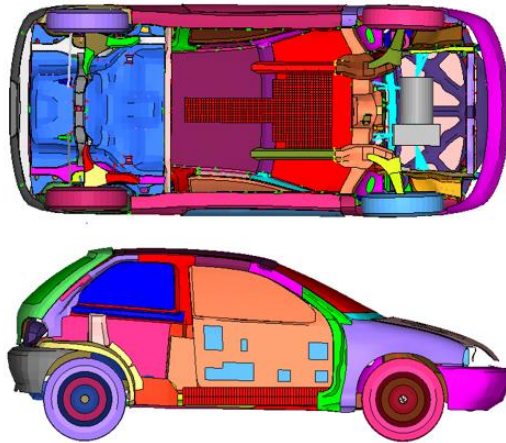
The designs presented in this paragraph utilize the cells exposed in chapter 4.2.1. Table 5.5 resumes the characteristics of five main designs.

<b>Total Score</b>	<b>Score [%]</b>	<b>X Cog [mm]</b>	<b>Z Cog [mm]</b>	
0.649	100	-1793	501.4	
<b>I<sub>zz</sub> [kg*mm<sup>2</sup>]</b>	<b>I<sub>yy</sub> [kg*mm<sup>2</sup>]</b>	<b>I<sub>xx</sub> [kg*mm<sup>2</sup>]</b>	<b>Safety score</b>	
1.18e7	1.39e7	5.41e6	-964	
<b>Total Score</b>	<b>Score [%]</b>	<b>X Cog [mm]</b>	<b>Z Cog [mm]</b>	
0.59	75	-1837	499.37	
<b>I<sub>zz</sub> [kg*mm<sup>2</sup>]</b>	<b>I<sub>yy</sub> [kg*mm<sup>2</sup>]</b>	<b>I<sub>xx</sub> [kg*mm<sup>2</sup>]</b>	<b>Safety score</b>	
1.16e7	1.39e7	5.24e6	-692	
<b>Total Score</b>	<b>Score [%]</b>	<b>X Cog [mm]</b>	<b>Z Cog [mm]</b>	
0.5297	50	-1814	501.26	
<b>I<sub>zz</sub> [kg*mm<sup>2</sup>]</b>	<b>I<sub>yy</sub> [kg*mm<sup>2</sup>]</b>	<b>I<sub>xx</sub> [kg*mm<sup>2</sup>]</b>	<b>Safety score</b>	
2.04e7	2.12e7	6.86e6	-1816	
<b>Total Score</b>	<b>Score [%]</b>	<b>X Cog [mm]</b>	<b>Z Cog [mm]</b>	
0.47	25	-1879	499.05	
<b>I<sub>zz</sub> [kg*mm<sup>2</sup>]</b>	<b>I<sub>yy</sub> [kg*mm<sup>2</sup>]</b>	<b>I<sub>xx</sub> [kg*mm<sup>2</sup>]</b>	<b>Safety score</b>	
7.05e7	7.05e7	8.69e6	-1564	
<b>Total Score</b>	<b>Score [%]</b>	<b>X Cog [mm]</b>	<b>Z Cog [mm]</b>	
0.412	0	-1886	499.43	
<b>I<sub>zz</sub> [kg*mm<sup>2</sup>]</b>	<b>I<sub>yy</sub> [kg*mm<sup>2</sup>]</b>	<b>I<sub>xx</sub> [kg*mm<sup>2</sup>]</b>	<b>Safety score</b>	
7.97e7	7.85e7	9.63e6	-1536	

**Table 5.5** Resume table of the results of the application of the methodology with the Panasonic NCR 18650 A cells.

It is worth observing the similarity of the shape of the models to the designs provided by the analysis with the Boston Power 5300 cells, although the cells dimensions are different. A more detailed analysis is provided at the end of this chapter (see chapter 5.7).

Moreover, in figure 5.6, an example of the integration is presented.

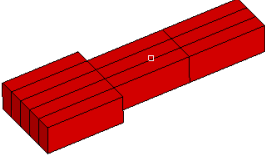
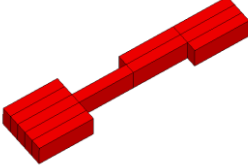
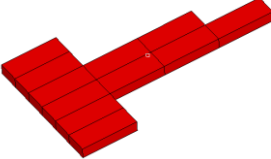
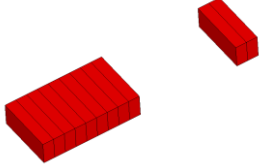
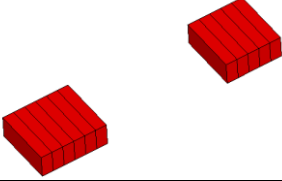


**Figure 5.6** Example of the integration of the battery pack with the best score into the vehicle.



## 5.6 Designs using the Panasonic concept modules

The features of the battery pack using modules based on the Panasonic 18650 cells are exposed in chapter 4.2.1. The analysis provided 13122 models that were evaluated using the first scenario described in chapter 4.3.2. Table 5.6 shows five different models selected due to the total score.

<b>Total Score</b>	<b>Score [%]</b>	<b>X Cog [mm]</b>	<b>Z Cog [mm]</b>	
0.6502	100	-1802	500	
<b>I<sub>zz</sub> [kg*mm<sup>2</sup>]</b>	<b>I<sub>yy</sub> [kg*mm<sup>2</sup>]</b>	<b>I<sub>xx</sub> [kg*mm<sup>2</sup>]</b>	<b>Safety score</b>	
1.72e7	1.96e7	4.64e6	-6	
<hr/>				
<b>Total Score</b>	<b>Score [%]</b>	<b>X Cog [mm]</b>	<b>Z Cog [mm]</b>	
0.5511	75	-1828	500	
<b>I<sub>zz</sub> [kg*mm<sup>2</sup>]</b>	<b>I<sub>yy</sub> [kg*mm<sup>2</sup>]</b>	<b>I<sub>xx</sub> [kg*mm<sup>2</sup>]</b>	<b>Safety score</b>	
4.21e7	4.46e7	4.51e6	-6	
<hr/>				
<b>Total Score</b>	<b>Score [%]</b>	<b>X Cog [mm]</b>	<b>Z Cog [mm]</b>	
0.4651	50	-1802	495	
<b>I<sub>zz</sub> [kg*mm<sup>2</sup>]</b>	<b>I<sub>yy</sub> [kg*mm<sup>2</sup>]</b>	<b>I<sub>xx</sub> [kg*mm<sup>2</sup>]</b>	<b>Safety score</b>	
2.91e7	2.81e7	1.06e7	-15	
<hr/>				
<b>Total Score</b>	<b>Score [%]</b>	<b>X Cog [mm]</b>	<b>Z Cog [mm]</b>	
0.3427	24	-1804	500	
<b>I<sub>zz</sub> [kg*mm<sup>2</sup>]</b>	<b>I<sub>yy</sub> [kg*mm<sup>2</sup>]</b>	<b>I<sub>xx</sub> [kg*mm<sup>2</sup>]</b>	<b>Safety score</b>	
3.31e7	3e7	1.01e7	-12	
<hr/>				
<b>Total Score</b>	<b>Score [%]</b>	<b>X Cog [mm]</b>	<b>Z Cog [mm]</b>	
0.2415	0	-1839	500	
<b>I<sub>zz</sub> [kg*mm<sup>2</sup>]</b>	<b>I<sub>yy</sub> [kg*mm<sup>2</sup>]</b>	<b>I<sub>xx</sub> [kg*mm<sup>2</sup>]</b>	<b>Safety score</b>	
6.65e7	6.34e7	1.01e7	-10	
<hr/>				

**Table 5.6** Resume table of the results of the application of the methodology with the Panasonic concept module.

It is worth observing the presence of battery packs divided in two parts also in this analysis. As exposed before, this solution is usually avoided as it leads to an increase of the total cost of the battery packs due to the need of two BMS. An example of the integration is proposed in figure 5.7.

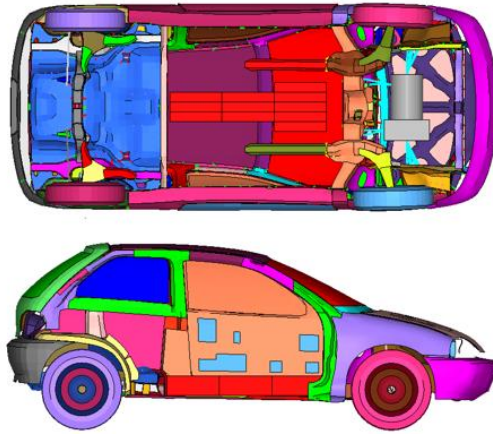


**Figure 5.7** Example of the integration of the battery pack with the best score into the vehicle.

## 5.7 Discussion

Through the application of the algorithm with different cells 'dimensions it is possible to analyse the influence of the battery pack in the features of the vehicle and the effect of the cells 'dimensions in the design of the battery pack.

The number of cells or modules of the battery pack affects the number of possible solutions, in fact, as the dimensions increase different boundary conditions lead to the same design due to the discretization of the vehicle in a reduced number of possible zones.

Moreover, changing the cells 'orientation, different maximum heights available for the algorithm produce the same design for the same reason exposed before. On the other hand, this increases the speed of the algorithm.

Nevertheless, observing the best overall models for every cell's and module's type it is possible to find that some zones are particularly favored for the positioning of the cells.

In effect, the models with the highest score present a battery pack that spreads for the entire length of the tunnel plus the zone under the front seats.

This can be explained with the observation of the map of probability exposed in chapter 2.3: these zones exhibit a low probability of deformation, therefore the use of these zones for the placement of the cells offers a higher safety for the battery pack.

Moreover the use of the previously exposed zones permits the battery pack to obtain low inertia around the Y and X axis and therefore reduces the negative influence, due to the added mass, in the dynamic of the vehicle.

It is worth highlighting the use of these areas also in EVs of the supermini class in the current market, as shown in figure 5.8.



**Figure 5.8** Examples of three EVs in the current market that use the tunnel zone and the area under the front seats for the integration of the batteries. From the left: Kia Soul electric 2015 model [46], Renault Zoe 2014 model [47] and Fiat 500 E 2014 model [48].

On the other hand, analysing the models with the lowest score for the baseline scenario, it is possible to find a common use of the rear zone of the vehicle. This enables the battery pack to lower the center of gravity of the vehicle and to achieve

a load ratio near to 50/50, but, on the other hand, increases the negative influence of the battery pack in the inertia moments.

In effect, examining the difference between the height of the center of gravity in the vehicle before the integration of the battery pack and the height of the same parameter in the vehicle after the integration, it was found that the best overall models present a slight variation of this parameter, while the worst models provide a wider range.

In fact, a battery pack with a higher dimension in the Z direction permits the integration of almost all the cells in the tunnel zone that, at the same time, increases the safety of the battery pack and decreases the negative influence of the mass of the cells to the inertia moments of the vehicle.

Moreover, the high influence of the variation of the score of the models analysed in chapter 4.3.2 between the baseline scenario and the scenario with an augmented weight for the height of the center of gravity can thus be clarified.

A similar trend is found also for the longitudinal position of the center of gravity; in effect, while the overall best models exhibit a variation of this parameter about 170 mm respect to the original model, the worst overall designs permit to shift the center of gravity up to 233 mm rearward, almost reaching a position that permits a 50/50 load ratio. In figure 5.9 are proposed the results with the Boston Power Swing 5300 cells, nevertheless similar results can be found for all the cells and modules analysed.

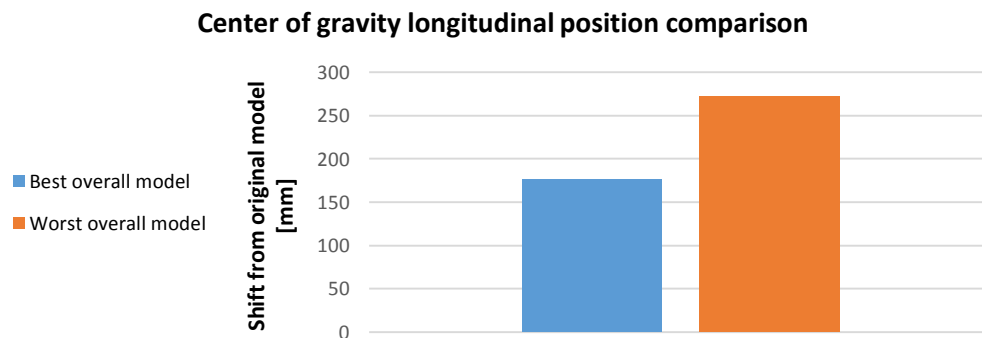


**Figure 5.9** Comparison of the transfer of the longitudinal position of the center of gravity of the vehicle with the application of the best overall and worst overall model of battery pack for the analysis developed with the Boston Power 5300 cells.

The safety evaluation deserves further considerations. In effect, the best overall designs do not present the best safety score.

Analysing the designs provided by different cells using a weighting parameter scenario focused upon the safety, it is possible to find that all the models with the maximum safety score exhibit a very similar shape (see figure 5.10).

In particular, the designs utilize, obviously, the zones with the minor probability of deformation and that leads to set the battery in the middle of the vehicle, using a longitudinal elongated shape. That allows the model to achieve the maximum score possible for the safety and to have good inertial properties, if compared to other designs, but on the other hand influences negatively the vertical position of the centre of gravity.

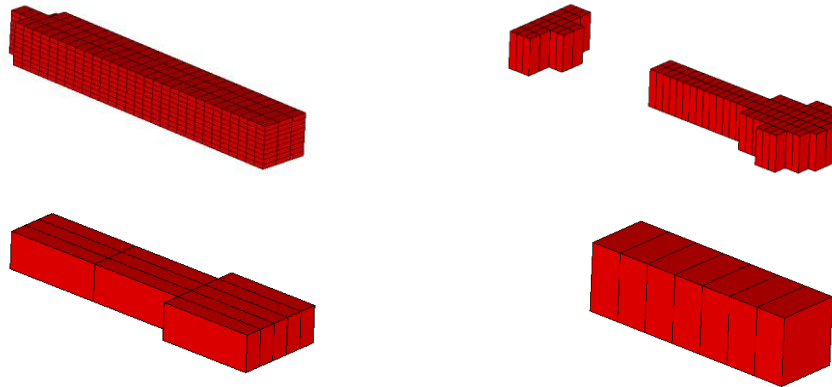


**Figure 5.10** Examples of the best designs of the battery pack found for 4 different analyses; in particular for the Boston Power 5300 cells (upper left), Boston Power modules (upper right), for the Panasonic modules (lower left) and for the Kokam modules (lower right).

It is worth analysing the position of the center of gravity in the different analyses developed. A common average position for the center of gravity can be found for best battery packs designed using different cells and the same can be claimed for the worst models.

In particular, observing the models with a maximum difference of 15% of the total percentage score, an average lowering of 26 mm of the center of gravity can be found while, examining the models with a total percentage score from 15% to 0% the average shift is 31 mm (see figure 5.11).

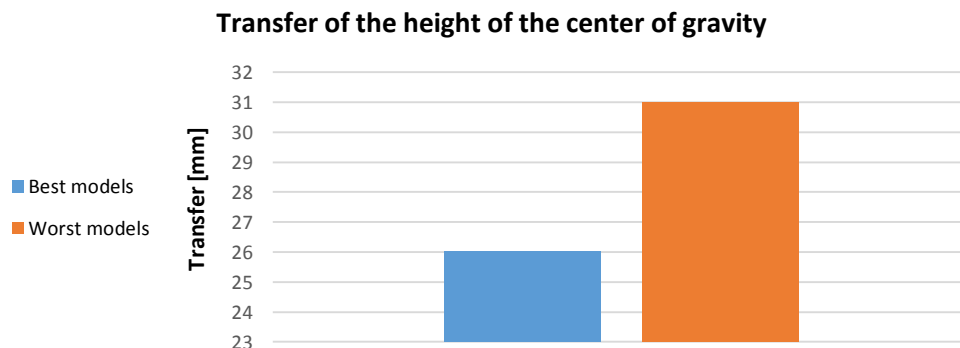


**Figure 5.11** Average transfer of the height of the center of gravity for the best and worst model for the different cells' and modules' types.

The difference in the height of the center of gravity leads to an increase of the SFF (see chapter 3.1.1) respectively about 5 % and 6% for the best and worst overall models (see figure 5.12).

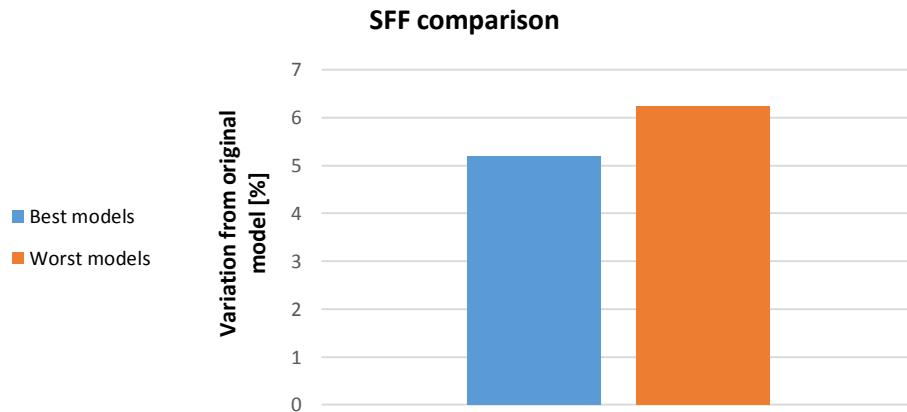


**Figure 5.12** Variation of the SFF for the best and worst models compared to the original vehicle before the integration of the battery pack.

Moreover, the critical speed to produce rollover rises from 9,5 km/h to 9,64 and 9,67 km/h for the best and worst models respectively, with a variation of 1,5% (see figure 5.13).

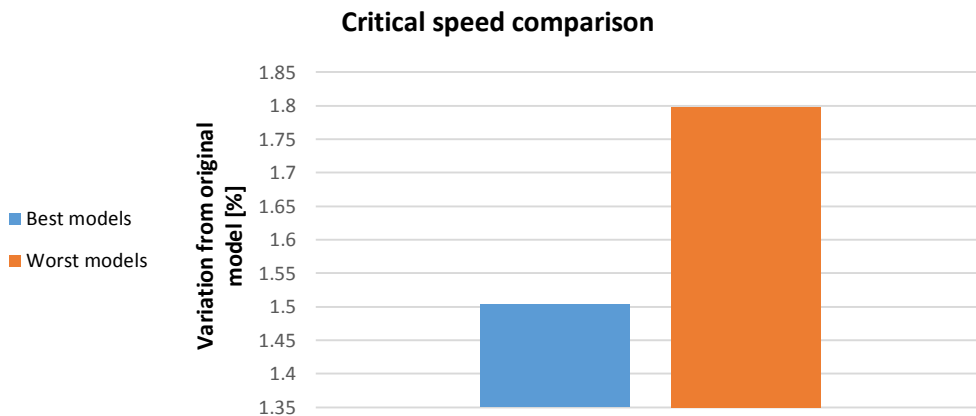


**Figure 5.13** Variation of the critical speed to produce rollover for the best and worst models compared to the original vehicle before the integration of the battery pack.

A common location for the best and worst overall models can be found also for the longitudinal position of the center of gravity. Inspecting the models in the

same ranges exposed before and averaging the transfer of the X coordinate of the center of gravity it was found that the best models show a center of gravity located 175 mm rearward, respect the model before the integration, while, in case of the worst models, this value reaches 230 mm (see figure 5.14).

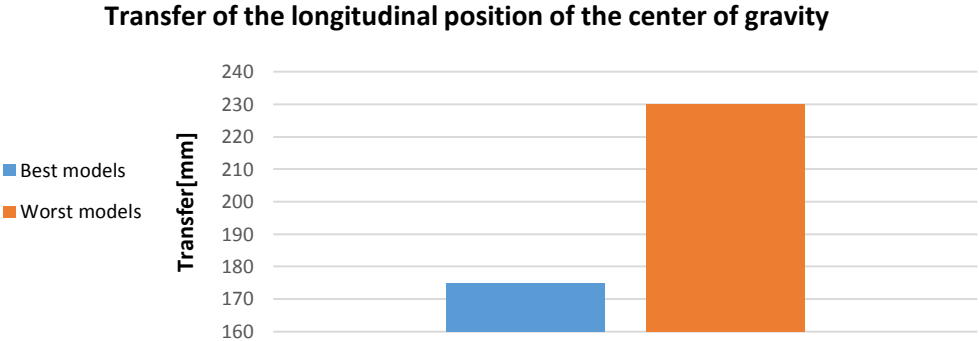


**Figure 5.14** Average transfer of the longitudinal position of the center of gravity for the best and worst models for the different cells' and modules' types.

## CHAPTER 6

### Crash test simulations

In order to verify the effective safety of the models achieved through the methodology, a campaign of FEAs was developed with the purpose to simulate the behaviour of the EV in real crashes through the LS-Dyna software.

The crash tests were realized with the battery pack model designed with the Boston Power 5300 Swing cells, described in chapter 4.2.2.

In order to integrate the battery pack into the vehicle a simple floor pan was designed. This leads to the elimination of the front crossbeam. Moreover, the internal combustion engine was removed, and an electric motor was installed.

The battery housing was simply designed with shell elements with the following features:

- number of integration points : 5;
- thickness 2 mm;
- material: steel, Young´s modulus 210000 MPa, Yield strength 411 MPa, density 7810 kg/m<sup>3</sup>, Poisson´s ratio 0,3, elasto-plastic behaviour. [49]

The connections between the original floor pan and the chassis of the vehicle were not modified after the installation of the modified floor pan,

The original vehicle was not modified, with the only exceptions described before (see figure 6.1).

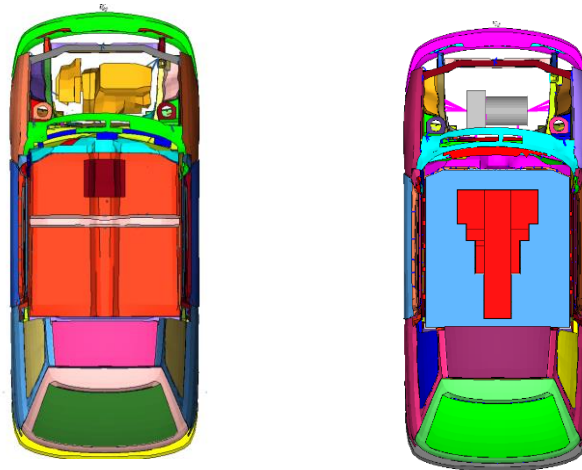


**Figure 6.1** Model of the original vehicle (left) and the EV simulated (right). Note the elimination of the front cross beam and the substitution of the original engine with an electric motor.



Seven different crash tests were simulated (see also table 6.1):

- a frontal crash test against a rigid wall;
- two pole crash tests;
- two frontal crash test against a deformable barrier with 100% overlap;
- a frontal crash tests against a deformable barrier with 40% overlap;
- an oblique crash test against a mobile deformable barrier.

### Crash test simulations developed

Test	Different configuration	Overlap [%]	Angle [°]	Vehicle speed [km/h]	Already used by
<b>Frontal crash – rigid wall</b>	1	100	0	56	FMVSS208,U.S. NCAP,KNCAP
<b>Pole crash test</b>	1- Impact point: R-point	Not defined	90	29	EuroNCAP, KNCAP,ANCAP
	2- Impact point: proximity of B-pillar	Not defined	90	29	/
<b>Frontal crash- Progressive Deformable Barrier</b>	1	100	0	50	/
	2	100	0	64	/
<b>Frontal crash - Offset Deformable Barrier</b>	1	40	0	64	EuroNCAP, IIHS, Latin NCAP, JNCAP, C-NCAP, KNCAP, ASEAN NCAP, ANCAP
<b>Oblique crash – Mobile Progressive Deformable Barrier</b>	1	40	30	Vehicle: 35 Trolley: 35	/

**Table 6.1 Resuming table of the crash tests simulated. [19]**

For every test the maximum Von Mises stress and the maximum strain in the cells and in the battery pack's housing were analysed, moreover the resultant acceleration pulse in proximity of the A and B pillar of the vehicle were recorded and compared to the original vehicle in order to find possible improvements (see figure 6.2). [29]

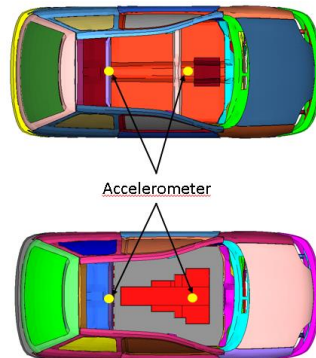


**Figure 6.2** Graphic explanation of the position of the accelerometers.

It is worth mentioning that due to the lack of informations about the mechanical properties of the cells, they have been modelled using an elastic material with the following characteristics:

- Young's modulus: 207 MPa;
- Poisson's ratio: 0,3;
- Density : 2200 kg/m<sup>3</sup>;
- One element per cell.

Thus in the strain graphs, the strain of the cells has to be intended as elastic strain, while the strain of the battery pack's housing represented is the effective plastic strain.

Moreover, it is worth mentioning that the FE model of the vehicle is validated only for front impacts with 100 % overlap, nevertheless, with the purpose to have a baseline for the evaluation of the results, it was subjected also to simulations for which it is not validated. [37]

## 6.1 Frontal crash test against a rigid wall

A frontal crash test against a rigid wall represents a hard test for the vehicle as the acceleration pulses are usually higher and the entire structure of the automobile is subjected to high and fast stresses. [29]

Due to its severity, it was the first crash test simulation developed.

The EuroNCAP crash test against a rigid wall set the vehicle's speed to 50 km/h, [50] however in order to increase the severity of the test the vehicle was speeded at 56 km/h against the wall (see figure 6.3), as in the US regulation [9]; the resulting deformations in the cells and in the battery pack housing were controlled, as well as the stresses.

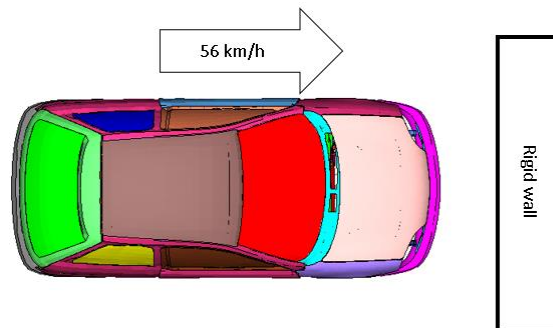


**Figure 6.3** Schematic representation of the configuration of the frontal crash test against a rigid wall simulation.

The possibility to extract realistic results from the simulation is proven by the trends of the energies, exposed in figure 6.4.

**Energies' trend in frontal crash test against a rigid wall simulation**

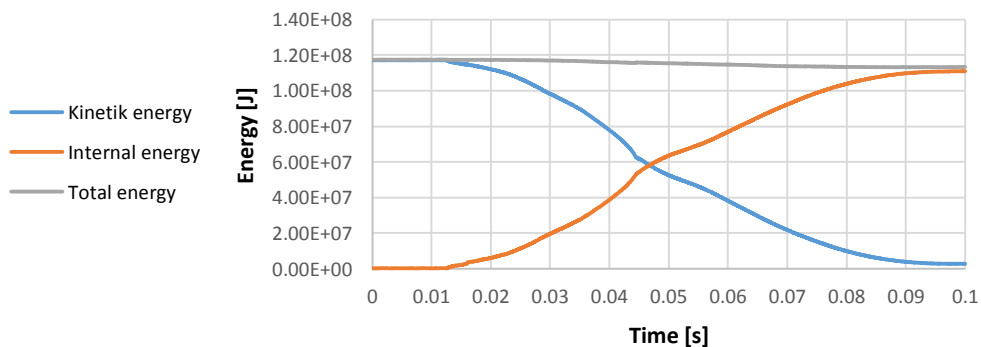


**Figure 6.4** Trends of the internal, kinetic and total energy in the crash test simulation against a rigid wall.

As the kinetic energy decreases, due to the impact, the internal energy of the model increases, due to the deformation of the elements, while the total energy of the system remains almost constant, with respect to the conservation of the total energy of the system.

In order to check the integrity of the battery pack the trends of the maximum stresses in the housing and in the cells were controlled as well as the strains. The results are proposed in figure 6.5 and 6.6.

**Maximum Von Mises stress in the frontal crash test against a rigid wall simulation**

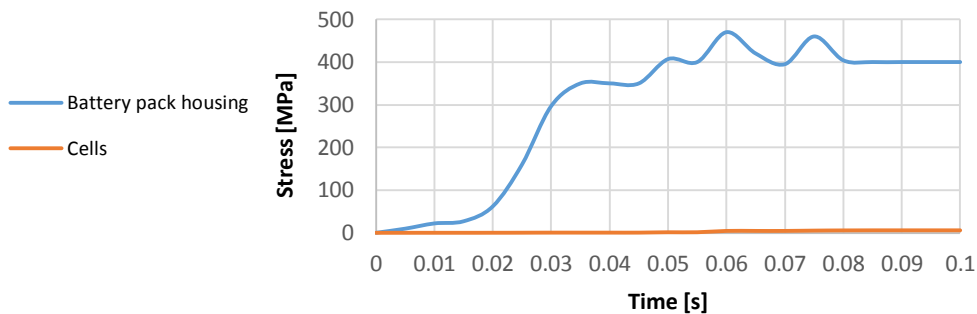


**Figure 6.5** Maximum Von Mises stress in the cells and in the battery pack housing in the crash test simulation against a rigid wall.

**Maximum strain in the frontal crash test against a rigid wall simulation**

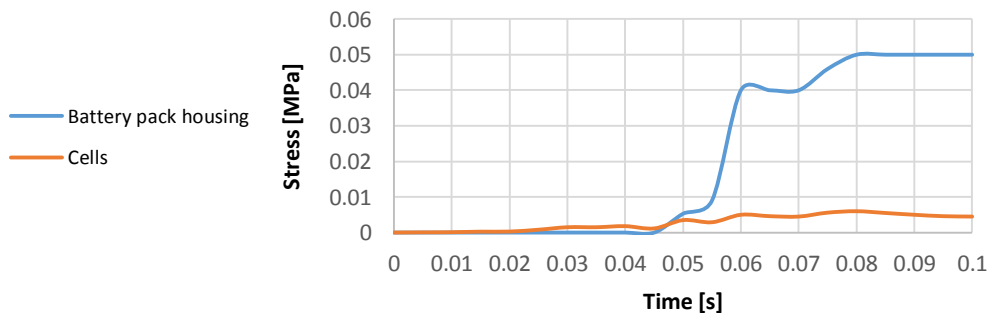


**Figure 6.6** Maximum strain in the cells and in the battery pack housing in the crash test simulation against a rigid wall.

Although the strain in the cells is not equal to 0, its maximum value is more than ten times smaller as in the battery pack's housing, while the stresses are never

higher than 6 MPa. This is the result of modelling the battery pack with an artificial material with a limited Young modulus, in order to find also a small variation in the deformation.

It can be concluded that a detailed model of the battery pack should then offer better results. Nevertheless, the simulation expresses that, in a real crash test, no excessive damage should be observed in the cells, due to their relative low deformation.

Moreover, it is possible to find in figure 6.7 an example of the simulation at 0,06 s and at 0,1 s.

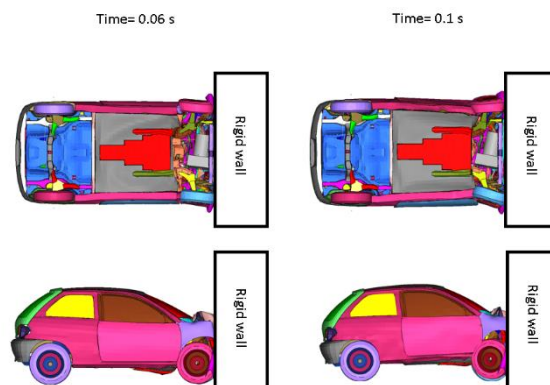


**Figure 6.7** Graphic comparison of the deformation of the vehicle after 0,06 and 0,1 second after the beginning of the simulation.

The acceleration pulses, shown in figure 6.8, offer more informations about the evaluation of the performances of the battery pack in the crash test and about the safety of the occupants.

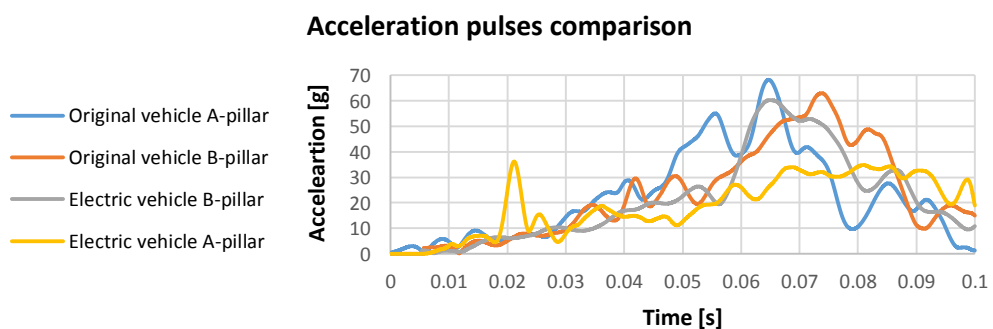


**Figure 6.8** Graphic comparison of the resultant acceleration pulses in the original model and in the vehicle after the integration of the battery pack. The accelerations were filtered using a SAE-J 211 CFC 60 filter, as the legislation advises. [19]

While the results of the rear accelerometers of the original vehicle and the EV exhibit a similar trend, the acceleration's pulses in proximity of the A-pillar are strongly different.

In particular, the EV exhibits a high pulse at 0,021s, where the accelerations reaches almost 40 g. This can be explained observing that, due to the not sufficient stiffness of the floor pan, at the moment of the impact the battery pack suffers an high acceleration in the horizontal direction, as shown in figure 6.9.

Nevertheless after this peak, the resultant of the accelerations in the EV exhibits an oscillating trend that does not reach the peak of the original vehicle.

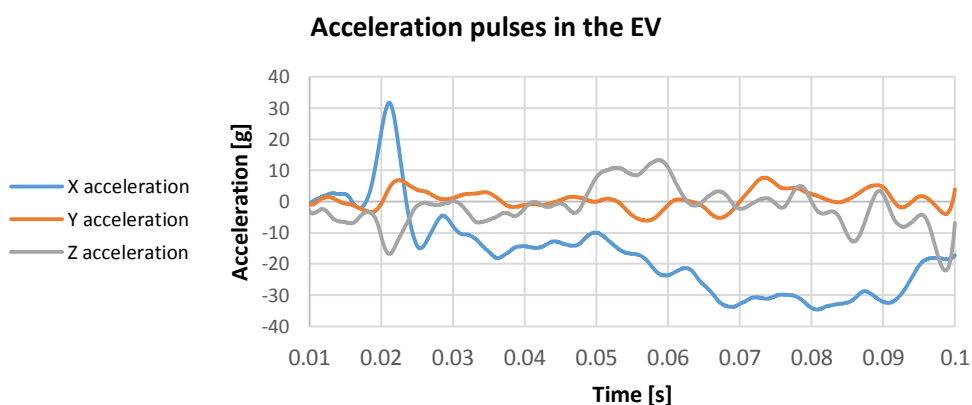


**Figure 6.9** Graphic comparison of the acceleration pulses in the vehicle after the integration of the battery pack in three directions. The accelerations were filtered using a SAE-J 211 CFC 60 filter, as the legislation advises. [19]

## 6.2 Pole crash test

The standard pole crash test simulates the impact of the vehicle against a narrow object that in the test is a rigid pole with the diameter of 254 mm. The impact position in the EuroNCAP test is set to the R point of the dummy (see figure 6.10) because the main goal is to verify the severity of possible injuries of the driver. [51]

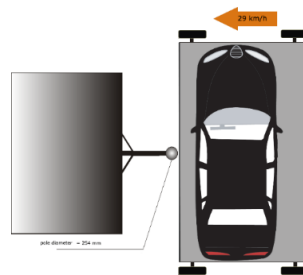


**Figure 6.10** Graphic explanation of the configuration of a pole crash test by EuroNCAP.

The standard configuration of the pole impact test was simulated, moreover, as the main purpose of the test is to verify the safety of the battery pack, also a different configuration was tested, in which the impact point was shifted rearward (see figure 6.11).

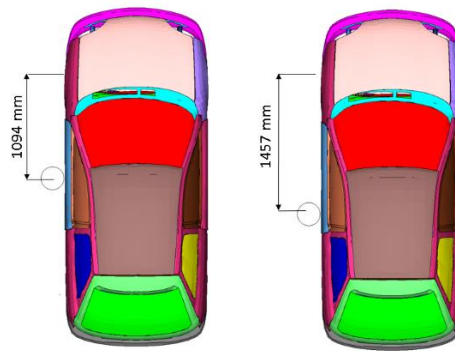


**Figure 6.11** Graphic explanation of the configuration of a pole crash test used in the simulations: on the left the standard configuration by EuroNCAP and on the right side the second configuration.

The energies ‘trends of the analysis (figure 6.12) express the possibility to use the results for further considerations.

It has to be noted the higher internal energy at the end of the simulation of the impact at the R point in comparison with the second configuration. In fact, the elimination of the front crossbeam increases the overall deformation of the components involved, which are not designed, in this case, to resist to such high stresses. Moreover, the rear impact causes a minor decrease of the kinetic energy due to the rotational effects depending on the relative position of the center of gravity of the vehicle and the impact point.

#### Energies’ trends in the pole crash test simulation

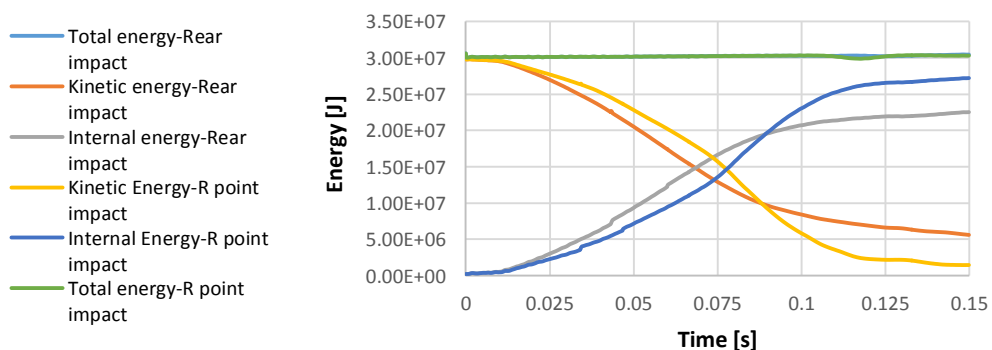


**Figure 6.12-** Trend of the kinetic, internal and total energy in the pole crash test simulation.

The same effect can be noted also observing the trend of the deformation of the cells and of the housing in the two configurations. In the R point impact test the frame does not prevent the contact between the impactor and the battery pack, thus an higher deformation can be observed in both the battery pack and the housing (see figure 6.13).

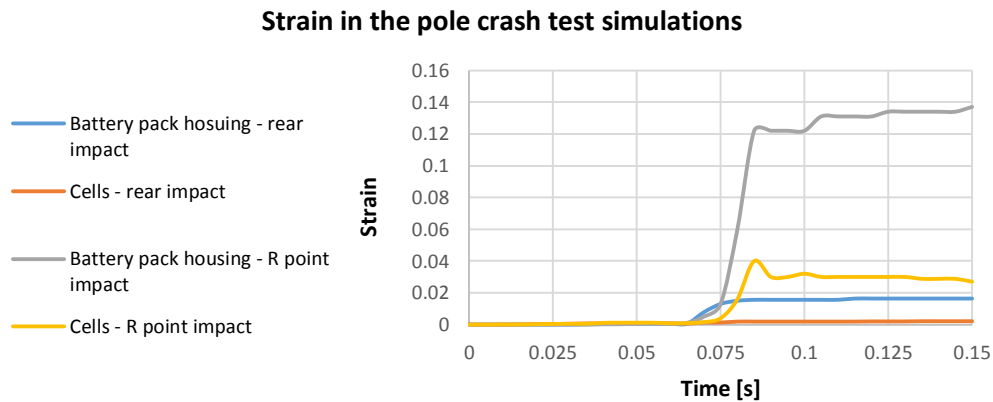


**Figure 6.13** Strain in the cells and in the battery pack housing in the two pole crash test simulations.

In the second configuration tested, the stress in the battery housing reaches the yield stress of the material, while the maximum Von Mises stress in the cells remains always less than 1 MPa. Instead, in the R point impact simulation the stress of the housing exceeds the yield stress of the material, resulting in the elevated strain observed in figure 6.11. Despite that, the cells do not exhibit stresses higher than 10 MPa, however ten times bigger than these in the second configuration.

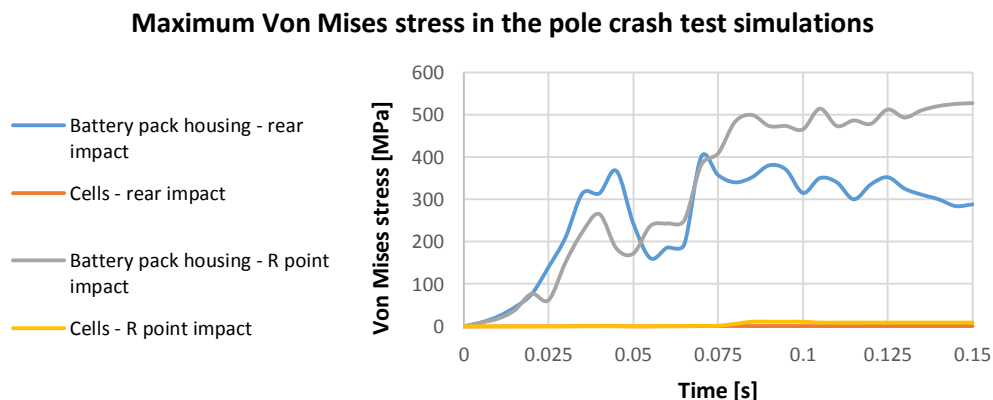


**Figure 6.14** Maximum Von Mises stress in the cells and in the battery housing in the pole crash simulation.



It is worth analysing the deformed shape of the vehicle in the two configurations during the simulation, in order to understand the results (see figure 6.12).

As visible in figure 6.12, the intrusion depth in the R point impact simulation is deeper than in the second configuration (see also figure 6.13). This is caused by the lack of a component that can absorb the energy of the impact, as originally was the front crossbeam. In the second configuration, the rear crossbeam fulfils this function. Moreover it is interesting to note that the intrusion depth in the pole impact at the R point for the EV is 35 mm less than that of the original vehicle.

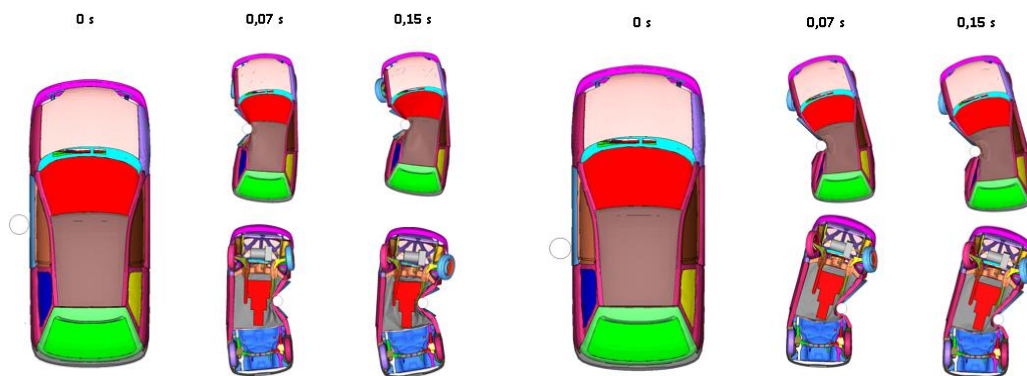


**Figure 6.15** Examples of the deformed shape of the vehicle in 3 instants of the simulations. On the left the results of the simulation with the impact point set to the R point, then on the right with the impact point translated rearward.

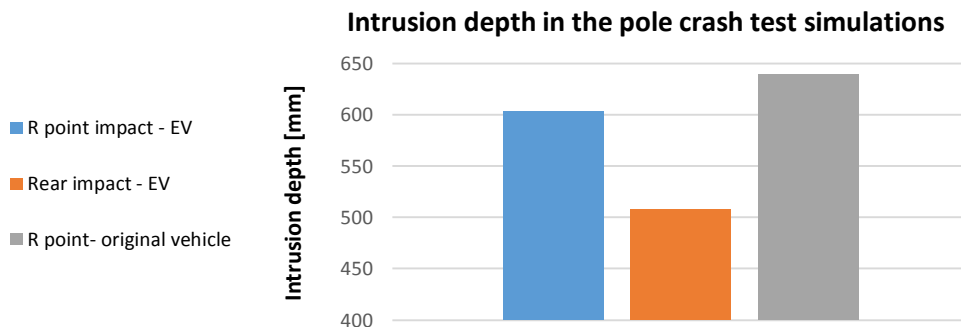


**Figure 6.16** Graphic comparison of the intrusion depth in the two configuration tested of the pole impact crash test and comparison to the original vehicle.

In conclusion, it can be stated that the safety of the battery pack is not a concern in the second configuration, nevertheless an impact at the R point can lead to serious consequences for the battery pack and for the driver due to the elevated

depth of penetration. Thus, particular attention has to be posed in the design of the floor pan and/or reinforcements in the further steps of the design. It is worth mentioning that no optimization process of the structure was adopted, as not part of the topics of the work.

### 6.3 Frontal crash test against a deformable barrier

The frontal crash test against a deformable barrier is set as a standard crash test thanks to the possibility to reproduce acceleration pulses similar to the ones that can be found in crashes against another vehicle. [19]

Three configurations were tested:

- two frontal crashes with 100 % overlap ;
- a frontal crash with 40% overlap.

#### 6.3.1 Frontal crash test with 100% overlap

In this crash test simulation the vehicle was speeded at 50 km/h against a progressive deformable barrier (PDB) (see figure 6.17). Moreover a second test was developed, where the speed was increased to 64 km/h.

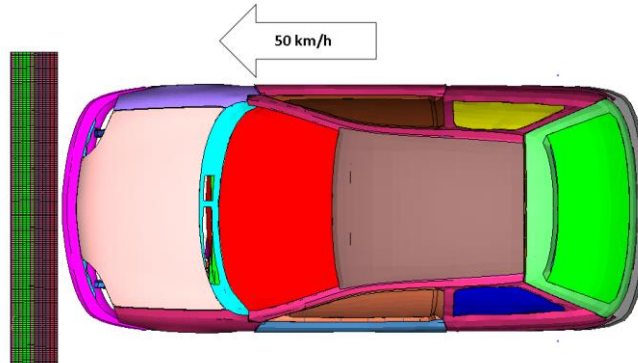
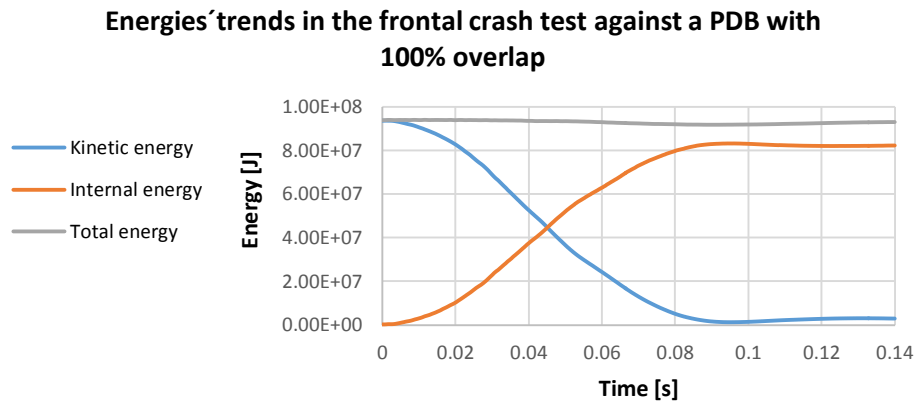


Figure 6.17 Graphic explanation of the configuration of the frontal crash test against a deformable barrier with 100% overlap.

The energies' trends (figure 6.18) exhibit a realistic behaviour and express the possibility to analyse the results.



**Figure 6.18** Energy trends in the frontal crash test against a deformable barrier with 100% overlap at 50 km/h.

Although the difference in the speed of the vehicle in comparison with the test against a rigid wall is only 6 km/h, a strong difference in the maximum Von Mises stress in the battery pack was found.

In the simulation against a deformable barrier, the maximum stress of the battery housing never exceeds 400 MPa, while the maximum value reached in the frontal crash test against a rigid wall simulation was 480 MPa (see figure 6.5 and 6.19), due to the different absorption of energy of the two barriers, 0 in case of a rigid wall, dependent from the vehicle's structure and speed in case of a PDB.

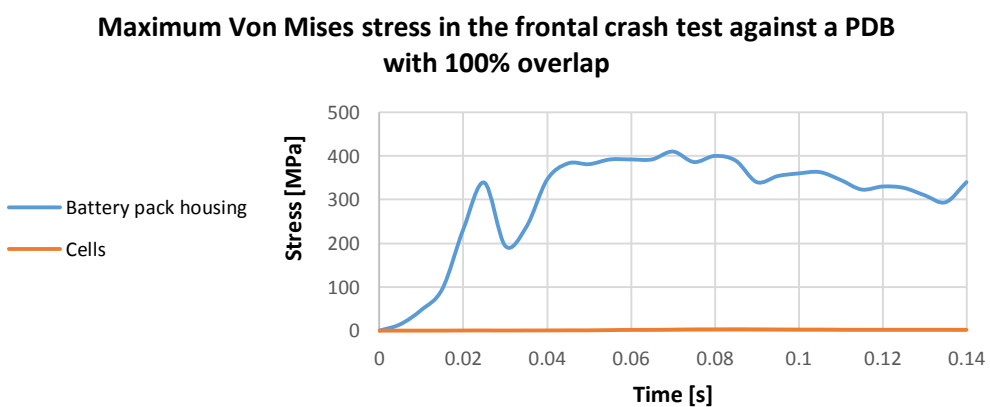


**Figure 6.19** Maximum Von Mises stress in the cells and in the battery pack housing.

Moreover, for the reason exposed previously, the strain's trend in the cells is reduced, compared to the other simulations developed, indicating a less hazardous situation for the battery pack, if involved in case of such a crash (see figure 6.20).

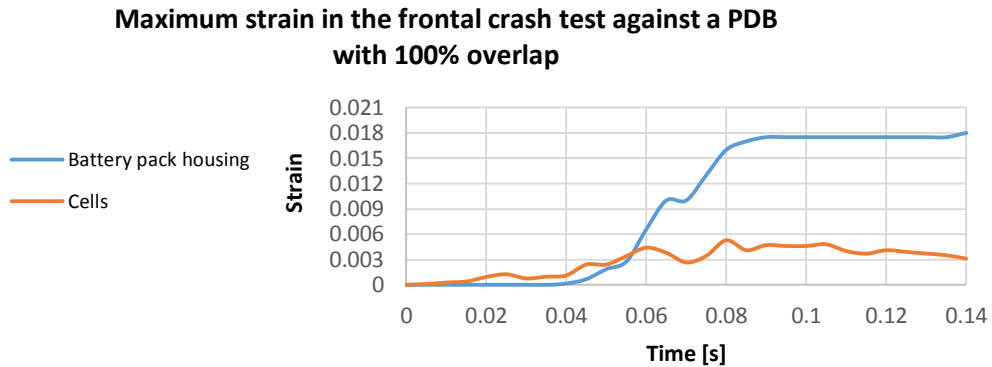


**Figure 6.20** Strain's trends in the cells and in the battery pack housing in the frontal crash test against a deformable barrier with 100% overlap simulation.

It is not possible to find a strong difference in the acceleration pulses in proximity of the B pillar of the two vehicles, nevertheless the front accelerometers exhibit a peak amplitude at different times due to the reduced stiffness of the floor pan in the EV, caused by the elimination of the front crossbeam and the introduction of the added mass of the battery pack (see figure 6.21).

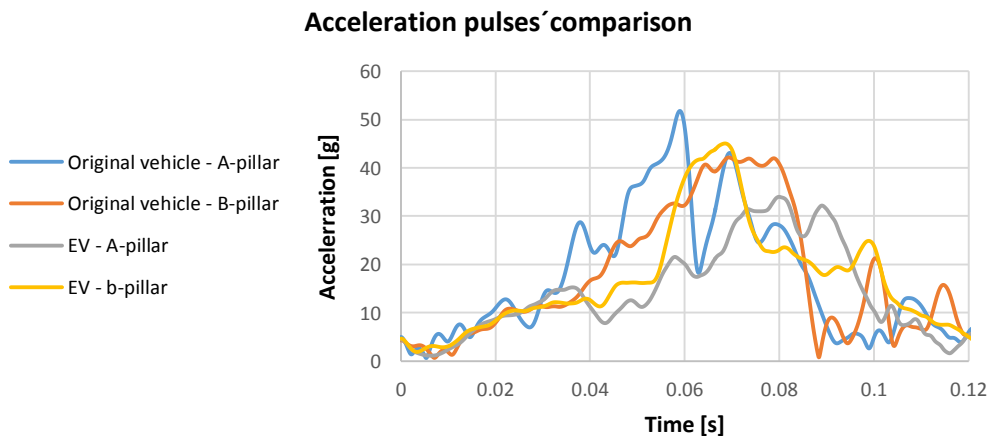


**Figure 6.21** Resultant accelerations 'trends in the original vehicle and in the EV in the frontal crash test against a deformable barrier at 50 km/h with 100% overlap simulation.

Observing the stresses' and strains' trends in the simulations developed with different speeds of the vehicles a notable difference can be found.

In particular, a maximum difference in the maximum Von Mises stress about 50 MPa it is observable (see figure 6.22), nevertheless, the maximum strain is almost the double in the configuration with an increased speed (fig 6.23), due to the trespassing of the yield strength of the material of the battery pack housing.

**Maximum Von Mises stress comparison**

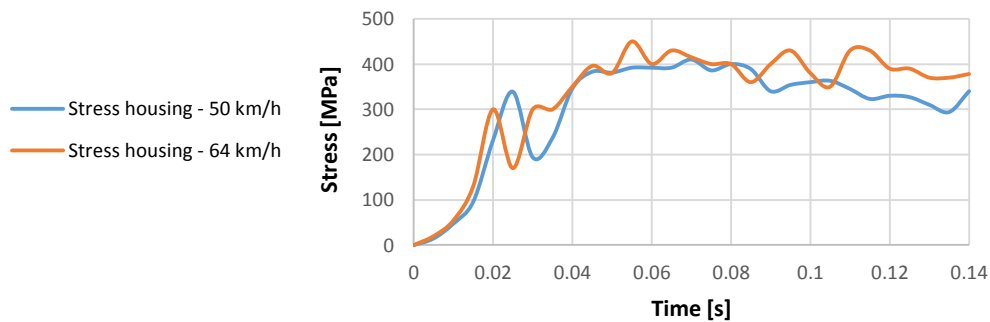


**Figure 6.22** Graphical comparison of the trends of the maximum Von Mises stress in the battery housing in the two simulations of the crash test against a deformable barrier with 100 % overlap.

**Maximum strain comparison**

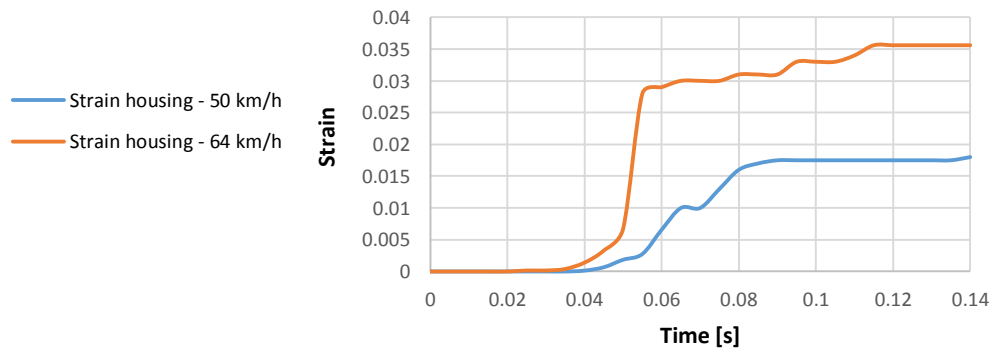


**Figure 6.23** Graphical comparison of the trends of the maximum effective plastic strain in the battery housing in the two simulations of the crash test against a deformable barrier with 100 % overlap.

Thus, while the frontal crash test against a PDB at 50 km/h does not represent a dangerous situation for the cells, more attention has to be posed in the design in order to improve the results of the simulation of the same test developed at 64 km/h.

### 6.3.2 Frontal crash test with 40% overlap

This test aims to check the effectiveness of the front structure of the vehicle in the absorption of the impact, when the impact itself regards a small portion of the front of the automobile. This is particularly critical because, if the structure of the vehicle is not adequately designed, high depths of intrusion are registered in the zone of the feet of the driver, although a deformable barrier is used (ODB). [29] The configuration of the simulation is shown in figure 6.24.

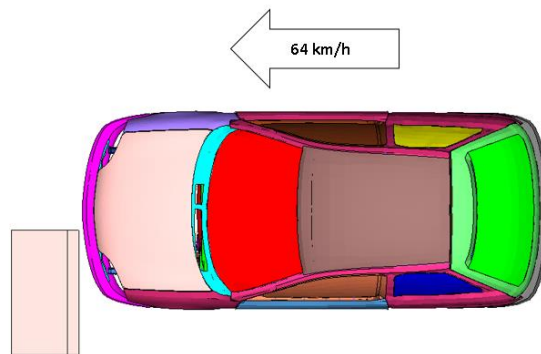


**Figure 6.24** Graphic explanation of the configuration of the frontal crash test against a deformable barrier with 40% overlap simulation.

The energy trends are exposed in figure 6.25.

It is important to note that, in this case, the internal energy reaches the total energy; this is not physically possible, nevertheless it has to be remembered that the FE model is not validated for such a simulation. It is worth anyway analysing the results.

**Energies' trends in the frontal crash test against a ODB barrier with 40% overlap**

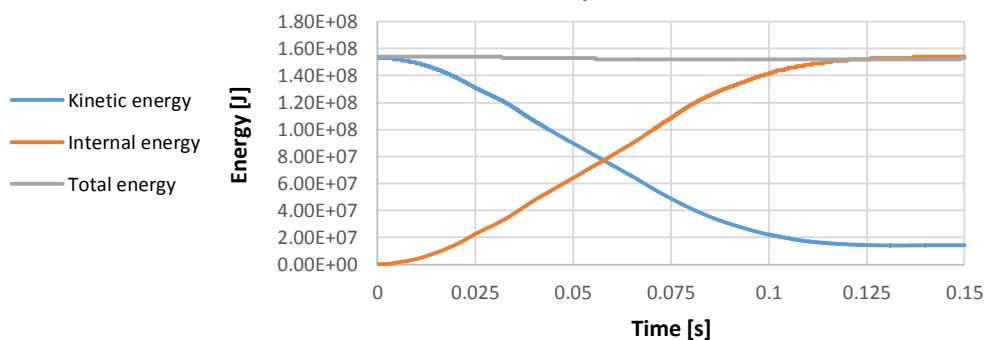


**Figure 6.25** Energies' trends in the frontal crash test against a deformable barrier with 40% overlap simulation.

Due to the high intrusions in the frontal structure of the vehicle, the stress in the battery housing exceeds the yield stress of the material (see figure 6.26), as visible also from the high value of the strain (see figure 6.27).

Nevertheless, the stress in the cells remains always under 8 MPa but the deformation reaches values double of the maximum obtained in the other tests, expressing the high possibility of severe danger to the cells.

#### Maximum Von Mises stress in the frontal crash test simulation against an ODB with 40 % overlap

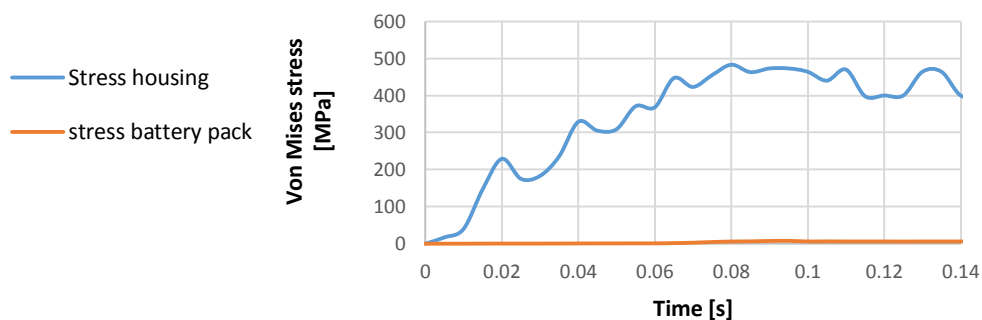


**Figure 6.26** Maximum Von Mises stress's trends in the cells and in the battery pack housing in the frontal crash test against a deformable barrier with 40% overlap simulation.

#### Maximum strain in the frontal crash test simulation against an ODB with 40% overlap

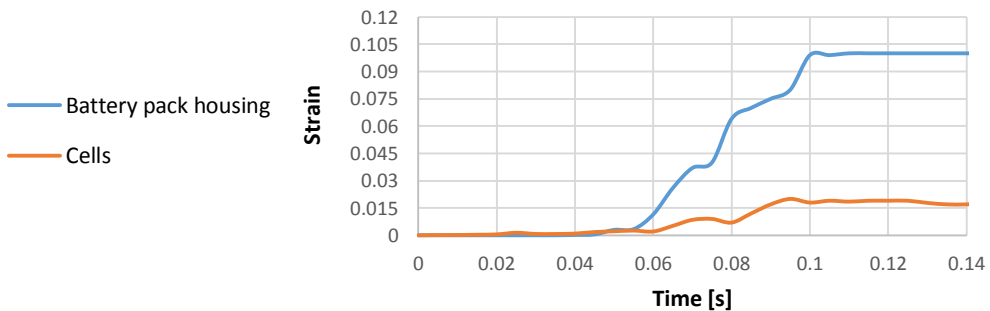


**Figure 6.27** Strain's trend in the cells and in the battery pack housing in the frontal crash test against a deformable barrier with 40% overlap simulation.

It has to be anyway noted that the structure of the car does not offer an adequate protection both for the battery pack and for the driver as it is possible to see from figure 6.28 and figure 6.29

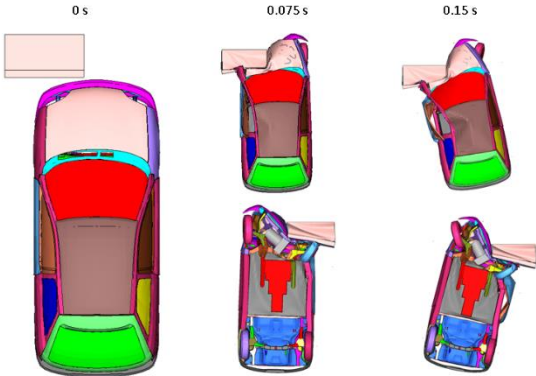


**Figure 6.28** Example of the deformation of the vehicle in three different instants of the crash test simulation against a deformable barrier with 40% overlap.

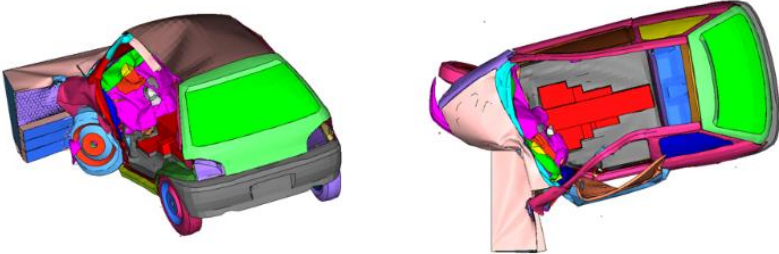


**Figure 6.29-** Deformed shape of the vehicle at the end of the crash test simulation against a deformable barrier with 40% overlap. Note the high deformation in the zone of the feet of the driver.



## 6.4 Oblique crash test

Crashes with an oblique PDoF are common in an urban scenario (see appendix D), nevertheless a crash test simulating these occasions is not set as standard crash test by EuroNCAP.

The configuration of the crash test simulation is exposed in figure 6.30. The vehicle and the mobile progressive deformable barrier (MPDB) were speeded both at 35 km/h with an angle of  $30^\circ$  between their respective speed vectors and the overlap was set to 40 %.

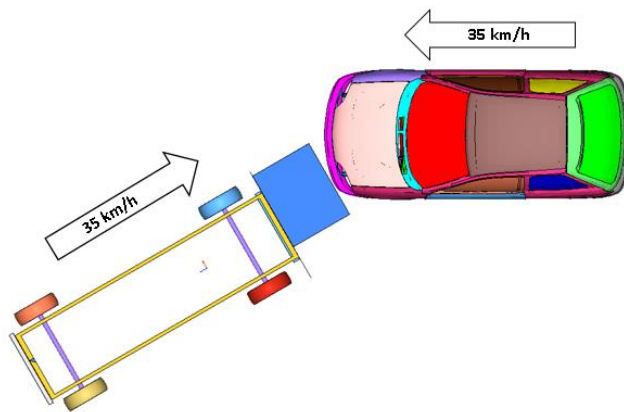


**Figure 6.30** Schematic representation of the configuration of the oblique crash test simulation.

Although the model is not validated for oblique or side impacts [37] the energies ‘trends exhibit a physical realistic behaviour (see figure 6.31).

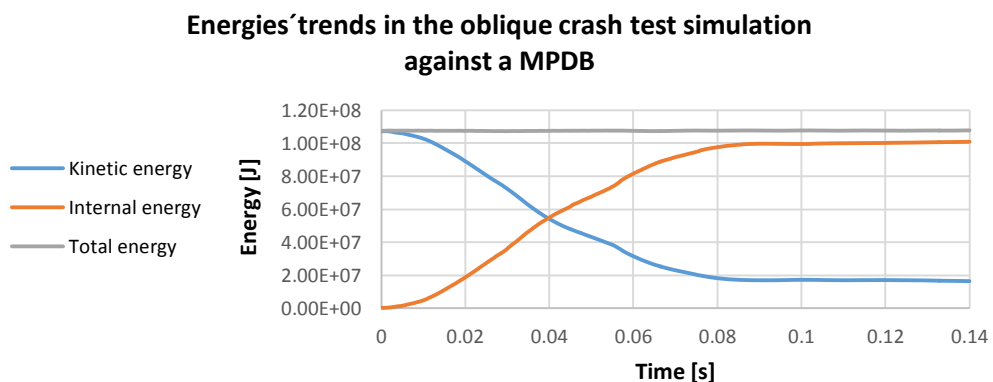


**Figure 6.31** Energies ‘trends in the oblique crash test simulation.

The maximum Von Mises stress exhibits a trend similar to the one registered in the frontal crash test simulation (see figure 6.32), nevertheless an increase of strains both in the cells and in the battery housing can be observed due to the reduced zone of impact that leads to an increase of the severity of the crash (see figure 6.33).

**Maximum Von Mises stress in the oblique crash test simulation against a MPDB**

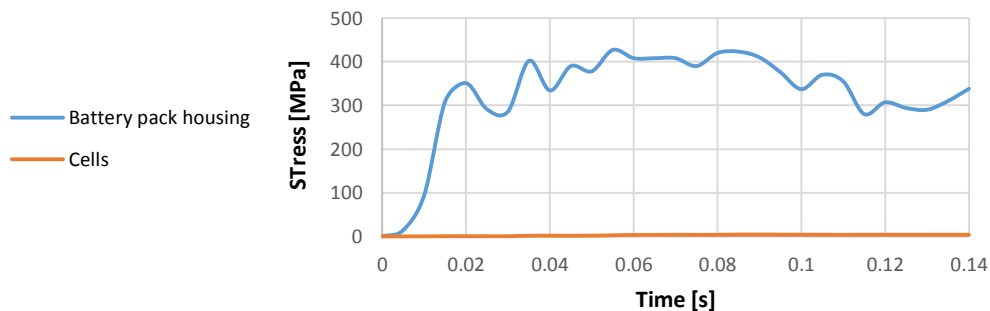


**Figure 6.32** Maximum Von Mises stress's trends in the cells and in the battery pack housing in the oblique crash test simulation.

**Maximum strain in the oblique crash test simulation against a MPDB**

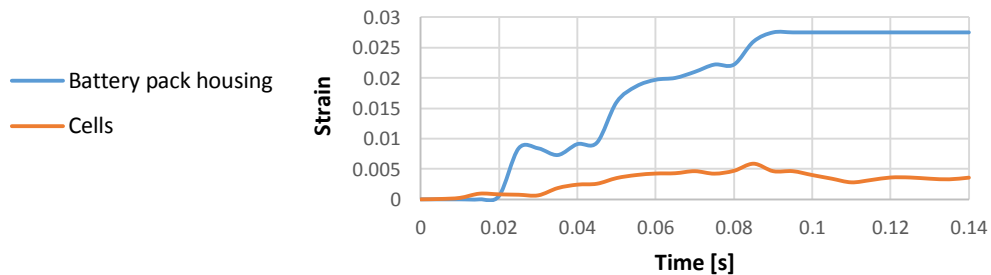


**Figure 6.33** Comparison of the strains in the cells and in the battery housing in the oblique crash test simulation.

Moreover, similar trends can be found in the accelerations 'pulses of the original vehicle and in the EV from the accelerometers in proximity of the B pillar, while the front ones reveal a different behaviour (see figure 6.34).

In particular, a decrease of the maximum peak of acceleration, as well as a temporal shift, can be observed due to the integration of the battery pack and the modification of the floor pan.

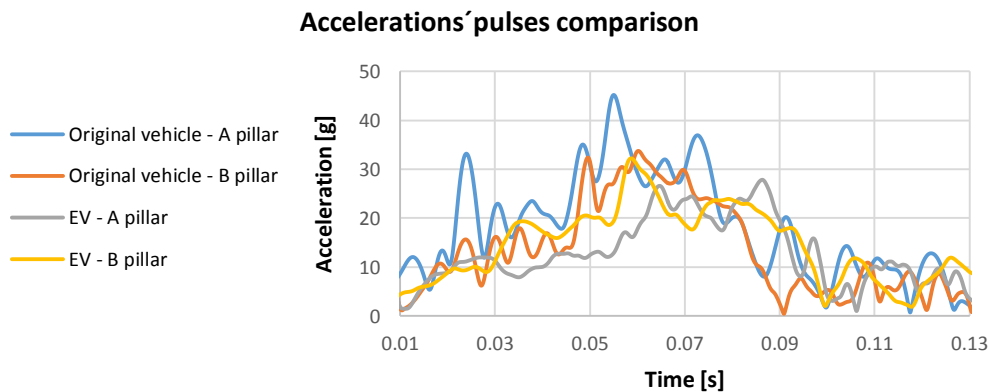


**Figure 6.34** Comparison of the resultant accelerations 'pulses in the original vehicle and in the EV.

It is important to note a maximum difference of 17 g in the measurements of the front accelerometers of the original vehicle and the EV.

As the acceleration peaks can be correlated to the severity of the injuries of the occupants [52], a variation of 17 g in the maximum crash pulse decreases the risk of a MAIS2+ injury, that defines injuries from moderate to lethal, by 52%, from 90 %, in case of 45 g, to 38% in case of 28 g. [52]

## 6.5 Discussion

Although the models used are not validated for all the crash test simulations considered, it is possible to retrieve important informations about the safety of the battery pack, observing the deformation of the cells in the different tests.

In particular, two tests deserve special attentions:

- the pole crash test with impact at the R-point;
- the frontal crash test against a deformable barrier with 40% overlap;

In these tests a high deformation ( $>0,02$ ) in the cells was found, indicating an hazardous situation for the battery pack.

The main cause is the improper structure of the vehicle that can not offer an appropriate protection of the battery pack, as well as of the occupants, as highlighted by the notable depth of intrusion in the pole crash test and by the high

deformation in the zone of the feet of the driver in the frontal crash test with 40 % overlap.

Moreover, the high peaks of the acceleration pulses of the original vehicle denote the possibility of serious injuries in case of crash, while the integration of the battery pack provides a decrement of the crash pulses in proximity of the A pillar of the vehicle.

The simulations can give important indications about possible improvements in the structure of the vehicle, as well as the particular risk of some crash configuration. Nevertheless, a more detailed and validated model of the vehicle, as well as a precise design of the battery pack and of the floor pan are necessary to provide an accurate assessment of the safety of the batteries.

## Conclusion and future works

The study proposes a novel approach for the battery pack design in the concept phase, basing the placement of the cells upon the probability of deformation in real accidents.

Thanks to the methodology, a fast battery pack design is possible, offering indications about the most adequate one for the vehicle considered, with respect to the evaluation parameters selected.

The tests of the results of the methodology indicate the possibility to a safe integration of the batteries in the desired vehicle, with the opportunity to modify actively the inertial properties and the location of the center of gravity of the automobile.

Moreover, the analysis of the crash test simulations suggests important improvements in the vehicle structure in order to increase the crashworthiness of the EV.

Although the methodology fulfils his role as helping tool in the concept phase, further improvements can be developed including:

- an expansion of the possible evaluation parameters, including, as example, the ratio between the surface and the volume of the battery pack, that can lead to an easier thermal management of the cells;
- the development of a detailed FE model of the battery pack, as well as of the floor pan, with the application of the right mechanical properties of the cells, retrieved by mechanical tests;
- the possibility to include cells with different orientations in the same battery pack in order to optimize the space utilization.



## References

- [1] Rick J., Marten I., *Batteries for electric cars-Challenges, opportunities and the outlook to 2020*, 2010, Boston consulting group;
- [2] Kuo T. C., Huang S. H., Zhang H. C., *Design for manufacture and design for "X" : concepts applications and perspectives*, May 2001, Computer & industrial engineering 41.3, 241-260;
- [3] Paine M., Paine D., Ellway J., Newland C., Worden S., *Safety precautions and assessments for crashes involving electric vehicles*, Australasian NCAP, Paper 11-0107;
- [4] Chan C. C., *The state of the art of electric, hybrid and fuel cell vehicles*, 2007, proceedings of the IEEE 95.4, 704-718;
- [5] Tesla models S 2012 battery pack, retrieved from <http://www.cnet.com/news/tesla-model-s-the-battery-pack/>;
- [6] Chevrolet Volt 2016 battery pack, retrieved from <http://www.autoevolution.com/news/2016-chevrolet-volt-propulsion-system-detailed-video-photo-gallery-88242.html>;
- [7] Nissan Leaf 2015 battery pack, retrieved from <http://cleantechnica.com/2014/07/01/nissan-leaf-replacement-battery-priced-5499/>;
- [8] ECE regulation number 100 (02 series);
- [9] FMVSS 305 regulation;
- [10] ISO 6491-1, ISO 6491-2, ISO 6491-3, ISO 6491-4 regulations;
- [11] Cicconi P., Germani P., Landi D., Mengarelli M., *Cooling simulation of an EV battery pack to support a retrofit project from Lead-acid to Li-ion cells*, 2013, Vehicle power and propulsion conference;
- [12] Thermal simulation's results, retrieved from [http://www.gauss-centre.eu/SharedDocs/Meldungen/GAUSS-CENTRE/EN/1\\_Year\\_of\\_Hermit.html](http://www.gauss-centre.eu/SharedDocs/Meldungen/GAUSS-CENTRE/EN/1_Year_of_Hermit.html);
- [13] Teibinger A., *SafeEV- Safe and small electric vehicles through advanced simulations methodologies*, November 2013, deliverable 3.1;
- [14] Luttenberger P., Ostrowski M., Kurz M., Sinz W., *Structural analysis of a body in white for battery integration using finite element and macro element with the focus on pole crash optimization*, September 2012;
- [15] Sinz W., Breitfuß C., Tomasch E., Gugler J., Feist F., Lacher H., *Integration of a crashworthy battery in a fully electric city bus*, 2012, International Journal of Crashworthiness 17.1: 105-118;
- [16] Wang Z., Shi S., Liu P., *Research progress on collision safety of electric vehicles*, 2011, Measuring technology and mechatronics automation;

- [17] Wierzbicki T., Sahraei E., *Homogenized mechanical properties for the jellyroll of cylindrical Lithium-ion cells*, 2013, Journal of power sources 241: 467-476;
- [18] Chen W., Wierzbicki T., *Relative merits of single-cell, multi cell and foam-filled thin-walled structures in energy absorption*, 2001, Thin-walled structures 39.4 : 287-306;
- [19] Hoffmann R., Reuter R., *Safety companion*, 2013, Carhs;
- [20] Chevrolet Volt pole crash test simulation image, retrieved from: <http://www.crash-analysis.com/pages/gallery.shtml> ;
- [21] Chevrolet Volt pole crash test photo, retrieved from: [http://en.wikipedia.org/wiki/Plug-in\\_electric\\_vehicle\\_fire\\_incidents](http://en.wikipedia.org/wiki/Plug-in_electric_vehicle_fire_incidents);
- [22] Barlow T. J., Latham S., McRae I. S., Boulter P. G., *A reference book of driving cycles for use in the measurement of road vehicle emission*, June 2009, TRL Limited ;
- [23] Young, K., Wang C., Wang L. Y., Strunz K., *Electric vehicle battery technologies - Electric vehicle integration into modern power networks*, 2013, Springer. 15-56;
- [24] Brousselly M., Biensan P., Bonhomme F., Blanchard P., Herreyre S., Nechev K., Staniewicz R. J., *Main aging mechanisms in Li ion batteries*, 2005, Journal of power sources, 146.1: 90-96;
- [25] Eckenstein L., Schmitt F., Hartmann B., *Lightweight measures for electric vehicles*, November 2012, ATZ worldwide, volume 112;
- [26] Kurz M., *Smartbatt- Smart and safe integration of batteries into electric vehicles*, 24 September 2012, EARPA safety workshop;
- [27] U.S. Department of Energy, *Advance battery development*, 2013, Annual progress report;
- [28] Vogt F., Große S., Hannawald L., *Method for the estimations of the deformation frequency of passenger cars with the German-in-depth-accidents study (GIDAS)*;
- [29] Huang M., *Vehicle crash mechanics*, 2010, CRC press, chapter 1;
- [30] Gillespie T. D., *Fundamentals of vehicle dynamics*, chap 4-6, 1990, Society of automotive engineers;
- [31] Vaidya R., Seshu P., Arora G., *Study of on-center handling behaviour of a vehicle*;
- [32] Mallick P. K., *Materials, design and manufacturing for lightweight vehicles*, 2010, Elsevier;
- [33] Roper L. D., *Physics of automobile rollovers*, 2001;
- [34] Automobile handling, retrieved from: [http://en.wikipedia.org/wiki/Automobile\\_handling](http://en.wikipedia.org/wiki/Automobile_handling);
- [35] D. Casanova, Sharp R. S., Symonds P., *Minimum time manoeuvring the significance of yaw inertia*, 2000, Vehicle System Dynamics;



- [36] Allen W. R., Klyde H. D., Rosenthal J. T., Smith M. D., *Estimation of passenger vehicle inertial properties and their effect on stability and handling*, 2003, Society of Automotive Engineers, SAE paper No. 2003-01-0966;
- [37] Geo Metro, reduced model, retrieved from <http://www.ncac.gwu.edu/vml/models.html> ;
- [38] Geo Metro characteristics, retrieved from [http://en.wikipedia.org/wiki/Geo\\_Metro](http://en.wikipedia.org/wiki/Geo_Metro);
- [39] Warner J., *Lithium-Ion battery packs for EVs*, 2014, Ed. G. Pistoia, Elsevier;
- [40] Panasonic NCR 18650 A photo and data, retrieved from <http://industrial.panasonic.com/lecs/www-data/pdf2/ACA4000/ACA4000CE254.pdf>;
- [41] Panasonic concept module, retrieved from <http://www.gizmag.com/panasonic-lithium-ion-battery-module/13030>;
- [42] Boston Power Swing 5300 photo and data, retrieved from <http://liionbms.com/pdf/bostonpower/swing5300.pdf>;
- [43] Boston Power Swing Key 442 photo and data, retrieved from <http://www.boston-power.com/products/swing442>;
- [44] Kokam Series 255 75 Ah photo and data, retrieved from [http://kokam.com/kokam/en/html/product/large\\_cells\\_over.html](http://kokam.com/kokam/en/html/product/large_cells_over.html);
- [45] Kokam KBM 255 75 Ah photo and data, retrieved from: [http://kokam.com/kokam/en/html/product/module\\_255\\_over.html](http://kokam.com/kokam/en/html/product/module_255_over.html);
- [46] Kia soul 2015 model photo, retrieved from: <http://www.kia-world.net/lithium-ion-polymer-batteries-soul-ev/>;
- [47] Renault Zoe 2014 model photo, retrieved from : <http://myrenaultzoe.com/>;
- [48] Fiat 500 E 2014 model photo, retrieved from : [http://www.motorauthority.com/news/1080522\\_2014-fiat-500e-2012-los-angeles-auto-show-preview](http://www.motorauthority.com/news/1080522_2014-fiat-500e-2012-los-angeles-auto-show-preview);
- [49] Livermore software technology corporation, *LS-Dyna keyword user's manual, Volume II-Materials models*, February 2014;
- [50] EuroNCAP regulation, *Full width frontal impact testing protocol*, June 2014, version 1.0
- [51] EuroNCAP regulation, *Pole side impact testing protocol*, June 2014, version 7.0;
- [52] Stigson H., Kullgren A., Rosén E., *Injury risk functions in frontal impacts using data from crash pulse recorders*, 2012, Annals of advances in automotive medicine/ annual scientific conference, vol. 56;
- [53] ECE regulation, *Classification and definition of vehicles*, 2013;
- [54] EuroNCAP regulation, *Vehicle specification, sponsorship, testing and retesting*, January 2015, version 6.4;

- [55] Passenger cars 'classification in the European market, retrieved from: [http://en.wikipedia.org/wiki/Euro\\_Car\\_Segment](http://en.wikipedia.org/wiki/Euro_Car_Segment);
- [56] Fiat 500 2012 model photo, retrieved from: [http://usnews.rankingsandreviews.com/cars-trucks/FIAT\\_500/2012/](http://usnews.rankingsandreviews.com/cars-trucks/FIAT_500/2012/);
- [57] Volkswagen Polo 2010 model photo, retrieved from: <http://www.parkers.co.uk/cars/prices/used/volkswagen/polo/>;
- [58] Ford Focus 2013 model photo, retrieved from: <http://quote.newcars.com/ford/focus/2013>;
- [59] BMW Series 3 2014 model photo, retrieved from: <http://www.topspeed.com/cars/bmw/2014-bmw-3-series-exclusive-sport-ar161871.html>;
- [60] Mercedes Class E 2014 model photo, retrieved from: [http://www.thecarconnection.com/overview/mercedes-benz\\_e-class\\_2014](http://www.thecarconnection.com/overview/mercedes-benz_e-class_2014);
- [61] Audi TT 2012 model photo, retrieved from: <http://atlantaga.auto.com/cars-for-sale89/audi-tt>;
- [62] Nissan Leaf 2014 model photo, retrieved from: <http://www.product-reviews.net/2014/12/08/nissan-leaf-replacement-battery-price-raises-longevity-concern/>;
- [63] Toyota Prius 2013 model, retrieved from: <http://blog.juicedhybrid.com/2012/03/15/how-are-hybrid-cars-efficient/>;
- [64] Chau K.T., *Pure electric vehicles*;
- [65] Battery pack for EVs, retrieved from: [http://en.wikipedia.org/wiki/Electric\\_vehicle\\_battery](http://en.wikipedia.org/wiki/Electric_vehicle_battery);
- [66] Drury W. D., Miller J. P., Jootel S. P., *An approach to cell selection to optimise battery pack size and mass for small battery electric vehicles*, November 2012;
- [67] Cylindrical cell structure drawing, retrieved from: [http://www.mpoweruk.com/cell\\_construction.htm](http://www.mpoweruk.com/cell_construction.htm);
- [68] 18650 cell photo, retrieved from: [http://batteryuniversity.com/learn/article/types\\_of\\_battery\\_cells](http://batteryuniversity.com/learn/article/types_of_battery_cells);
- [69] Trattinig, G., Werner L., *Battery Modelling for Crash Safety Simulation*, 2014, Automotive Battery Technology, Springer International Publishing, 19-35;
- [70] Pouch cell's volume variation photo, retrieved from: <http://www.epectec.com/batteries/prismatic-pouch-packs.html>;
- [71] Keil P., Burda P., *Development of a lithium-ion battery system*, March 2012;
- [72] Trigg T., Telleen P., *Global EV outlook: Understanding the electric vehicle landscape to 2020*, April 2013, Electric Vehicle Initiative;
- [73] Gartner J., Wheelock C., *Electric vehicles: 10 predictions for 2010*, 2009, Pike research;

- [74] Teibinger A., *SafeEV- Safe and small electric vehicles through advanced simulations methodologies*, December 2013, deliverable 2.2;
- [75] Wohlecker R., *Report on most likely crash scenarios for APVs (horizon in 2025) and projection methodology*, August 2013, MATISSE deliverable D1.1;
- [76] EuroNCAP regulation, *Assessment protocol-Adult occupant protection*, July 2014, version 7.0.1;
- [77] EuroNCAP regulation, *Offset deformable barrier frontal impact testing protocol*, June 2014, version 7.0;
- [78] Otte D., Sferco R., Schäfer R., Volker E., Thomas P., Welsch R., *Assessment of injury severity of nearside occupants in pole impacts to side of passenger cars in European traffic accidents- Analysis of German and UK in-depth data*, 2009;
- [79] EuroNCAP regulation, *Side impact mobile deformable barrier testing protocol*, June 2014, version 7.0.
- [80] Dodge Neon FE model, retrieved from <http://www.ncac.gwu.edu/vml/models.html> ;
- [81] Renault Twizy drawing, retrieved from: <http://www.renault.co.uk/cars/electric-vehicles/twizy/twizy/#/cars/electric-vehicles/twizy/twizy/ze-battery.jsp>.



## Appendix A Motor vehicles' classes

"Motor vehicle" means any power-driven vehicle, which is normally used to carry persons or goods by road. Vehicles such as agricultural tractors, which are only incidentally used for carrying persons or goods by road or for drawing, on the road, are not covered in the definition.

The work focuses about two particular classes of vehicles, described by the UNECE regulation [53]:

- category L;
- category M.

### A.1 Category L

Class L refers to motor vehicle with less than 4 wheels and it is divided in 7 sub categories:

- *category L1*: a two-wheeled vehicle with an engine cylinder capacity in the case of a thermic engine not exceeding 50 cm<sup>3</sup> and whatever the means of propulsion a maximum design speed not exceeding 50 km/h;
- *category L2*: a three-wheeled vehicle of any wheel arrangement with an engine cylinder capacity in the case of a thermic engine not exceeding 50 cm<sup>3</sup> and whatever the means of propulsion a maximum design speed not exceeding 50 km/h;
- *category L3*: a two-wheeled vehicle with an engine cylinder capacity in the case of a thermic engine exceeding 50 cm<sup>3</sup>, or whatever the means of propulsion a maximum design speed exceeding 50 km/h.
- *category L4*: a vehicle with three wheels asymmetrically arranged in relation to the longitudinal median plane with an engine cylinder capacity in the case of a thermic engine exceeding 50 cm<sup>3</sup> or whatever the means of propulsion a maximum design speed exceeding 50 km/h (motor cycles with sidecars);
- *category L6*: a vehicle with four wheels whose unladen mass is not more than 350 kg, not including the mass of the batteries in case of electric vehicles, whose maximum design speed is not more than 45 km/h, and whose maximum net power output does not exceed 4 kW;
- *category L7*: a vehicle with four wheels, other than that classified for the category L6, whose unladen mass is not more than 400 kg (550 kg for vehicles intended for carrying goods), not including the mass of batteries in the case of electric vehicles and whose maximum continuous rated power does not exceed 15 kW.

## A.2 Category M

Category M refers to power-driven vehicles having at least four wheels and used for the carriage of passengers and it includes three sub-classes:

- *category M1*: vehicles used for the carriage of passengers and comprising not more than eight seats in addition to the driver's seat;
- *category M2*: vehicles used for the carriage of passengers, comprising more than eight seats in addition to the driver's seat, and having a maximum mass not exceeding 5 tonnes;
- *category M3*: vehicles used for the carriage of passengers, comprising more than eight seats in addition to the driver's seat, and having a maximum mass exceeding 5 tonnes.

## A.3 Motor vehicle classes by EuroNCAP

As Euro NCAP is the most followed car safety performance assessment programme in Europe, its vehicles' classification is taken as example.

Euro NCAP groups cars into five main structural categories [54]:

- passenger car;
- MPV;
- off-roader;
- roadster;
- pickup.

As this thesis focuses on the passenger cars, just that category will be analysed though the results can be applied also to the other categories.

### A.3.1 Passenger car

A passenger car is a road motor vehicle having at least four wheels, intended for the carriage of passengers and designed to seat no more than nine persons including the driver. Passenger cars refer to the M1 category of the UNECE regulation.

The terms "*passenger car*" covers the following categories: [55]

- *Supermini*: is a class of automobile that covers the A and B segment of the Euro Market segment. A-segment or mini cars refers to cars limited approximately to 3600 mm in length; the most representative cars of this segment are Fiat 500, Fiat Panda, Volkswagen Up!, Mini, Hyundai i10.

B-segment or small cars refers to cars with a length from 3600 mm to 4200 mm, some representative vehicle of this class are Ford Fiesta, Renault Clio, and Volkswagen Polo.



**Figure A.1** Photo of a Fiat 500 2012 model (left) [56] representative of the A segment of the European market and a Volkswagen Polo 2010 model (right) [57], representative of the B segment of the European market.

- *Small family car*: is a class that cover the C-segment, or medium cars, of the Euro market and refers to vehicle limited from 4200 to 4600 mm in length, such a vehicle can be an hatchback (3 or 5 doors), sedan, station wagon and also cabrio for some market. This segment represents the most important class for the automotive markets; some representative vehicle of this class are Volkswagen Golf, Ford Focus, Skoda Octavia and Audi A3;



**Figure A.2** Photo of a Ford Focus 2013 model [58], representative of a vehicle of the C segment of the European market and of the small family car class.

- *Large family car*: is a class that corresponds to the D-segment of the Euro market and it refers to vehicle with a length from 4600 to 5000 mm approximately. Some representative vehicles of this class are: BMW 3 series, Volkswagen Passat and Audi A4.



**Figure A.3** Photo of a BMW series 3 2014 model [59], representative of a vehicle of the D segment of the European market and of the large family car class.

- *Executive*: is a class that corresponds to the E-segment or executive cars of the Euro Market and it refers to cars usually longer than 5000 mm and characterized by a luxury setup. The main representative of this sector are BMW 5 series, Mercedes E class and Audi A6.



**Figure A.4** Photo of a Mercedes class E 2014 model [60], representative of a vehicle of the E segment of the European market and of the executive class.

- *Roadster sport*: this class, included in the S-segment or sport coupes of the Euro market, refers to vehicles with just two seats and characterized by a sport setup and by the absence of a rigid and fixed roof; some exponents of this class are Audi TT, BMW Z4, Lotus Elise.



**Figure A.5** Photo of an Audi TT 2012 model [61], representative of a vehicle of the S segment of the European market and of the roadster sport class.



## Appendix B      Electric vehicle's definition and main components

An electric vehicle (EV) is a vehicle type that uses one or more electric motors for propulsion. An electric vehicle can be powered through a collector system by electricity from off-vehicle sources, or may self-contain a battery or generator to convert fuel to electricity. EVs include road and rail vehicles, surface and underwater vessels, electric aircraft and electrically powered space vehicles.

The work will focus in a particular way to battery electric road vehicles (BEV) and hybrid electric road vehicles (HEV).

The term BEV refers to a type of electric vehicle (EV) that uses only chemical energy stored in rechargeable battery packs. BEVs use electric motors and motor controllers instead of internal combustion engines (ICEs) for the propulsion.

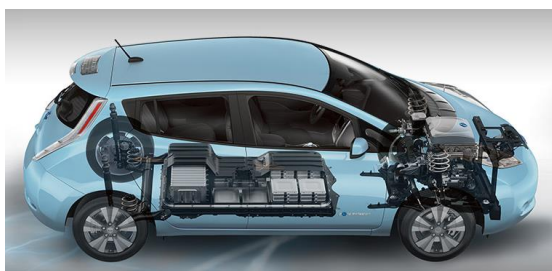


**Figure B.1**      Example of an electric road vehicle. [62]

A hybrid electric vehicle (HEV) uses instead a combination of an electric motor and an ICE for the propulsion, usually the electric motor provides the traction for low speeds, after that the ICE starts. As a BEV, a HEV utilizes batteries to store the energy needed for the traction but, since the electric kilometres range is much smaller than that of a BEV, the battery pack has usually a smaller energy. It has to be noted that the recharge of the batteries of an HEV can be through the electric network, these vehicle are called plug-in hybrid electric vehicle (PHEV) or just through regenerative braking and/or the power produced by the ICE.

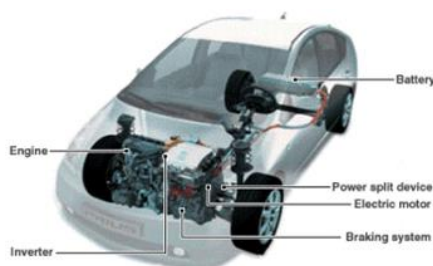


**Figure B.2**      Example of a hybrid electric vehicle. [63]

An electric vehicle is characterized by the complete absence of an internal combustion engine (ICE) and by the presence of the following main components:

- one or more electric motors;
- a battery pack composed by the cells, the housing and one or more battery management system (BMS);
- auxiliary components: an inverter (if needed), a charging system and a cooling system (if necessary).

### B.1 Electric motors

An electric motor is an electrical machine that converts electrical energy into mechanical energy.

Two main different categories of electric motors are available [64]:

- *Direct current (DC) motors:* A DC motor (figure B.3) takes advantage of the phenomena of repulsion of magnetic poles with different charge. An electromagnetic field is generated by a coil of wire charged by current. By switching the current on or off in a coil, its magnetic field can be switched on or off, moreover the magnetic field can be switched by  $180^\circ$  inverting the flow of the current. A commutator permits each armature coil to be activated in turn. Therefore, DC motors suffer from a problem due to the use of commutators and brushes. In fact, commutators cause torque ripples and limit the motor's speed, while brushes are responsible for friction. Moreover, due to the wear and tear, periodic maintenance is always required. These drawbacks make them less reliable and unsuitable for maintenance-free operation. The major advantages of DC drives are their maturity and simplicity. DC motors used to be widely accepted for EVs however, due to their relatively low efficiency and need of maintenance, DC drives are no longer attractive for the modern EVs.

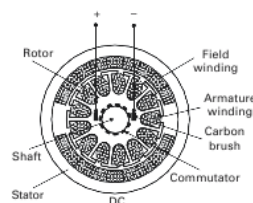
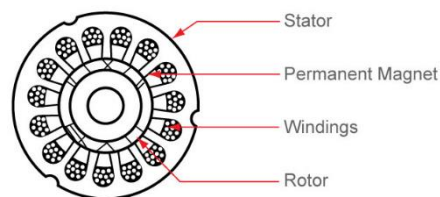


Figure B.3 Schematic section of a DC motor. [64]

- *Alternate current (AC) motors* : in opposition with the DC motors, AC motors are driven by alternate current (AC) so an inverter is always needed .Three subcategories are particularly attractive for EV's applications:
  - *Permanent-magnet synchronous motors (PMSM)*: In this type of motors (figure B.4), the magnetic field is generated by permanent magnets (almost exclusively rare earth magnets) therefore no power is required to generate the rotor field. As a result, the PMSM is extremely compact and can be simply controlled with high dynamic performances. The torque is fully available starting at zero speed, and it is constant over a wide speed range. Therefore such a motor is well-suited to traction applications. Furthermore, the efficiency is very high also in the partial load range. The only disadvantage of the PMSM is their use of rare earth magnets. These are expensive, and are subjected to significant price fluctuations.



**Figure B.4-** Schematic section of a permanent magnet synchronous motor. [64]

- *Electrically excited synchronous motors (ESM)*: in this motors (figure B.5) the copper coil in the rotor, fed through slip rings, is responsible for the rotor field. This excitation circuit requires more space than do permanent magnets, therefore ESMs are usually bigger than a PMSM. One of their advantages is the possibility to control the magnetic field without generating additional losses. As a result, the efficiency rate falls less sharply at high speeds, nevertheless it is less than that for a PMSM as a result of the required field current. A high excitation field current is required if the machine is operated at high torques. As a consequence, the rotor temperature increases significantly.

After such boost operation, a no-load interval is required so that the rotor can cool down again. This restricts the possible number of acceleration cycles. Another point worth mentioning is the additional degree of freedom regarding functional safety. The electrical excitation can be switched off, so that just like an induction motor, a voltage is no longer induced.

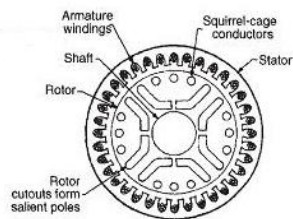


**Figure B.5** Schematic section of an electrically excited synchronous motor. [64]

- *Induction motors* (IM): in an IM (figure B.6) the current induced in a squirrel-cage rotor as a result of the differential frequency (slip) with respect to the stator field generates the rotor field. The rotor has a simple and robust mechanical design, can withstand high speeds and has no wearing parts. An induction motor is relatively less efficient in the partial load range than a PMSM, due to the rotor losses. The speed-torque characteristic curve is linear up to the corner speed. After this point, the torque decreases quadratically with respect to the speed, thus more significantly than for a PMSM. One advantage is its high peak power in the middle of the speed range.

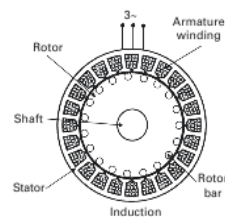


**Figure B.6** Schematic section of an induction motor. [64]

## B.2 The battery pack

The battery pack is both the energy source of an electric vehicle and currently its most expensive component.

It contains the following main components:

- *the cells*, that provide the energy necessary for the traction;
- *the battery management system (BMS)*, that is responsible for the collection of data from the battery pack's sensors and for the communications with the world outside the battery pack;
- *the relays*, which control the distribution of the battery pack's electrical power to the output terminals and of course, a variety of temperature, voltage, and current sensors;
- *the housing*, that has to provide structural protection for the cells in case of accident and it has to avoid any possible penetration of fluid in order to prevent any possible damage of the cells.

It has also to be noticed that due its considerable weight the battery pack can strongly influence the dynamic response of the vehicle.

Because of its crucial importance for the safety of the user and the correct operation of the vehicle the battery pack designs are complex and vary widely by manufacturer and specific application. [65]

## B.3 Cells for an electric vehicle

A wide range of batteries is currently available for EVs application, and many researches are developed in order to increase the electrical properties and decrease the production costs. As the chemistry of the components of the cell influences the energy features of the cell, it is worth analysing the most used chemistries so far, they can be resumed in [66]:

- *Lead acid batteries*
- *Nickel metal hydride batteries*
- *Li-ion batteries.*

### B.3.1 Lead acid battery batteries

The lead–acid battery is the oldest type of rechargeable battery. Despite having a very low energy-to-weight ratio and a low energy-to-volume ratio, its ability to supply high currents means that the cells have a relatively large power-to-weight ratio. As they are inexpensive compared to recent technologies, lead-acid batteries are widely used even when peak current is not important.

These features, along with their low cost, makes it attractive for use in motor vehicles, but usually just to provide the high current required by automobile starter motors.

Nevertheless it is possible to find in the current market also deep cycle batteries used for electric vehicles like forklifts or golf carts.

Traditionally, most electric vehicles have used lead-acid batteries due to their mature technology, high availability, and low cost.

Lead-acid batteries' use in EV applications leads to a notable increase of the total vehicle mass, for this reason this type of battery is not more interesting for EVs' application. [66]

### **B.3.2 Nickel metal hydride batteries**

NiMH batteries were considered the most interesting option for an EV. The primary advantage of this chemistry is its proven longevity and safety. The primary drawbacks are limitations in energy and power density, and low prospects for future cost reductions. Not only are energy and power densities unlikely to improve much further but NiMH costs are not expected to drop much further with increased production. For these reasons the attention of the EVs' producer is no more pointed to this type of battery. [66]

### **B.3.3 Lithium ions batteries**

Lithium-ion (and similar lithium polymer) batteries, widely known through their use in laptops and consumer electronics, dominate the most recent group of EVs in development. They permit almost 200 Wh/kg energy density and 80 to 90% charge/discharge efficiency. Nevertheless it has to be noted that traditional lithium-ion batteries suffer from a short cycle lives and significant degradation with age. Moreover, they can pose a fire safety risk if punctured or charged improperly.

A notable attention it is currently posed to the possibility to increase the features of lithium ions batteries through the use of metals and alloy for the cathode.

As currently most of the attentions are posed to Li-ion batteries, a more detailed description is needed, due to the different features that these cells exhibit due to their different shapes. Li-ion cells can be divide into 3 categories:

- *cylindrical cell;*
- *prismatic cells;*
- *pouch cells.*

Table B.1 offer a comparative view of the principal advantages and disadvantages of the different shapes available for the Li-ion cells. [39]

	<b>Cylindrical</b>	<b>Prismatic</b>	<b>Pouch</b>
<b>Energy density</b>	Medium	High	Highest
<b>Mechanical stability</b>	High	Medium	Low
<b>Thermal performance</b>	High	Highest	Medium
<b>Space utilisation</b>	Low	High	Highest
<b>Manufacturing cost</b>	High	Medium	Low
<b>Pressure withstand</b>	High	Medium	Low

**Table B.1** Comparative view of the characteristics of the different shapes available for the Li-ion cells

### B.3.3.1 Cylindrical cells

The main advantages of this type of cells are the ease of manufacture and the good mechanical stability; in fact, thanks to their shape they can withstand high internal pressures without deforming. In addition, a cylindrical design does not change size during a charging/discharging cycle. [39]

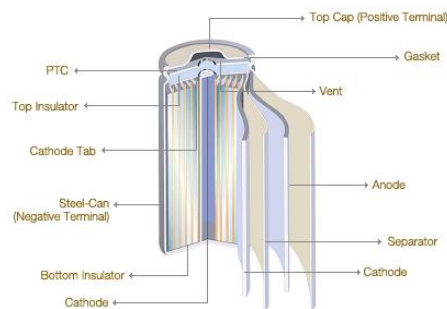


**Figure B.7** Schematic representation of a cylindrical cell. [67]

The 18650, illustrated in figure B.8, is one of the most popular cell packages.



**Figure B.8** Photo of cylindrical 18650 cells. [68]

The 18650 is the most optimized cell and offers the lowest cost per Wh. Even though the cylindrical cell does not fully utilize the space by creating air cavities on side-by-side placement, the high energy density of these cells can compensate for its non-ideal stacking characteristics, moreover the empty space can be used for the cooling system in order to improve the thermal management of the battery pack.

Most lithium and nickel-based cylindrical cells include a positive thermal coefficient (PTC) switch that acts as safety system in case of malfunctioning : when exposed to excessive current, the normally conductive polymer heats up and becomes resistive, acting as short circuit protection. Once the short circuit is removed, the PTC cools down and returns to conductive state. [69]

### B.3.3.2 Prismatic cells

The modern prismatic cell (figure B.9) satisfies the demand for thinner sizes. Prismatic cells make optimal use of space by using the layered approach. No universal format exists and each manufacturer designs its own. The prismatic cell requires a slightly thicker wall to compensate for decreased mechanical stability compared to the cylindrical design. [39]

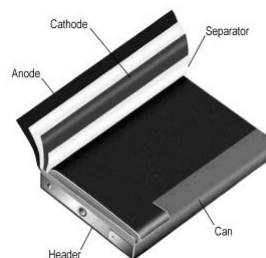


**Figure B.9** Schematic representation of a prismatic cell. [67]



### B.3.3.3 Pouch cells

The pouch cell offers a radical new design. Rather than using a metallic cylinder, conductive foil-tabs are welded to the electrodes and brought to the outside in a fully sealed way (see figure B.10).

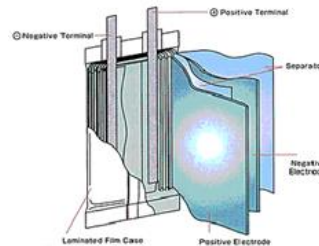


**Figure B.10** Schematic representation of a pouch cell. [67]

The pouch cell makes the most efficient use of space and achieves a 90–95 % packaging efficiency, the highest among all the cells considered. Eliminating the metal enclosure reduces weight but leads to the need of an external structure for the support and protection of the cell. No standardized pouch cells exist; each manufacturer designs its own.

The capacity is lower than cylindrical cells, moreover, provision must be made in the battery compartment for expansion during the charging and discharging cycle (figure B.11). [39]



**Figure B.11** Example of the variation in volume of a pouch cell during the charging/discharging cycle. [70]

## B.4 Battery housing

The battery housing is responsible for the structural safety of the cells and for the connections of the battery pack to the vehicle.

There is no standard design and every manufacturer utilises its own design principles in order to have the best compromise between safety and weight.

The design of the battery pack is strongly influenced by the cells' shape and characteristics as well as the cells disposition inside the vehicle. A notable

attention is currently posed about improving the ratio between the total weight of the battery pack and the battery housing weight.

In order to reduce the manufacturing costs and increase the safety, inside the battery housing, the cells are organized in modules, in which usually, for safety reason, each module has a voltage less than 60 V (figure B.12). [71]

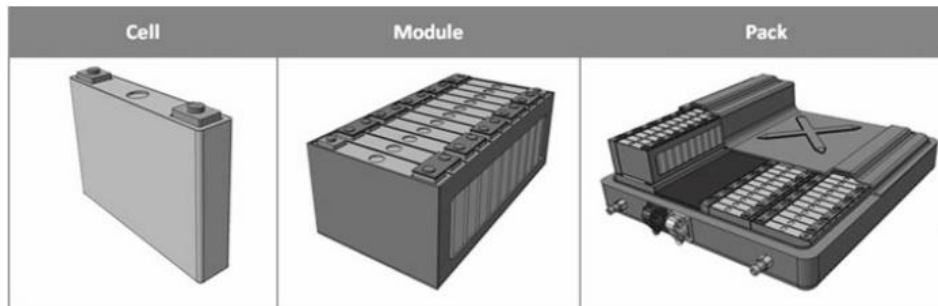


**Figure B.12** Example of the assembly of cells in modules and arrangement of modules in a battery pack. [71]

Inside each module the cells are connect in parallel or series in order to achieve the desired voltage and capacity, the same happens to the modules inside the battery housing (figure B.13). [19]

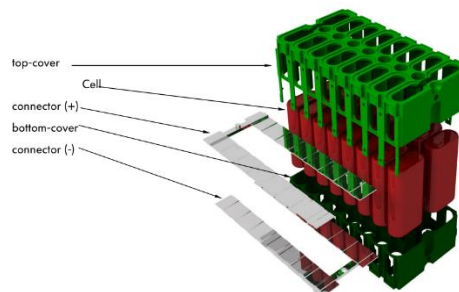


**Figure B.13** Example of the assembly of cells in modules and of the connections between the cells. [71]

## B.5 The battery management system (BMS)

To guarantee the safe operation of the batteries, a battery management system (BMS) is essential. Its task is to continuously monitor voltages, currents and temperatures inside the batteries. [71]

In case of overvoltage, undervoltage, as well as too high currents or temperature, the BMS requests the load to be reduced or shuts down the battery pack in case

of emergency. The BMS is also required for state of charge determination in order to display the remaining energy and control cell balancing mechanisms during the charging process.

The main parameters controlled by the BMS are:

- voltage: total voltage, voltages of individual cells;
- temperature: average temperature, coolant output temperature, or temperatures of the single cells;
- state of charge(SOC) or depth of discharge (DOD): to indicate the charge level of the battery and the residual energy;
- coolant flow: for cooled batteries;
- current: current in or out of the batteries;

## **Appendix C      Electric vehicles ‘market**

Although the first electric car appeared in the 1884, the electric vehicle market had a particular history.

Electric cars were very popular at the beginning of the 20<sup>th</sup> century as they could provide a level of comfort and ease of operation that could not be achieved by the ICE vehicles of that time.

Soon the advances in the ICE cars, the greater range provided by internal combustion engines, as well as the much faster refuelling time, caused a rapid growth of the petroleum infrastructure.

This led the mass production vehicle manufactures, especially Ford, to choose the gasoline engine as preferred engine for automotive traction. As consequence, the price of gasoline powered vehicles decreased to less than an half of an equivalent electric car, resulting in the total elimination of the electric vehicles from the US automobile market by the beginning of 1930s.

Nevertheless, the increasing cost of petroleum as the always-growing concern about the environment and the pollution in the cities led to a new interest in electric vehicle in the 2000s.

Such an interest has been growing, driven by the continuous advance in the technology and the promise of the decrease of the cost of electric vehicles.

At the current time, the electric vehicle market has just a little share of the entire car fleet but need to be accurately analysed in order to understand its real importance.

Due to the wide range of factors that influences this market and the lack of a real statistical trend, due to the recent expansion of the sector, an analysis of the latest forecasts has been developed. Furthermore the European market, as well as the Austrian and German market, have been considered as examples in order to check the correctness of the forecasts.

### **C.1.1 Electric vehicle market forecast analysis**

At the present time, two are the main negative factors that limit the EVs’ market expansions by the view of the customers [1]:

- The elevated cost of the vehicle;
- The limitation in the kilometres range.

As the second factor seems to be less important in the future thanks to the advance in the battery technology and an accurate study of the kilometres range needed by the customers, the actual cost of an electric car is actually the most influencing factor as shown also by the past history of this sector.

For this reason, it is claimed by many experts that, as the costs will decrease, the market will be subject to a rapid growth; as currently the most expensive component of an electric vehicle are the batteries, the variation of the cost of an electric vehicle can be directly linked to the cost of the batteries.

As the battery market for EVs is directly dependent from the EV market itself, an increase of the sale will produce a decrease of the cost of the batteries, which will lead to a decrease of the total cost of the vehicle. Moreover, an increase of the sales will produce more interest in the manufactures about the investments in R&D researches, which will produce both an increase of the quality as a decrease of the price, as effect of the economy of scale.

However, the process would have a slow growing rate if no external action were applied.

Recent studies claim that national financials policy initiatives could be the kick-starter of the process. Through this hypothesis, the cost of the batteries can be forecasted, as well as the spreading of the electric vehicle [1].

By these studies, the cost of the batteries is supposed to drop in the next 5 years (see figure C.1).

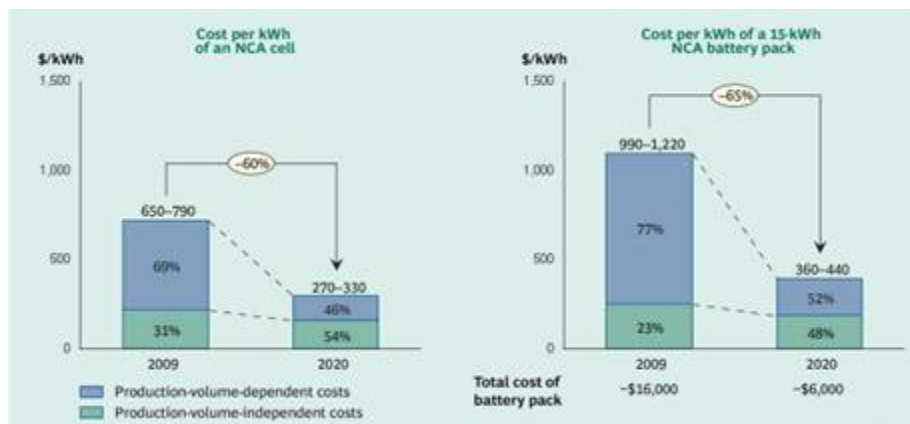
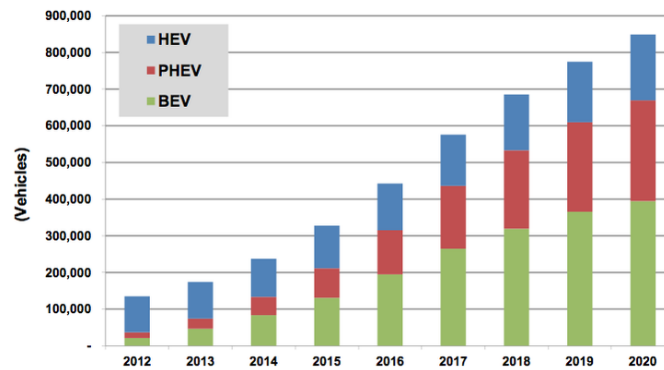


Figure C.1 Resume of the drop of the cost of the electric vehicle cells forecasted. [1]

These factor will act as a booster for the EVs' market, that it is believed to have an exponential grown worldwide in the next years (figure C.2). [72]



**Figure C.2** Resuming graph of the increase in the new matriculation of EVs forecasted.

The EVs' market it is supposed to be subject to a worldwide expansion as claimed by Pike research, nevertheless the next attentions will focus on the European market in order to check the validity of the forecast [73].

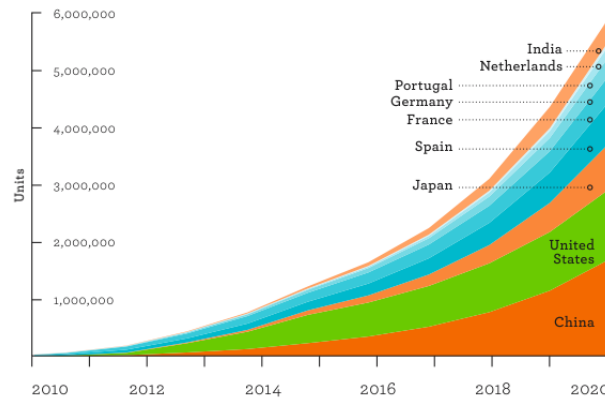


**Figure C.3** Resuming graph of the increase in the of EV fleet forecasted.

### C.1.2 Electric vehicle market in Europe

As a general vision of the electric cars 'market is necessary to provide the right trend information the European market has been analysed before focusing on other specific countries' markets.

A new vehicle matriculation analysis was at first performed, thanks to the data provided by the Eurostat database. As it is possible to note in figure C.4 the number of matriculation increased considerably since 2010.

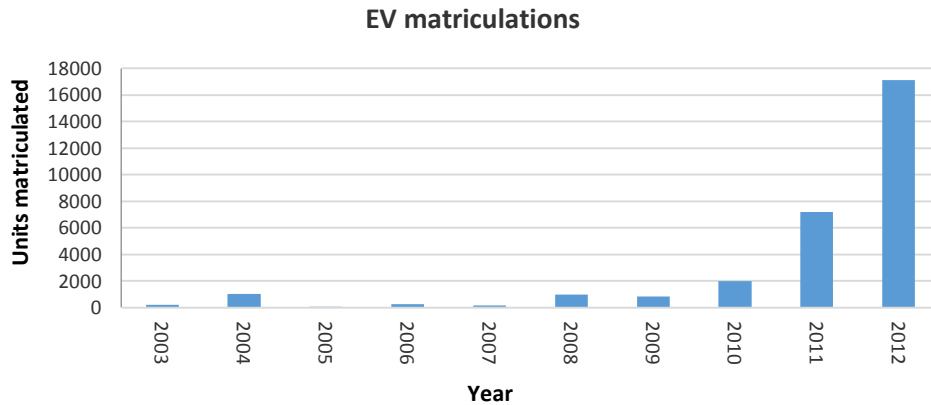


**Figure C.4** EVs matriculation registered by the Eurostat database.

Nevertheless, the analysis of the number of matriculations itself can not provide the right identification of a trend. For this reason the grow rate of the matriculations was examined.

The growth rate, calculated as in equation C.1, permits a rapid identification of the trend of a series as it directly compares the data of two different periods, underlining the difference. The trend of the growth rate of the EV's market found is exposed in figure C.5 with a graphic comparison to the ICE cars' growing rate.

$$\text{Growth rate} = \left( \frac{X_t}{X_{t-1}} - 1 \right) * 100 \quad \text{C.1}$$

**Equation C.1** Definition of the growing rate; it is defined trough the ratio between the value of a variable at the time t ( $X_t$ ) and the same variable in the previous period ( $X_{t-1}$ ) minus 1, and the multiplied per 100 in order to have a percentage value.

While ICE cars shows a negative trend in the last three years period, with a decreasing rate about -4 % in 2012, EVs' growth rate exhibits a growing trend always over 100% since 2008.

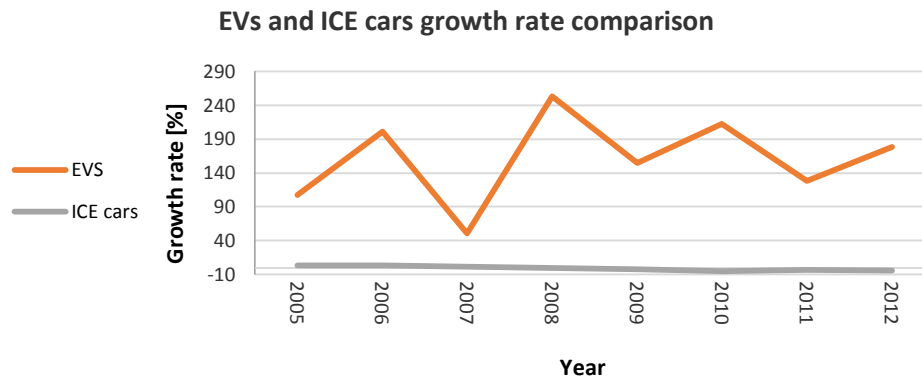


**Figure C.5** Graphic comparison between the growth rate of the EVs' matriculations and the ICE cars' one thanks to the data provided by the EUROSTAT database. Note the extreme difference in the growth rate in the entire period analysed.

Nevertheless has to be noted that the number of EVs matriculated remains a small percentage of the total fleet as shown in table C.1.

Year	EV's matriculations [units]	ICE vehicles 'matriculations [units]	EV/ICE
2010	1998	15824828	0.0126
2011	7205	15652855	0.0460
2012	170107	14708997	0.1163

**Table C.1** Resuming table of the comparison in the number of matriculations between EVs and ICE cars. Note the small ration between the two categories.

A high correlation between the forecasts and the statistical analysis has been found with a difference of about 3000 unit in 2012, confirming the validity of the forecast.



### C.1.3 Electric vehicle market in Germany and Austria

In order to check presence of the previously exposed trends in national markets, two countries' markets were analysed: German and Austrian one.

The two countries present a notable difference in population, nevertheless similar trends can be found analysing the national databases.

The matriculation rate for ICE passenger cars exhibit in both markets a slightly decreasing trend, with just two energy source with a positive matriculation growth: hybrid and electric vehicles (see figure C.6 and C.7).

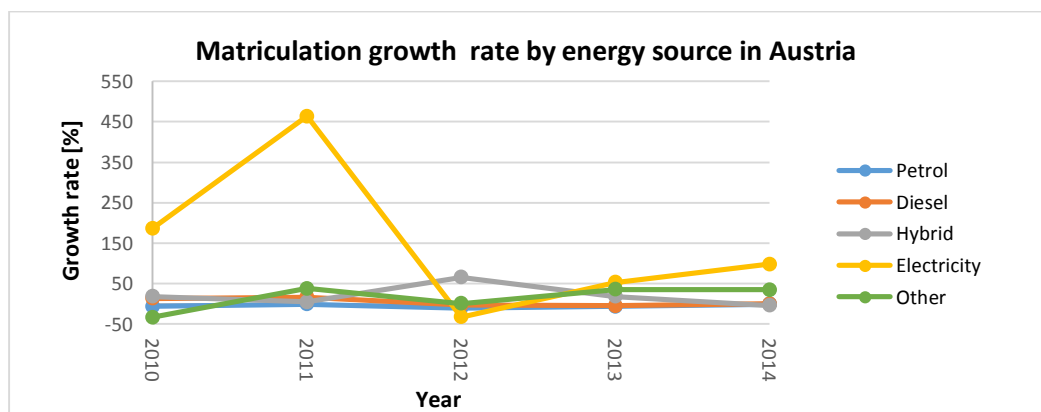


Figure C.6 Graphic comparison of the growth rate of passenger cars by different energy source in the Austrian market in the period between 2010 and 2014 (until August 2014).

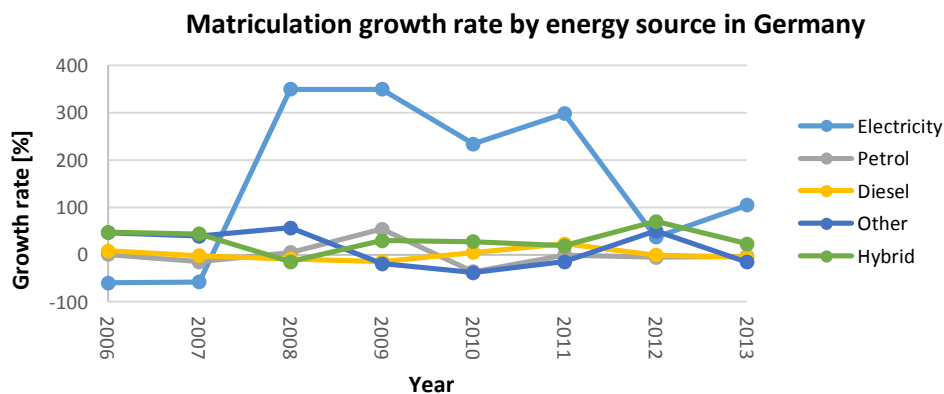


Figure C.7 Graphic comparison of the growth rate of passenger cars by different energy source in the German market in the period between 2006 and 2013.

It can be observed that, despite a negative growth rate of the passenger cars based on the use of petrol and diesel, the trend of EVs and HEVs is always positive in the period observed, although wide oscillations are present.

Nevertheless, it has to be noted that the small number of units causes the oscillations in the trends, in fact, just a little variation in the units matriculated produces a sensible change in the trend.

It is worth mentioning that despite the high growth rate the share of EVs' matriculations remains a small percentage of the total matriculation, as shown in figure C.8 and C.9

**Matriculation by energy source in 2013 in Austria**

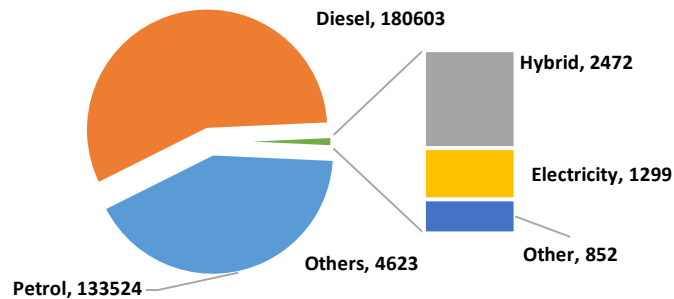


**Figure C.8** Graphic comparison of the matriculation of passenger cars in Austria in 2013 by energy source.

**Matriculation by energy source in 2013 in Germany**

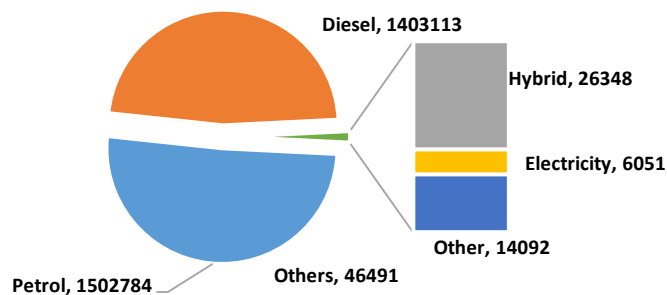


**Figure C.9** Graphic comparison of the matriculation of passenger cars in Germany in 2013 by energy source.

## Appendix D Accidents in urban scenarios

As the work focuses at the development of a vehicle for an urban scenario it is worth analysing the accidents in the urban roads in order to understand the level of danger to which a vehicle can be subject.

### D.1 Accidents scenario in Europe, Germany and Italy

In order to have a view of the problem as complete as possible, the UNECE database, that contains accidents in the entire Europe, was at first analysed.

It was found in the analysis that urban roads are the road type in which accidents are most frequent.

In the year 2012, a total number of 1547106 car-to-car accidents were reported to the UNECE database, among these almost 70% happened in urban roads, corresponding to a total number of 1078067 accidents, against just 89407 accidents in highways (see figure D.1).

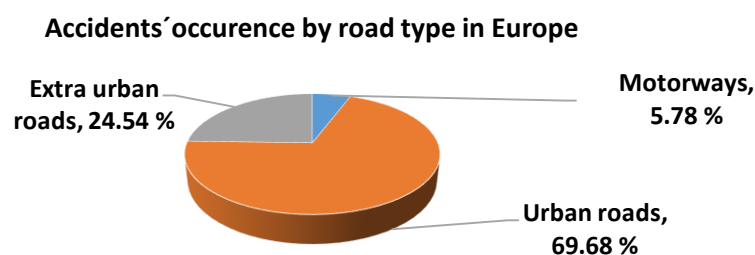


**Figure D.1** Distribution of incidents reported in the UNECE database by road type.

A similar share was found also in the German roads, analysing the GIDAS database (see figure D.2).

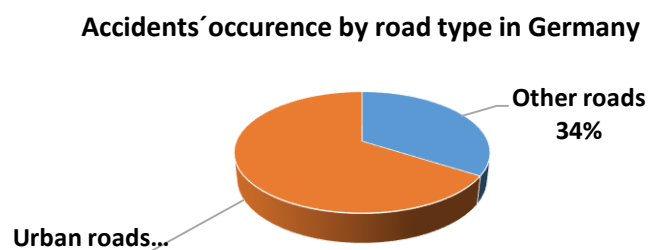


**Figure D.2** Distribution of incidents reported in the GIDAS database by road type.

Italian roads do not differ from the trends found in Germany and Europe, with a percentage of urban accidents major than 75%. Nevertheless, it has to be noted that the database analysed could not permit to distinguish car-to-car accidents from car-to-pedestrian accidents.

**Accidents' occurrence by road type in Italy**

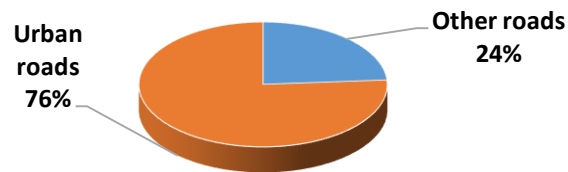


**Figure D.3** Distribution of accidents reported in the ISTAT database by road type.

As the Italian database presents a wide number of historical data, a statistical analysis was performed in order to underline the possible presence of a trend. Through the investigation of the data from 1954 to 2011, it was possible to extrapolate a forecast for the trend of the urban accidents in the Italian roads (figure D.4).

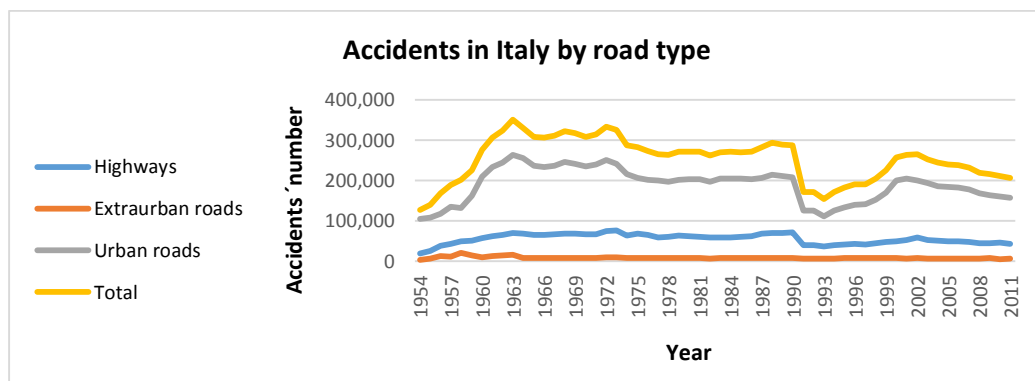


**Figure D.4** Number of accidents in the Italian urban roads in the period from 1954 to 2011, as found in the ISTAT database.

As presumable, the number of accidents increased as the Italian cars 'fleet grew', especially between 1954 and 1962, showing, after that year, an oscillating decreasing trend.

As the actual cars are considerably different from the vehicles, that can be found before 1990s, thanks to the advance in the driving performances as well as the introduction of active safety systems (ABS, ESP,....), just the data after 1990 were considered in the further analysis.

In order to smooth the oscillations, the data were averaged with a mobile bandwidth of 11 years, observing a linear trend proposed in figure D.5.

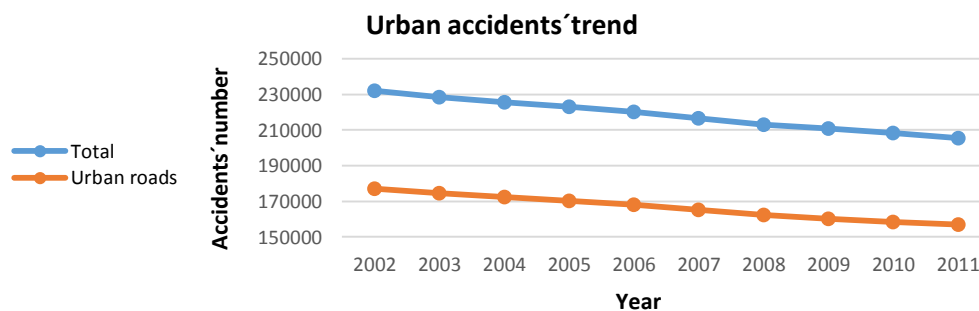


**Figure D.5** Trend of the number of accidents found applying a mobile bandwidth of 11 years to the data of the ISTAT database.

The series presents an easily recognisable descending trend; therefore, a linear interpolation was applied in order to forecast the trend in the years between 2012 and 2028.

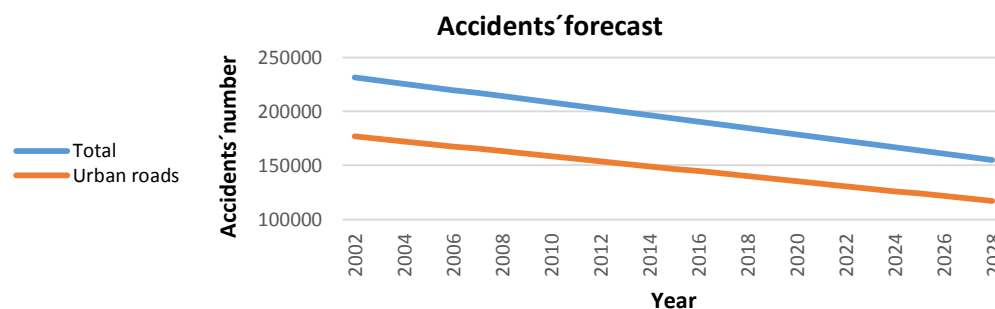


**Figure D.6** Forecast on the number of accidents in Italy.

It is worth observing that, although the total number of accidents will decrease, the percentage of urban accidents will remain almost constant in the next 15 years (see figure D.7) as proof of the importance of the safety design of a vehicle for the urban environment.

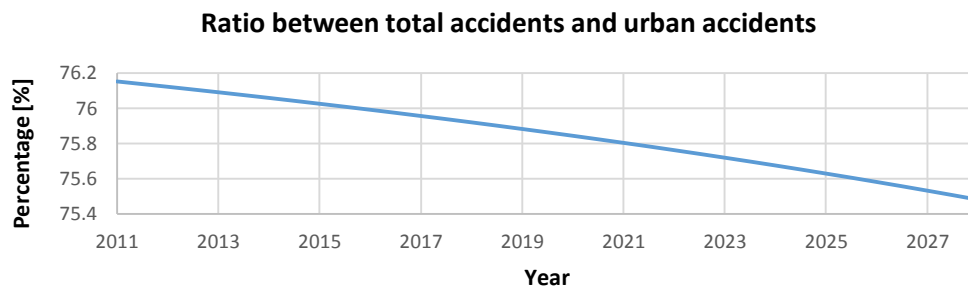


**Figure D.7** Ratio between the total number of accidents and the urban accidents, based upon the forecast developed with the ISTAT database data.

It is possible to find in the literature previous studies that indicate the most frequent, and dangerous, causes of accidents in urban scenarios [74].

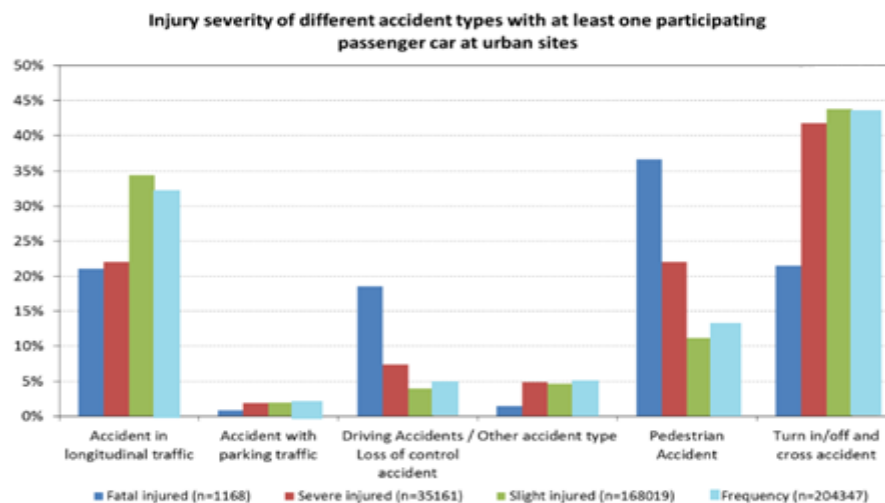


**Figure D.8** Injuries distribution by type of accident in urban scenarios.

Due to the high total number of accidents in the first and last configuration, they were analysed in detail in order to identify common trends.

In particular, the principal direction of force (PDoF) was controlled with the purpose to verify the need to introduce a new crash test to verify the safety of a vehicle in an urban environment.

Side impacts, in particular, show a wide variation of the PDoFs, nevertheless two principal directions can be found (figure D.8).

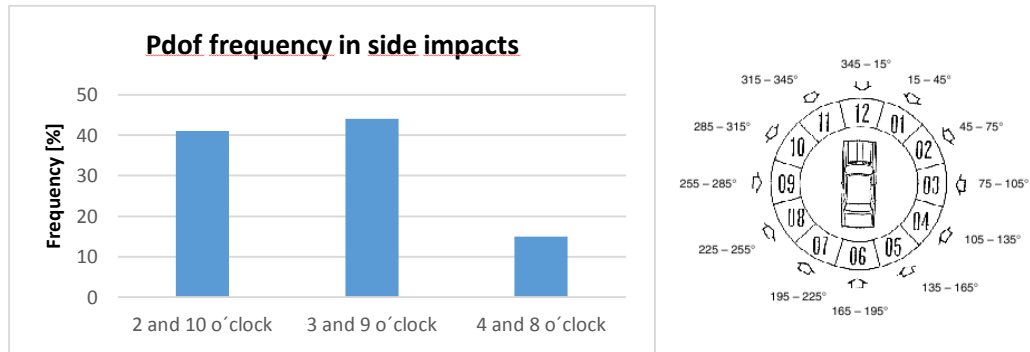


**Figure D.9** PDoF frequencies in side impacts, found in the GIDAS database.

It is worth noting the high frequency of accidents with PDoF with a direction of 2 and 10 o'clock (40 %), just 4 % less than the frequency of perpendicular crashes. Moreover, focusing the attention to junction accidents, it can be found that oblique PDoFs have an higher frequency than perpendicular or longitudinal PDoFs (figure D.10). [75]

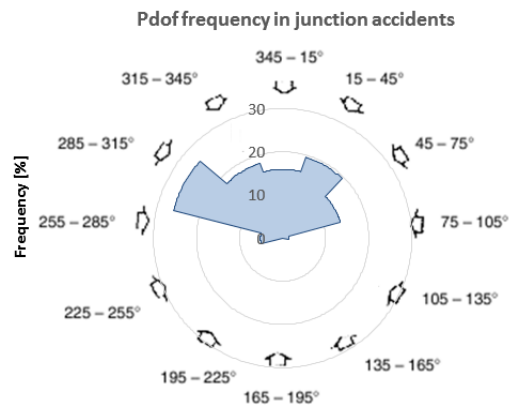


**Figure D.10** PDoF frequencies in side junction impacts.

Due to the high frequencies of an oblique PDoF, found both in side and junction accidents, this configuration was considered important in an urban environment and will therefore be tested.

## Appendix E EuroNCAP crash tests

EuroNCAP is one of the main performance assessment program worldwide, for this reason its crash tests are taken as reference both by consumers and producers. Although many are the tests possible the main are [76]:

- frontal crash test against a rigid wall;
- frontal crash test against a deformable barrier;
- side pole crash test;
- side impact crash test.

### E.1 Frontal crash test against a rigid wall

Euro NCAP tests cars against a rigid barrier with full overlap at a test speed of 50km/h. A small female frontal impact dummy (hybrid III 5% dummy) is used in the front driver's seat and in the rear passenger side seat. [50]

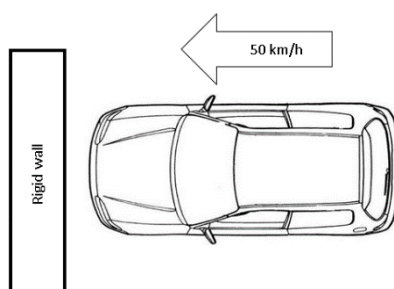


**Figure E.1** Schematic representation of the configuration of the vehicle in the crash test against a rigid wall by EuroNCAP.

### E.2 Frontal crash test against a deformable barrier

The second standard crash test is configured with a vehicle at 64 km/h against a deformable barrier with a 40 % overlap. This condition is particularly critical as just a part of the frontal structure of the vehicle absorb the entire energy of the impact. This usually leads to a bigger deformation in the zone of the feet of the driver.

For this crash test 3 different dummies are used:

- in the front seats are set two Hybrid III 50% dummies;
- in the rear left seat is set a Q3 dummy;



- in the rear right seat is set a Q1.5 dummy. [77]

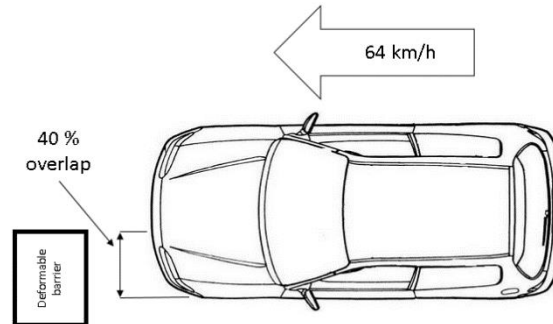


**Figure E.2** Schematic representation of the configuration of the vehicle in the crash test against a deformable barrier with 40% overlap by EuroNCAP.

### E.3 Pole crash test

The pole test crash test is developed in order to check the safety of the driver and passengers in case of impact against a narrow object. The pole's diameter is set to 254 mm and the vehicle is speeded at 29 km/h, with the impact point in line with the R-point of the dummy, which in this test is an ES-2. [51]

It has to be noted that it has been proposed to raise the impact speed to 32 km/h and to develop a test with the speed direction set to 75° due to the higher depth of intrusion that this configuration can produce. [78]

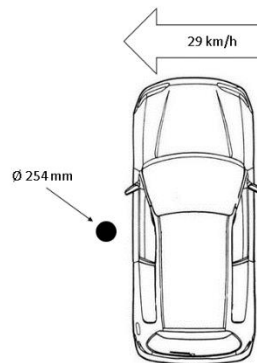


**Figure E.3** Schematic representation of the configuration of the vehicle in the pole crash test by EuroNCAP.

#### E.4 Side impact crash test

The side impact crash test represents the simulation of an impact between 2 vehicles driving in perpendicular directions. In order to test the safety of the driver and the passengers, the crash is simulated speeding a mobile deformable barrier at 50 km/h against the vehicle. An ES-2 dummy is set at the driver seat, while a Q 1.5 dummy is posed on the rear left seat and a Q 3 dummy in the rear right seat. [79]

The trolley mass is actually 950 kg, although it has been proposed to raise it to 1300 kg and modify the barrier type by year 2015. [19]

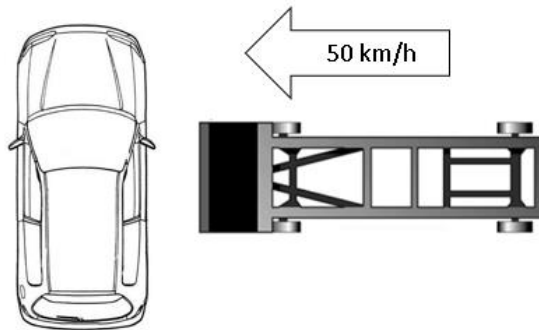


**Figure E.4** Schematic representation of the configuration of the vehicle in the side impact crash test by EuroNCAP.

## Appendix F Application of the methodology to different vehicles

With the purpose to test the universality of the application of the methodology, it was applied, successfully, to vehicles member of the M1 and L7e class; nevertheless the results were not tested with FEAs due to the notable amount of time required or the lack of validated finite element models of the vehicle considered.

In particular the following vehicles were considered:

- the Dodge Neon, a M1 car, member of the large family car segment [80];
- the Renault Twizy, a vehicle belonging to the L7e class;
- a concept of an L7e vehicle, thanks to the TU Graz.

The battery packs for the vehicles were modelled with the Boston Power 5300 cells; due to the diversity in dimensions and masses of the vehicle considered, different number of cells are required.

For the Dodge Neon a range of 200 km was set as goal, due to the design kilometres range and a total mass of 1400 kg, the vehicle requires 35 Kwh for the electric propulsion that are provided by 1817 cells.

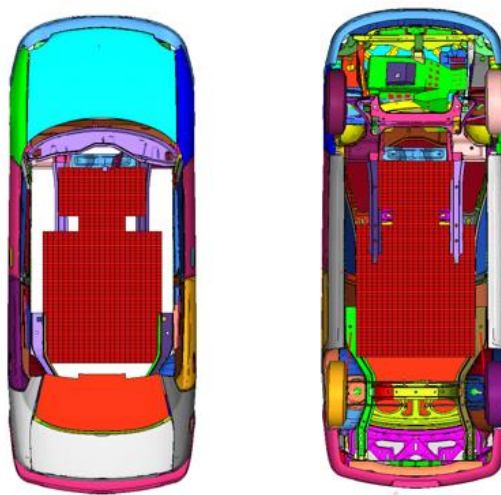
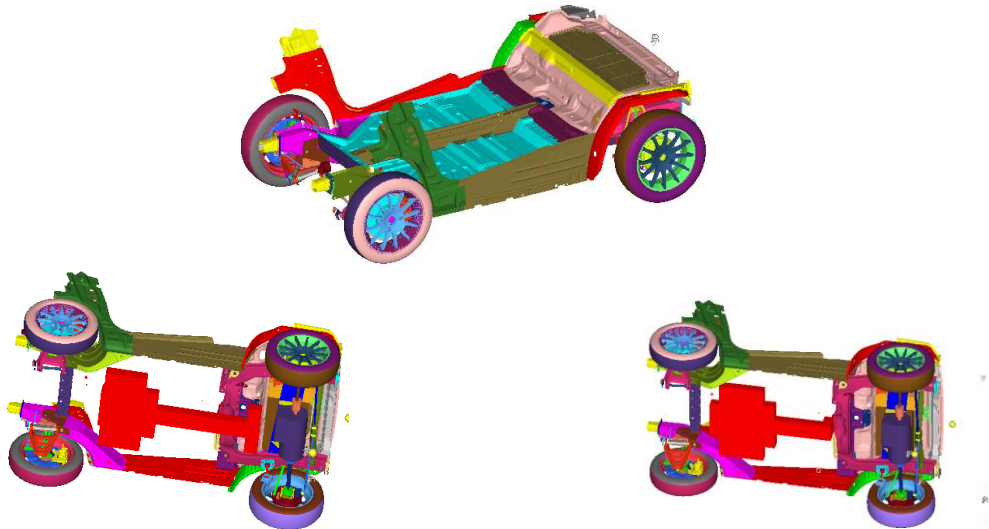


Figure F.1 Example of the application of the methodology to the Dodge Neon. [80]

For the concept of L7e vehicle provided by the University of Graz a total mass of 500 kg was estimated and the goal kilometre range was set to 100 km. Thus, 540 cells are needed.



**Figure F.2** 3D model of the concept L7e provided by the TU Graz (upper) and examples of the integration of the cells.

The Renault Twizy is an existing EV designed for the urban environment. Due to the lack of a 3D model of the vehicle, the dimensions needed for the application of the methodology were estimated. In order to achieve 100 km of full electric autonomy, the battery pack was modelled with 450 cells. It is worth mentioning that the best solutions provided by the methodology is similar to the shape of the battery pack used currently in the Renault Twizy.

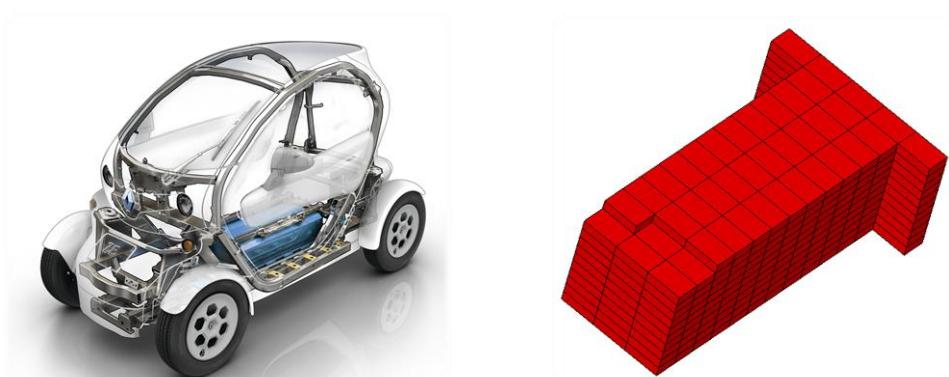


**Figure F.3** Representation of a Renault Twizy (left) [81] and example of a battery pack modelled through the application of the methodology.